

Measuring how lipid membranes respond to physical perturbations:

How charge alters lipid miscibility, how shear disrupts interleaflet coupling, and how prebiotic compounds affect membrane stability

Matthew C. Blosser

A dissertation submitted in partial fulfillment
of the requirements for the degree of:

Doctor of Philosophy

University of Washington

2014

Reading Committee:
Sarah Keller, Chair
Michael Schick
Paul Wiggins

Program Authorized to Offer Degree:
Physics

© Copyright 2014
Matthew C. Blosser

University of Washington

Abstract

Measuring how lipid membranes respond to physical perturbations:
How charge alters lipid miscibility, how shear disrupts interleaflet coupling, and how prebiotic
compounds affect membrane stability

by Matthew C. Blosser

Chair of the Supervisory Committee:

Professor Sarah L. Keller

Departments of Chemistry and Physics

The physical and chemical properties of lipid bilayers determine their biological function as the main structural component of cell membranes. The response of lipid membranes to various perturbations is, in general, difficult to predict. This dissertation will discuss four sets of experiments to probe the behavior of lipid membranes in different conditions.

In the first set of experiments, we show that the presence of charged lipids has a much smaller effect on the miscibility phase separation of lipid bilayers than predicted by simple theories. This conclusion is supported by the finding that the transition temperature of systems containing charged lipids are similar to the transition temperatures of systems without charged

lipids, and by the finding that the addition of monovalent salt, which screens charge interactions, has a small effect on the transition temperatures of bilayers containing charged lipids.

The second set of experiments examines the effect of high shear on phase-separated membranes. We find that an external shear is sufficient to move domains in each leaflet out of registration. By quantifying these results, we obtain a value for the free energetic cost per unit area of misregistration.

In the third set of experiments, we show that it is possible to create bilayers containing high fractions of charge and in highly salty solutions. We achieve this using the method cDICE, where vesicles are created by centrifuging aqueous droplets through a layer of lipids dissolved in oil. We further show that in this scheme, no detectable amount of cholesterol is incorporated into bilayers.

Finally, we examine interactions between bilayers of fatty acids and the building blocks of RNA, nucleobases and sugars. We show that the nucleobases and sugar that are found in RNA bind to fatty acid aggregates, and do so more strongly than chemically similar molecules. We also find that nucleobases and sugar stabilize fatty acid vesicles against flocculation in salty solutions. In contrast, under control conditions, salt induces the aggregation of vesicles into dense structures. These two effects suggest a role for fatty acid vesicles in the origin of life as a stable membrane in a salty ocean that could select and concentrate the components required to make RNA.

Table of Contents

| | |
|--|-----|
| Table of Contents | v |
| List of Figures | vii |
| Acknowledgements | x |
| Chapter I: Introduction | 2 |
| 1.1 Overview | 2 |
| 1.2 Physical properties of lipids..... | 3 |
| 1.3 Biological roles of lipids..... | 9 |
| 1.4 Fatty acids and the origin of life | 12 |
| Chapter II: Effect of Charge on Miscibility Phase Separation..... | 17 |
| 2.1 Introduction..... | 17 |
| 2.2 Materials and Methods..... | 21 |
| 2.3 Results | 26 |
| 2.4 Discussion..... | 40 |
| 2.5 Conclusion..... | 46 |
| Chapter III: Measuring interleaflet couplet in bilayers under shear..... | 47 |
| 3.1 Introduction..... | 47 |
| 3.2 Materials and Methods..... | 51 |
| 3.3 Model..... | 57 |

| | |
|--|-----|
| 3.4 Results | 63 |
| 3.5 Discussion..... | 71 |
| 3.6 Conclusion..... | 75 |
| Chapter IV: Fabricating vesicles by cDICE..... | 76 |
| 4.1 Introduction..... | 76 |
| 4.2 Materials and Methods..... | 79 |
| 4.3 Results | 81 |
| 4.4 Future Challenges..... | 85 |
| Chapter V: Fatty acids and the origin of life..... | 87 |
| 5.1 Introduction..... | 87 |
| 5.2 Results: | 90 |
| 5.3 Discussion..... | 107 |
| 5.4 Materials and Methods:..... | 109 |
| References | 116 |
| Appendix I: Code | 131 |

List of Figures

| | |
|---|----|
| Figure 1 Structures of three different lipids..... | 3 |
| Figure 2 Schematic depiction of phase separation..... | 6 |
| Figure 3 Schematic phase diagram | 7 |
| Figure 4 Titration curve of fatty acids | 13 |
| Figure 5 Structures of lipids used in experiments..... | 19 |
| Figure 6 Integrated mass spectrometry ion currents | 27 |
| Figure 7 Miscibility phase diagrams at different temperatures | 29 |
| Figure 8 Representative micrographs of DiPhyPG-DPPC-Chol vesicles..... | 30 |
| Figure 9 Transition temperature of charged system compared to a neutral system..... | 31 |
| Figure 10 Difference in miscibility transition temperatures | 32 |
| Figure 11 The fraction of membrane area covered by L_o | 34 |
| Figure 12 Effect of salt on charged GUVs..... | 36 |
| Figure 13 Phase separation of DiPhyPS-DPPC-Chol..... | 38 |
| Figure 14 Artifacts of vesicle preparation method | 41 |
| Figure 15. Schematic representation of the experimental system and hypotheses | 49 |
| Figure 16 Schematic representation of formation of a supported lipid bilayer | 53 |
| Figure 17 Ruptured GUV under flow | 54 |
| Figure 18 Automated edge tracking process..... | 55 |
| Figure 19 Controls using supported bilayers made from ruptured GUVs backfilled with ruptured SUVs | 64 |
| Figure 20 POPC bilayer under a bulk flow..... | 65 |

| | |
|---|-----|
| Figure 21 Velocity of the front edge of supported lipid bilayers made from SUVs composed of a single lipid type | 66 |
| Figure 22 Micrographs of domains under flow | 67 |
| Figure 23 Threshold shear required to move domains..... | 69 |
| Figure 24 Micrographs of dark regions under flow | 70 |
| Figure 25 Schematic depiction of the cDICE method | 78 |
| Figure 26 Vesicles made from aqueous droplets traveling through a solution of 1:1:100 DOPC:DPPC:Chol in oil..... | 82 |
| Figure 27 Liquid domains in a cDICE vesicle repleted with cholesterol | 83 |
| Figure 28 cDICE vesicle composed entirely of charged lipids (50:50 DiPhyPG:DPPG), | 83 |
| Figure 29 cDICE vesicles of 1:1 DiPhyPG:DPPC in PBS | 84 |
| Figure 30 Schematic of proposed production of asymmetric vesicles by cDICE | 86 |
| Figure 31 Fatty acids, like other amphiphiles, can form both micelles and vesicles..... | 88 |
| Figure 32 Nucleobases and ribose lower the pH at which vesicles form | 90 |
| Figure 33 Vesicles form when pH is decreased by heating a decanoic acid solution | 91 |
| Figure 34 Quantification of the heating-induced increase in vesicle density | 92 |
| Figure 35 Addition of nucleobases to a solution of 80 mM decanoic acid..... | 93 |
| Figure 36 Addition of ribose and glucose to a solution of 80 mM decanoic acid | 93 |
| Figure 37 Decanoic acid aggregates selectively bind heterocyclic nitrogenous bases | 94 |
| Figure 38 Scatchard analysis of adenine binding to decanoic acid micelles | 98 |
| Figure 39 Binding of bases to micelles does not correlate with their hydrophobicity | 99 |
| Figure 40 Vesicles grow faster in the presence of adenine..... | 101 |
| Figure 41 Nucleobases and sugars inhibit flocculation of decanoic acid induced by salt..... | 103 |

List of Tables

| | |
|---|-----|
| Table 1 Instrument parameters for mass spectrometry | 24 |
| Table 2 Effect of buffer on charged vesicles | 37 |
| Table 3 The rank order of effects of nucleobases and sugars | 96 |
| Table 4 Inhibition of salt-induced flocculation..... | 105 |

Acknowledgements

I would like to thank all of the amazing people that have made my time in graduate school such a pleasure. Foremost, I thank my advisor Sarah Keller for her contagious enthusiasm and clear, comprehensive command of her field. Her dedication as a scientist, mentor, teacher, and all-around awesome person is a constant inspiration. I thank Roy Black for introducing me to a field I never would have explored on my own. I thank all the members of the Keller lab: Aurelia Honerkamp-Smith, Jake Ashcraft, Cynthia Stanich, Joan Bleecker, Thomas Portet, Jonathan Litz, and Scott Rayermann, for their helpful advice, interesting science problems, and consistently fun conversation. I particularly want to thank the excellent undergraduate researchers I have worked with: Jordan Starr, Cameron Turtle, Ben Horst, and Moshe Gordon, who helped take much of the data in this dissertation. I thank the wonderful community of the amphiphiliphiles. I thank Martin Sadilek and Jim Bollinger for their help with mass spectrometry. Finally, I thank my family for their constant support.

Chapter I: Introduction

1.1 Overview

In this dissertation we will discuss the physical properties of lipid bilayers, how these properties influence biological function, and how they change in response to various stimuli. This document details four distinct projects exploring [1] the effect of charge on miscibility phase separation; [2] the magnitude of interleaflet coupling in phase separated systems and how bilayers respond to shear; [3] a method for creating vesicles using physiological lipids and buffers; and [4] the propensity of fatty acid membranes to bind to and be stabilized the precursors of RNA, and their possible role in the origin of life. These projects address different questions, while sharing several common themes. Each project involves the phase behavior of lipid bilayers. Each employs the strategy of introducing a well-controlled perturbation in order to probe complex interactions between lipids that would otherwise be difficult to quantify. Other commonalities are the role of charged lipids and solutes, the role of coupling between leaflets, and the response of lipid bilayers to changes in temperature.

The remainder of Chapter I includes a brief introduction to the physical and biological properties of lipids, with special attention paid to concepts that are important to understanding later experiments. We will start in Section 1.2 with the physical properties of lipid molecules and their aggregates, with a particular focus on miscibility phase separation. Section 1.3 will discuss lipids in a biological context: what are the lipids in cells, where are they, and how are they organized, with an emphasis on the raft hypothesis. Finally, in Section 1.4, we will discuss the special case of fatty acids, and how they fit into the larger picture of the beginning of life.

1.2 Physical properties of lipids

Chemical properties

Lipids are a ubiquitous class of biological small molecule. This thesis is concerned with the behavior of amphiphilic lipids, meaning the lipids have both hydrophobic and hydrophilic moieties. The chemical structures of three different lipids are shown in Figure 1.

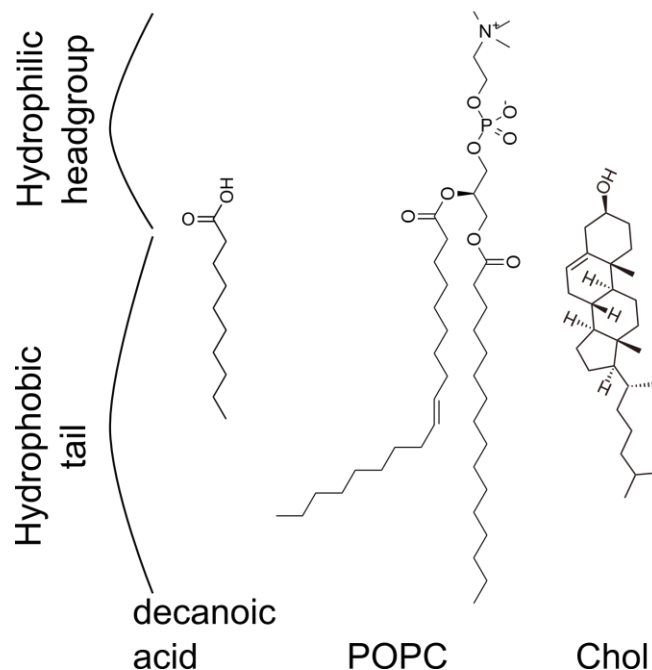


Figure 1 Structures of three different lipids: decanoic acid, palmitoyl-oleoyl-phosphatidylcholine (POPC), and cholesterol (chol). Structures are from commons.wikimedia.org.

The hydrophobic tail generally consists of a chain of repeating carbons (typically 10 to 26 carbons). These chains are flexible because individual carbon-carbon bonds can transition between two states, termed *trans* and *gauche*. For a lipid with all bonds in the *trans* state, the chain zig-zags at every carbon so that the chain is maximally extended in one direction. If a carbon-carbon bond is in a *gauche* state, the chain is bent or kinked at that position. The transition between these two states occurs readily at room temperature (1, 2). The straightness of

chains, or the prevalence of *trans* bonds, is referred to as the chain order. In addition to linear, saturated chains, lipid tails can be branched (such that additional carbon side chains branch from the main chain) or unsaturated (with a double bond between two carbons, as in POPC in Figure 1). These modifications change the physical properties of lipids, and in general disrupt packing interactions in a way that decreases order.

The hydrophilic headgroup, can consist of a variety of chemical groups. The head can have a net charge, as in phosphatidylglycerol, fixed charges that cancel overall to zero, as in phosphatidylcholine, or a readily polarized group, such as a hydroxyl (-OH) group. The headgroup and tail are commonly linked by a glycerol, with two tails per headgroup. A representative lipid of mammalian cell membranes is the phospholipid POPC, a phosphatidylcholine (PC) headgroup with one saturated sixteen carbon tail and one eighteen carbon tail with an unsaturation at the middle bond.

In addition to the phospholipids, another important class of lipids is that of the sterols. The sterol found in animal cells is cholesterol. Cholesterol has a small hydroxyl headgroup. Its hydrophobic moiety consists of four rings and a short hydrocarbon tail. Because the rings of cholesterol cannot bend like a hydrocarbon chain, cholesterol is significantly stiffer than phospholipids.

The polar headgroups of lipids interact favorably with the polar solvent water. In contrast, the hydrocarbon tails disrupt the hydrogen-bonding network of water, which is a highly unfavorable interaction. There can also exist interactions between headgroups, such as hydrogen bonding or dipole-dipole interactions, and van der Waals attraction between tails (3).

Bilayers

Because of their amphiphilic nature, lipids aggregate in water to form a wide variety of structures, all of which shield the hydrophobic tails from the polar solvent. Of particular interest to this dissertation is a bilayer configuration, shown schematically in Figure 2. This quasi-two dimensional structure is extensive in two dimensions and 2 molecules thick in the other, generally spanning about 5 nm. A bilayer has several properties that are convenient for biological function. It is relatively impermeable to hydrophilic compounds, despite its small thickness. It is soft bends to accommodate deformations (4). Holes in a bilayer rapidly close spontaneously, so a bilayer is self-healing (5). A bilayer formed into a closed shell is called a vesicle.

At temperatures above a transition temperature, T_m , characteristic of the lipid species, lipid bilayers are in a liquid state. The liquid phase is characterized by a high concentration of *gauche* bonds and a high rate of 2-dimensional diffusion of individual lipids. Below T_m , the area per lipid is lower (*i.e.* lipids are packed more tightly together), almost all of the bonds are in *trans* configurations, and diffusion is much slower (6, 7). This is called the gel or solid phase. The transition between these two phases is known as the main chain transition, the melting transition, or the gel-liquid transition. Most biological membranes are in the liquid phase; the only known gel phase in biological membranes occurs in the outermost skin cells, which are actually dead (4). The gel-liquid transition has been well studied because it is easy to observe, because it requires only a single lipid species, and because it demonstrates principles of lipid packing that are important in biology. The melting temperature, T_m , varies widely from species to species (*e.g.* -2 °C for POPC and 41 °C for DPPC), and T_m of a species provides a useful characterization of that lipid's ability to pack densely in a bilayer.

Miscibility phase separation

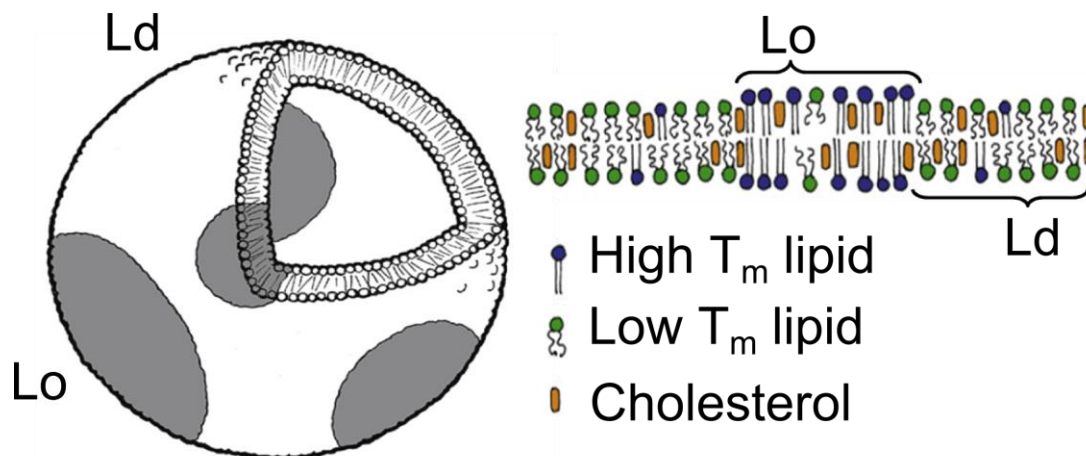


Figure 2 Schematic depiction of phase separation. (left) Cartoon of a phase separated vesicle, with the Ld and Lo phases labeled. (right) Side view of phase separated bilayer, showing the more densely packed ordered phase enriched in high T_m lipids and the disordered phase enriched in low T_m lipids. Figure adapted from Honerkamp-Smith et al. (8).

This dissertation focuses on a different phase transition in bilayers, namely the demixing from one single, homogenous liquid phase to two coexisting liquid phases. For demixing to occur, at least three components are required: a high T_m lipid, a low T_m lipid, and a sterol such as cholesterol (9, 10). At sufficiently low temperatures, such a mixture can separate into coexisting liquid phases, the liquid ordered (Lo) and liquid disordered (Ld), shown schematically in Figure 2. The Lo phase is enriched in saturated lipids, and, to a lesser extent, cholesterol. The chain order is also higher in the Lo phase, and the area per lipid lower (11). A binary mixture of high T_m and low T_m lipids would produce coexisting gel and liquid phases. In a ternary mixture, the presence of cholesterol disrupts the packing of the gel phase. However, the presence of all three components is necessary for liquid-liquid phase separation. In other words, Lo phases can form

at temperatures higher than the temperature at which the gel phase would occur without cholesterol (12). A qualitative phase diagram at constant temperature is found in Figure 3. This phase diagram shows a region of two coexisting liquid phases (Lo and Ld) surrounded by a region of one liquid phase (either Lo or Ld), which is known as a closed loop miscibility gap. Phase diagrams such as this one have been the subject of intensive study (13).

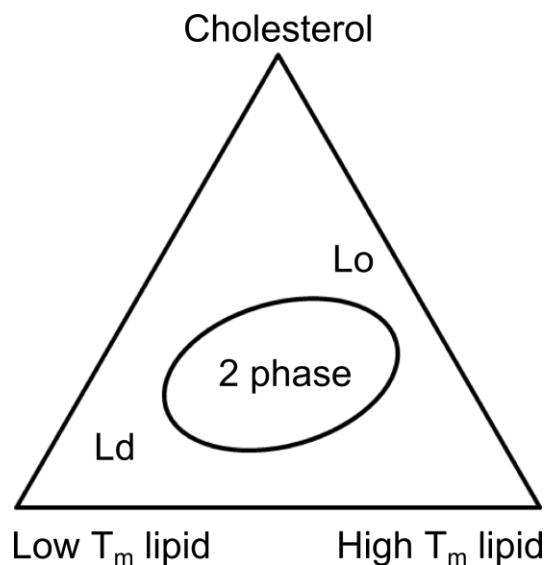


Figure 3 Schematic phase diagram. Points within the Gibbs phase triangle correspond to ternary lipid mixtures. At high concentrations of low T_m lipids, the bilayer is in a single, disordered phase, while at high concentration of high T_m lipids it is in a single, ordered (but still liquid) phase. Separation into two phases only occurs in the central region where all three components are present. Not depicted is the fact that cholesterol has a limited solubility in lipid bilayers, often 0.66 cholesterol (14). Bilayers with cholesterol concentrations higher than this are not stable, instead forming cholesterol crystals.

Studies of the phase behavior of lipid membranes have primarily utilized fluorescence microscopy, where separation into two phases is visualized by the partitioning of a

fluorescently labeled lipid. The compositions of the two phases, represented on the phase diagram as the end points of tie lines, have been obtained by NMR (12). Because phase separation is sensitive to lipid-lipid interactions, this data is often used to argue for the existence of preferential interactions between, say, high T_m lipids and cholesterol.

1.3 Biological roles of lipids

Lipids in biological systems are the primary structural component of cell membranes. They serve to compartmentalize the cell from its environment, and to compartmentalize different organelles from each other. It is estimated that an entire human contains approximately 100 km² of lipid membrane (4). Lipid bilayers provide a passive barrier to diffusion, an environment for membrane proteins, and are a site of signal transduction and catalysis. In addition to the role of lipid acting collectively, individual lipids can act as signaling molecules (15), and anchors for membrane proteins (16).

Cells contain many different species of lipid, thousands in the case of eukaryotes (17). This abundance of species has given rise to the field of lipidomics, and raised the question of what reason (if any) exists for this diversity. Lipids of different types are distributed differently between the different membranes of the cell, and even between different leaflets between a single bilayer. The endoplasmic reticulum is composed of (by percent phospholipid) ~60% PC lipids, ~30% phosphoethanolamine (PE) and ~20% phosphoinositide (PI) or phosphatidylserine (PS), and ~5% cholesterol, whereas the plasma membrane has ~40% PC, 25% PE, ~15% PS/PI, and ~25% sphingomyelin, with ~50% cholesterol (18). Associated with each headgroup is a wide variety of lipid tail compositions. For example, considering only PC lipids from one cell line, at least 20 different tail combinations have an abundance of at least 1% (19). Within the plasma membrane of red blood cells, 75% of PCs and 80% of sphingomyelin are in the outer leaflet, while 80% of PE and 100% of PS are in the inner leaflet (20). Lipids make up only part of most membranes. Integral membrane proteins account for ~20% of the area fraction of red blood cells (21). 27% of the genome codes for membrane proteins (22), and they account for more than 40% of pharmaceutical targets (23).

Membrane Heterogeneity

Historically, lipid bilayers were thought of as a passive background; a barrier to diffusion and a fluid solvent in which membrane proteins laterally diffuse. In this model (termed the “fluid mosaic” model), membrane proteins interact only with a small number of specific lipids and with specific other proteins (24). One of the most exciting (and controversial) ideas in the study of cell membranes is that rather than being homogeneous, lipid composition is non-uniform and that the membrane contains distinct regions called rafts (25), although the idea of microdomains in cell membranes is somewhat older (26).

These rafts are thought to be (or are defined as, depending on one’s viewpoint) “small (10–200 nm), heterogeneous, highly dynamic, sterol- and sphingolipid-enriched domains that compartmentalize cellular processes. Small rafts can sometimes be stabilized to form larger platforms through protein-protein and protein-lipid interactions” (27). Biochemical evidence suggests that rafts affect signaling and trafficking across the membrane (28, 29). Raft formation has been proposed to influence a wide range of diseases, including Alzheimer’s, influenza, and diabetes (30). One way rafts could affect protein function is through concentration and partitioning. If certain proteins and lipids were enriched (or depleted) in rafts, their chances of interacting would be changed due to this confinement. Another mechanism by which rafts could control protein function is by changing the behavior of single proteins based on its lipid environment. For example, the channel protein alamethicin spends different amounts of time in different conductance states depending on the composition of the lipid surrounding the channel (31). While there is still a great deal of controversy about the properties (and existence (32)) of

rafts, the idea that the lipid bilayer interacts with proteins, and that lipid properties can drive protein behavior (instead of merely the other way around) is widely accepted.

The first evidence to suggest that lipid rafts might exist came from detergent solubilization studies (33). When cell membranes were mixed with a detergent solution, it was found that a fraction of the membrane remained unsolubilized. Analysis of this fraction showed that it was enriched in high- T_m sphingolipids, cholesterol, and particular proteins. These fractions were identified as being from rafts. It was proposed that the lipids in these fractions were not solubilized because they were packed at a higher areal density than the rest of the membrane, but that the lipids were still fluid enough to permit protein function. Later, detergent solubilization was found to be capable of causing artifacts, such as inducing domains in model membranes that were originally uniform (34, 35). The similarity between the composition of the liquid ordered phase and rafts (as determined by detergent resistance), and the general idea that phase separation allows for the coexistence of disparate physical environments, suggested a correspondence between the two phenomena (36).

The direct detection of rafts in living cells has proven challenging. Because of their small, dynamic nature, rafts push the limits of current optical techniques. Groups using NMR, FRET, neutron scattering, x-ray scattering, atomic force microscopy (AFM), and imaging mass spectrometry, and have reported results consistent with the existent with small scale structure (28). Other groups have been more skeptical (32), and the field still searches for incontrovertible evidence of a raft “in the act.” Stronger evidence exists that the lipids in plasma membranes are capable of separating into regions of different lipid composition: Membranes of vesicles derived from cell membranes phase separate into two coexisting liquid phases (37, 38).

1.4 Fatty acids and the origin of life

Fatty acid bilayers

Fatty acids are in some sense the simplest lipid. They have a single hydrocarbon tail terminating in a carboxylic acid. Because of their small size and relatively weak interactions), fatty acids produce vesicles that are stable over smaller ranges of pH and temperature than vesicles made of phospholipids. Fatty acid's carboxylic acid headgroup can be either protonated or not depending on the local pH (which is in turn dependent on the global pH and the local chemical environment in a way that is often difficult to predict).

Fatty acid protonation affects aggregation, as shown in Figure 4 (39). At high degrees of protonation (low pH), most fatty acids are neutral, and form an oil that tends to exclude water. At low degrees of protonation, the charged fatty acids form micelles, because unfavorable like-charge interactions between fatty acid headgroups lead to a large positive spontaneous curvature. Only at intermediate degrees of protonation, where approximately one half of fatty acids are charged, do fatty acids form bilayers. Because the local pH can vary substantially based on the concentration of both fatty acid and other solutes, this narrow range of stability can be easily disturbed. In part because of these challenges, fatty acid vesicles were first reported only in 1973 (40), and vesicles from saturated fatty acids only in 1978 (41).

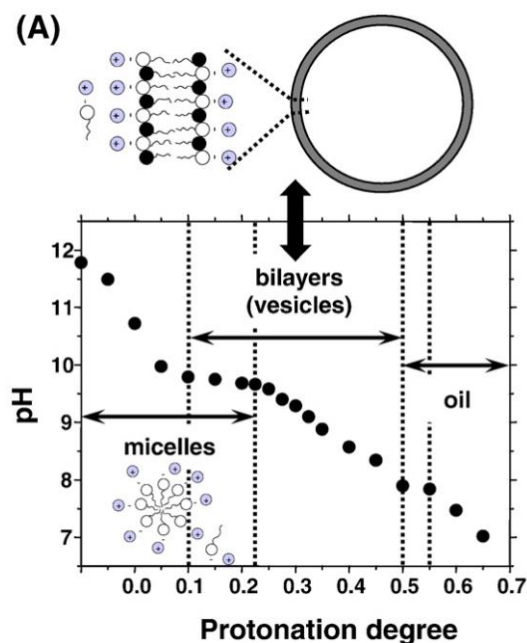


Figure 4 Titration curve of fatty acids showing the effect of protonation and bulk pH on the aggregation of fatty acids. Vesicles exist for a sizeable range of fatty acid protonations, but which corresponds to a relatively narrow range of pHs. Data shown is for oleic acid, which has 18 carbons and one double bond. Figure from Morigaki et al. (39)

Fatty acids are much less stable in bilayers than are phospholipids. In a mixture of DPPC and water, the overwhelming majority of DPPC will be in bilayers; the equilibrium monomer concentration is $\sim 10^{-10}$ M (42). In the case of fatty acids, the equilibrium monomer concentration is six orders of magnitude higher, $\sim 10^{-4}$ M (43). Because this monomer concentration is so high, fatty acid vesicles are capable of quickly changing size by exchanging monomer with the solution. Vesicles composed of phospholipids of at least 10 carbons (as is most common in biological membranes) exchange lipids with the solution much more rarely, and can be modeled as having a fixed number of lipids on experimental time scales. Fatty acid

vesicles also have much faster transport of lipids between leaflets (44), and much faster permeability of small polar molecules across the bilayer (45).

A phenomenon of particular interest for the work in this thesis is the effect of salt on fatty acid vesicles. It is known that high levels of salt destroy the colloidal stability of fatty acid vesicles, causing them to aggregate. Instead of forming an oil or micellar phase, the fatty acids form flocs, which have a higher concentration of lipids than vesicles but still contain a significant amount of water. Though few studies have been made of the structure of these flocs, presumably the local structure is still a bilayer (46).

Fatty acids and the origin of life

Fatty acids are of particular interest because of the role they are thought to have played in the chemical origins of life. It is thought that fatty acid vesicles provided encapsulation for the first cells. Encapsulation allowed the maintenance of chemical gradients, separated the machinery of the first cell from its environment, and separated the genetic material of the first population of cells from each other so that Darwinian evolution could occur (47).

There are several reasons to think that fatty acid vesicles could have played this role. The first is that fatty acids were available in a prebiotic environment (unlike relatively complex phospholipids that require biological synthesis). Analysis from meteorites finds significant fractions of saturated fatty acid. Fatty acid vesicles self-assemble. An experiment by Deamer et al. (48) showed that an organic extraction from the Murchison meteorite spontaneously formed vesicles when reconstituted in water. Fatty acid vesicles are relatively leaky to small molecules, so an autotrophic organism could obtain nutrients without specialized pores or channel, but remain impermeable to large polymers such as RNA. Decanoic acid is a representative prebiotic lipid, as it is small enough to be relatively abundant, but long enough to form membranes.

While fatty acids were present prebiotically, and vesicles can self-assemble, there is still an issue of vesicle stability in the presence of salt. Most (though not all) schemes for the origin of life occur in the oceans, which are thought to have been salty enough to induce flocculation of fatty acid vesicles. Some propose that this issue necessitates that life began in fresh water (48), or the existence for some mechanism stabilizing fatty acid vesicles against flocculation (49).

Researchers have proposed many different theories of how the first protocells formed on the early Earth, some mutually exclusive and some not. These theories often attempt to explain one step within a larger putative pathway to life. However, as the other steps in the pathway are often uncertain, there is wide disagreement about what plausible beginning and end points to an individual step are.

One of the more influential theories, though still far short of a standard model of abiogenesis, is the RNA world (50). This theory states that the first biomolecule was RNA, which was responsible for storing genetic information and catalyzing reactions, most notably its own replication. This theory is inspired in part by the fact that RNA in modern cells store genetic information (though primarily for short periods of time) and catalyze reactions as ribozymes. These ribozymes are thought to be living fossils of a time when all catalysis was carried out by RNA. This theory is supported by experiments that show that under certain circumstances RNA can catalyze its own replication (51). Arguments against the RNA world include (among others) the fact that it is incredibly difficult to synthesize RNA under prebiotic conditions, and after it has formed, it is vulnerable to degradation by hydrolysis (52). It remains the case that finding a pathway for the emergence of RNA is one of the most promising targets for establishing a pathway for the emergence of life. While the existence of fatty acid vesicles

encapsulating early cells is not strictly dependent on the identity of the first genetic molecule, the RNA world provides a promising framework for thinking about the prevailing conditions.

Chapter II: Effect of Charge on Miscibility Phase Separation

2.1 Introduction

Roughly a dozen years ago, the first fluorescence micrographs of model vesicle membranes demixing into liquid-ordered (L_o) and liquid-disordered (L_d) phases were published (53). Since that time, biophysicists have amassed a wealth of phenomenological data on the physical basis of phase separation. We know that vesicles that produce micron-scale coexisting liquid phases must, at minimum, be composed of a ternary lipid mixture. We know that the three components must be a lipid with a high melting temperature (T_m), a lipid with a low melting temperature, and a sterol such as cholesterol (9, 10). We know that the acyl chains of lipids in the L_o phase have higher conformational order than of lipids in the L_d phase (54). A variety of physical parameters, such as bending rigidities, line tensions, and diffusion constants have been quantitatively mapped and measured (55). An exciting recent development in the field of membrane biophysics is that a sufficient number of miscibility phase diagrams have been compiled such that comparisons between different lipid systems and measurement methods can be made (55). These diagrams synthesize information for membranes of different compositions, namely their transition temperatures, tie lines, and critical points. However, to date, the majority of these phase diagrams have been mapped for systems that contain only lipids without an overall net charge. Here we explore miscibility within membranes containing charged lip

Charged lipids introduce monopole electrostatic interactions into calculations of membrane miscibility phase behavior. In pure, bulk water, these electrostatic interactions are

This chapter is adapted from Blosser, M. C., J. B. Starr, C. W. Turtle, J. Ashcraft, and S. L. Keller. 2013. Minimal effect of lipid charge on membrane miscibility phase behavior in three ternary systems. *Biophys. J.* 104:2629-2638. (56)

long range: the screening length (called the Debye length, λ_D) is:

$$\lambda_D = \sqrt{\frac{\epsilon_r \epsilon_0 k_B T}{\sum_j n_j q_j}} \quad \text{Eq 1}$$

where ϵ_0 is the permittivity of free space, ϵ_r is the relative permittivity of the solvent, the sum runs over j charged species in solution, n_j is the concentration of the j^{th} species, and q_j is the charge of the j^{th} species. The Debye length is at least 2 orders of magnitude larger than the lipid-lipid distance. Electrostatic interactions between adjacent charged lipid headgroups in this scenario are strong, on the order of $k_B T$. These interactions, in contrast to those that arise from lipid acyl chain packing or hydrogen bonding, are relatively well understood and straightforward to calculate (57, 58), although mixed lipid systems present challenges (59, 60). Consequently, introducing charged lipids into membranes and mapping phase diagrams at low salt conditions is a valuable method to benchmark the free energy scales that lead to demixing of liquid phases. Miscibility phase diagrams of charged lipids will be of particular relevance to test simulation methods (61-63).

In addition to their important physical properties, charged lipids are biologically relevant. They constitute a significant fraction of biological membranes, where they are asymmetrically distributed between the inner and outer leaflets. For example, in mammalian red blood cells, 15 mole percent of lipids are charged, almost all of which reside in the cytoplasmic leaflet (64). Previously, it has been argued that repulsion between charged lipids may preclude heterogeneous lipid compositions in the inner leaflet (65) even though ionic strengths in biological systems correspond to ~ 140 mM salt. Nevertheless, the clustering of anionic lipids is often associated with interactions between proteins and membranes (66-68). Charged lipids also play important roles in signaling. Multivalent phosphoinositides (e.g. PI, PIP, and PIP₂) are the most extensively studied in this class of lipids (68-70).

Here, we map miscibility transition temperatures of two systems containing charged phosphatidylglycerol (PG) lipids. The PG lipids are mixed with uncharged phosphatidylcholine (PC) and cholesterol (Chol), to make either DiPhyPG-DPPC-Chol or DiPhyPC-DPPG-Chol. Structures of lipids are given in Figure 5. Diphytanoyl (as in DiPhyPG) was chosen for the chains of the low-T_m lipids and dipalmitoyl (as in DPPG) was chosen for the chains of the high-T_m lipids. These chains were chosen for two reasons. First, these choices facilitate comparison of our phase diagrams with previously published, extensively characterized diagrams of the corresponding uncharged system of DiPhyPC-DPPC-Chol (12). Second, neither lipid chain contains double bonds, and hence all lipid membranes that we produce are minimally prone to artifacts of photo-oxidation (71).

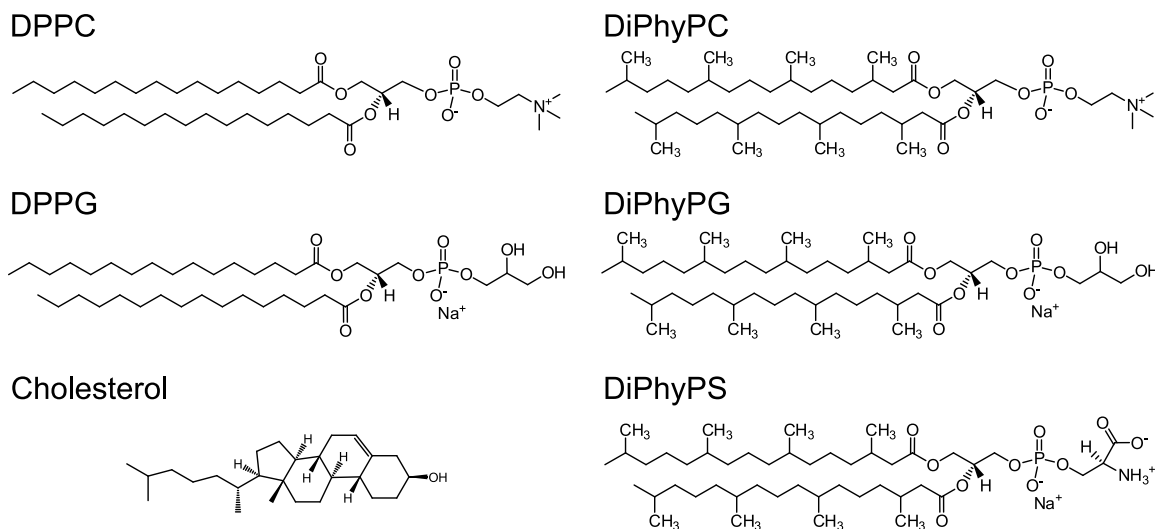


Figure 5 Structures of lipids used in experiments. DPPG, DiPhyPG, and DiPhyPS are depicted with counterions that are diluted in the solutions used in this study.

PG was chosen as the charged headgroup for three reasons. First, it has a relatively low pK_a. Therefore, PG remains charged in unbuffered solutions, even when effects of salt concentration and local bilayer environment, both on the local pH and the pK_a of the PG lipids,

are taken into account (72-74). Second, the melting temperatures of PG lipids are similar to those of PC lipids with the same chains (e.g. those of DPPG and DPPC are both 41°C) (75). Likewise, binary mixtures of PC and PG lipids have similar melting temperatures to binary mixtures of PC lipids with the same acyl chains (74, 76, 77). Since there exists some correlation between lipid melting temperatures and membrane miscibility temperatures (9), it is plausible that miscibility temperatures of all of the ternary systems that we study will be similar. Third, PG lipids are sometimes added as a minor component to neutral lipids of interest to increase vesicle yield (78).

In a separate set of experiments, we examine the phase diagram of charged membranes of DiPhyPG-DPPC-Chol in the presence of 10 mM monovalent salt, in order to determine the effect of screening the charges of the PG headgroup. The modest concentration of 10 mM is sufficient to shorten the Debye length to the same order of magnitude as the lipid-lipid spacing. Salt has been shown to reduce the effect of charge on membrane properties (79). The phase behavior of pure PG lipids has been shown to be strikingly different in pure water vs. high salt conditions (80-82).

2.2 Materials and Methods

Lipids

1,2-diphytanoyl-*sn*-glycero-3-phosphocholine (DiPhyPC); 1,2-dipalmitoyl-*sn*-glycero-3-phosphocholine (DPPC); 1,2-diphytanoyl-*sn*-glycero-3-phosphoglycerol (DiPhyPG); 1,2-dipalmitoyl-*sn*-glycero-3-phosphoglycerol (DPPG); and 1,2-diphytanoyl-*sn*-glycero-3-phosphoserine (DiPhyPS) were obtained from Avanti Polar Lipids (Alabaster, AL). Cholesterol was obtained from Sigma (St. Louis, MO). All lipids were used without further purification and were stored in chloroform at -20°C until use. Texas Red 1,2-dipalmitoyl-*sn*-glycero-3-phosphoethanolamine (TR-DPPE, Invitrogen, Eugene, OR) was included at 0.8 mol% as a dye for contrast between phases in fluorescence experiments. 18 M Ω -cm water was produced by a Barnstead filtration system. All other chemicals were obtained from Sigma (St. Louis, MO).

Making vesicles

We produced GUVs by a gentle hydration protocol (83) modified for high yield. Briefly, 0.25 mg of lipids were mixed in chloroform and spread on a clean glass slide at 60°C , which is above the gel-liquid melting transition of all lipids used here. Slides were dried under vacuum for >30 min., then hydrated overnight in 300 μL of aqueous solution at 60°C to produce vesicles. Vesicles were imaged within 4 hours of production. In our studies, miscibility transition temperatures are reported within a window of all possible ratios of the three lipids in our membranes. This window is determined by vesicle yield and dye partitioning. Specifically, compositions that produced a sufficient yield of vesicles are constrained by an upper limit on cholesterol concentration set by the cholesterol solubility limit (14, 84) and by a lower limit on charged lipids set by the gentle hydration method. Miscibility transition temperatures were measured only for samples that produced a high yield of vesicles. Dye partitioning constraints

render the DPPG-cholesterol binary axis inaccessible, since the fluorescent probe used here does not preferentially partition into the L_o or solid phase, as has been previously reported (9). To control for salt leaching from glass, a sample made with only 18 M Ω -cm water was prepared as above. At the end of the protocol, the conductivity of the water was measured using a HM Com-100 EC meter (Culver City, CA). Conductivity was measured to be 0.011 M Ω -cm, equivalent to a KCl concentration of 340 μ M aqueous solution. We used gentle hydration rather than electroformation because we are unaware of an electroformation protocol that produces high yields of vesicles without introducing new components (e.g. sucrose) to vesicle solutions.

Imaging Vesicles

To measure miscibility transition temperature (T_{mix}), GUVs were observed by fluorescence microscopy as in Veatch et al. (9). Briefly, vesicle samples were diluted \sim 5:1 in the appropriate solution and deposited between two coverslips. The coverslip assembly was sealed with vacuum grease and coupled with thermal paste (Omega Engineering, Stamford, CT) to a stage. Temperature control of the stage was achieved with a Wavelength controller connected to a Peltier device and a thermistor temperature probe with a manufacturer quoted accuracy of 0.02°C (Wavelength Electronics, Bozeman, MT). Epifluorescence microscopy was performed with a 40x objective on a Nikon microscope with either a Coolsnap HQ or QuantEM charge-coupled device camera (Photometrics, Tucson, AZ).

Only vesicles that appeared unilamellar and free from defects were included in measurements. Upon cooling, micron scale domains nucleated in vesicle membranes. The sample was allowed to equilibrate for >2 min. at each temperature before vesicle phases were assessed. The transition temperature was recorded as the temperature at which half of vesicles had visible domains. In most cases, all vesicles in a sample underwent phase separation within a

range of 3°C, which is wider than for uncharged vesicles formed by electroformation (12), but nevertheless implies that lipid compositions did not vary drastically from vesicle to vesicle. All compositions were measured at least twice (i.e. reheated and cooled at least once) to ensure that domains were indicative of equilibrium phenomena. Liquid domains have round shapes and merge quickly upon collision with other liquid domains (85, 86). Solid domains have static, typically noncircular shapes. Texas Red DHPE differentially labels the L_d phase, such that we distinguish L_d from L_o or solid phases, but not L_o from solid. Low illumination was utilized whenever possible to minimize the effect of light. Transition temperatures were constant over multiple measurements spanning >15 minutes, suggesting photooxidation was not significant, consistent with results with similar lipid mixtures (71).

Lipid extraction

Vesicles for mass spectrometry were prepared by the same method above, but without dye. Lipids extracted from vesicles were compared to lipids in stock solutions. Vesicle samples were first diluted in water to 0.5 mL, and then mixed with 3 mL 2:1 chloroform:methanol. Stock solutions in chloroform were diluted to 2 mL, and then mixed with 1.5 mL of 2:1 methanol:water. After this point, the vesicle and stock mixtures above were treated identically. The mixture was vigorously vortexed for >1 min. The mixture was spun on a bench top centrifuge for >10 min. until separate organic and aqueous phases resolved. The organic phase was removed by syringe, dried under nitrogen, and placed under vacuum for >30 min. Dried lipids were stored at -20°C until analyzed by mass spectrometry.

Mass Spectrometry

Electrospray mass spectrometry for PC vs. PG lipids was performed using a Waters Quattro triple quadrupole mass spectrometer, a 2795 Alliance HT LC/autosampler system, and

the QuanLynx software package (PC/PG). Spectrometry for Chol vs. PC used a Bruker Esquire Liquid Chromatograph ion trap mass spectrometer (Chol/PC). Samples were dissolved in 300 μL [34.3]:[57.1]:[8.6] hexane:isopropyl alcohol:water with 10 mM ammonium acetate (PC/PG) or 300 μL [47.5]:[47.5]:[5] hexane:isopropyl alcohol:water (Chol/PC). PC/PG was determined in negative mode, Chol/PC in positive mode. Parent and fragment ion m/z values, cone voltages, and collision energies are in Table 1.

Phospholipid Ratio:

| | |
|-------------------------|-----------------------------|
| Ion Polarity | Negative |
| Ion Source Type | ESI |
| Capillary | 2.60 kV |
| Cone | 25.00 V |
| Extractor | 3.00 V |
| RF Lens | 0.2 V |
| Source Temperature | 120 °C |
| Desolvation Temperature | 400 °C |
| Cone Gas Flow | 25 L/Hr |
| Desolvation Gas Flow | 900 L/Hr |
| LM Resolution | 14.0 |
| HM Resolution | 14.0 |
| Ion Energy 1 | 1.0 |
| Entrance | -2 |
| Collision | 2 |
| Exit | 1 |
| LM 2 Resolution | 15.0 |
| HM 2 Resolution | 15.0 |
| Ion Energy 2 | 2.5 |
| Multiplier | 650 |
| Syringe Pump Flow | 20 $\mu\text{L}/\text{min}$ |

Cholesterol Ratio:

| | |
|-----------------------|---------------------|
| Ion Polarity | Positive |
| Ion Source Type | ESI |
| Trap Drive | 45.0 |
| Octopole RF Amplitude | 100.0 V |
| Lens 2 | -60.0 V |
| Capillary Exit | 105.0 V |
| Lens 1 | -5.0 V |
| Dry Temp | 250 °C |
| Nebulizer | 9.00 psi |
| Dry Gas | 5.00 L/min |
| HV Capillary | 4000 V |
| HV End Plate Offset | -500 V |
| Fragmentation Width | 10.00 m/z |
| Fragmentation Time | 40000 μs |
| Fragmentation Delay | 5000 μs |

Table 1 Instrument parameters for mass spectrometry. Parameters are specific to the instrument used.

Mass spectrometry measures the current of daughter ions produced by a molecule of interest (i.e. PC, PG or Chol). That current is integrated over a sample injection, and a

background (solvent) value is subtracted to give a peak area. The area is assumed to be proportional to the initial concentration of the molecule of interest, with the constant of proportionality determined by the extraction and ionization efficiency. By comparing the peak areas of two different molecules, the relative abundance of ions produced can be compared without carefully controlling the total amount of sample. By comparing the peak area ratio for a sample to that of a stock solution of known concentrations under identical instrument conditions, we determined the relative abundance of parent molecules independent of ionization efficiency. With this method, internal standards are not necessary. Ion ratios were averaged for at least two samples. Run to run deviations in ion ratios were found to be similar for all samples of the same type (vesicle or stock). The uncertainty of each point was estimated to be the root mean square of these deviations.

2.3 Results

This section details our four major results for systems of DiPhyPG-DPPC-Chol and DiPhyPC-DPPG-Chol, which are briefly summarized as follows: [1] Charged PG/PC/Chol vesicles formed by gentle hydration have the same composition as the lipid stocks from which they are made. [2] Phase diagrams of vesicles containing charged PG lipids are qualitatively similar to corresponding phase diagrams of vesicles with only neutral lipids, namely: [2a] charged membranes demix into two liquid phases at high temperatures (T_{mix}), and [2b] the charged lipids in our system strongly partition into one liquid phase. [3] The concentration of salt in solution of charged vesicles has only a small effect on membrane miscibility transition temperatures of charged vesicles. Specifically, using pure water vs. 10 mM KCl in the production of charged vesicles has only small effects on T_{mix} over a broad range of lipid compositions. The same results are seen at 100 mM KCl, at least for one lipid composition. [4] Results 2 and 3 are valid over a range of experimental conditions, including the substitution of PS lipids for PG lipids.

Result 1: Charged PG/PC/Chol vesicles formed by gentle hydration have the same composition as the lipid stocks from which they are made.

In order to accurately map the phase behavior of lipids in vesicles, it is first necessary to produce vesicles of known composition. Vesicle compositions are important to investigate because strong electrostatic interactions between charged lipids may result in some lipid species incorporating more readily into vesicles than others (87). To verify vesicle compositions, we used mass spectrometry of lipids from vesicles composed of ternary mixtures of DiPhyPG, DPPC and cholesterol, without any fluorescently labeled lipids. As seen in Figure 6, ion current ratios for lipids extracted from vesicles are indistinguishable within experimental uncertainty

from ion ratios for lipids from stock solutions, both for cholesterol and phospholipids. The two ratios are sufficient to completely determine vesicle compositions. In addition, differences in the phospholipid ion ratio of 1:1 DiPhyPG:DPPC vesicles with 0, 20, and 40 mol% cholesterol were smaller than the sample to sample variation (data not shown). Taken together, these results show that the gentle hydration method produces vesicles with the same ternary ratios of DiPhyPG, DPPC, and cholesterol as in original stock solutions.

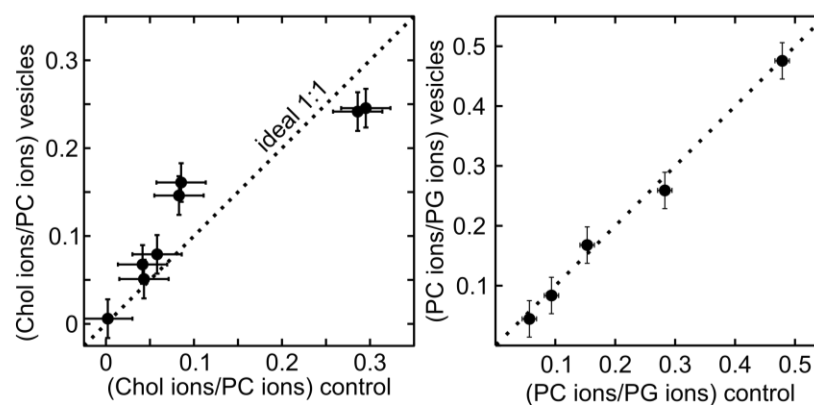


Figure 6 Integrated mass spectrometry ion currents for lipid solutions extracted from vesicles produced by gentle hydration (y-axis) vs. from lipid stock solutions (x-axis), for PC/PG (left) and cholesterol/PC (right). The dotted line is the expected relationship for vesicles that incorporate lipids from stock solutions with perfect fidelity. All data fall close to this line. Uncertainty represents the root mean squared deviation among three aliquots extracted from the same vesicle preparation, averaged over all compositions.

Two tests were conducted to verify that the presence of non-vesicle lipid aggregates does not skew mass spectrometry results. First, ion ratios were measured for vesicle samples that were determined to have high vs. low vesicle yields and high vs. low prevalence of aggregates. In all cases, ion ratios between vesicle and stock solutions agreed, as in Figure 6 (data not shown).

Second, a centrifugation step was added, which removed most aggregates. Ion ratios were indistinguishable for lipids extracted from vesicle solutions with and without the centrifugation step (data not shown).

Result 2: Phase diagrams of vesicles containing charged PG are qualitatively similar to the corresponding phase diagram of vesicles with only neutral lipids.

Vesicles composed of the two different ternary lipid mixtures containing charged PG lipids studied here (DiPhyPG-DPPC-Chol and DiPhyPC-DPPG-Chol) phase separate over a wide range of compositions and temperatures, even in low-conductivity aqueous solutions created here by placing 18 M Ω -cm water in glass chambers (Figure 7, Figure 8, Figure 10). In all membrane systems, micron-scale liquid-liquid phase separation is observed only when at least three lipid types are present: a lipid with a high melting temperature, a lipid with a low melting temperature, and a sterol such as cholesterol. Vesicles with compositions that fall on the binary axis of 0% cholesterol exhibit phase separation between solid (gel) and liquid phases. An unusual feature of the DiPhyPC-DPPG-Chol system is that solid-liquid coexistence is observed above the quoted melting temperature of both DiPhyPC (< -120 °C) and DPPG (41 °C), possibly due to widening of the melting transition in solutions of low ionic strengths (82). This phenomenon was later seen in work by Himeno et al. (88). However, it is difficult to quantitatively compare our results to those from calorimetry experiments, which are performed at significantly higher concentrations of lipids (and their counterions).

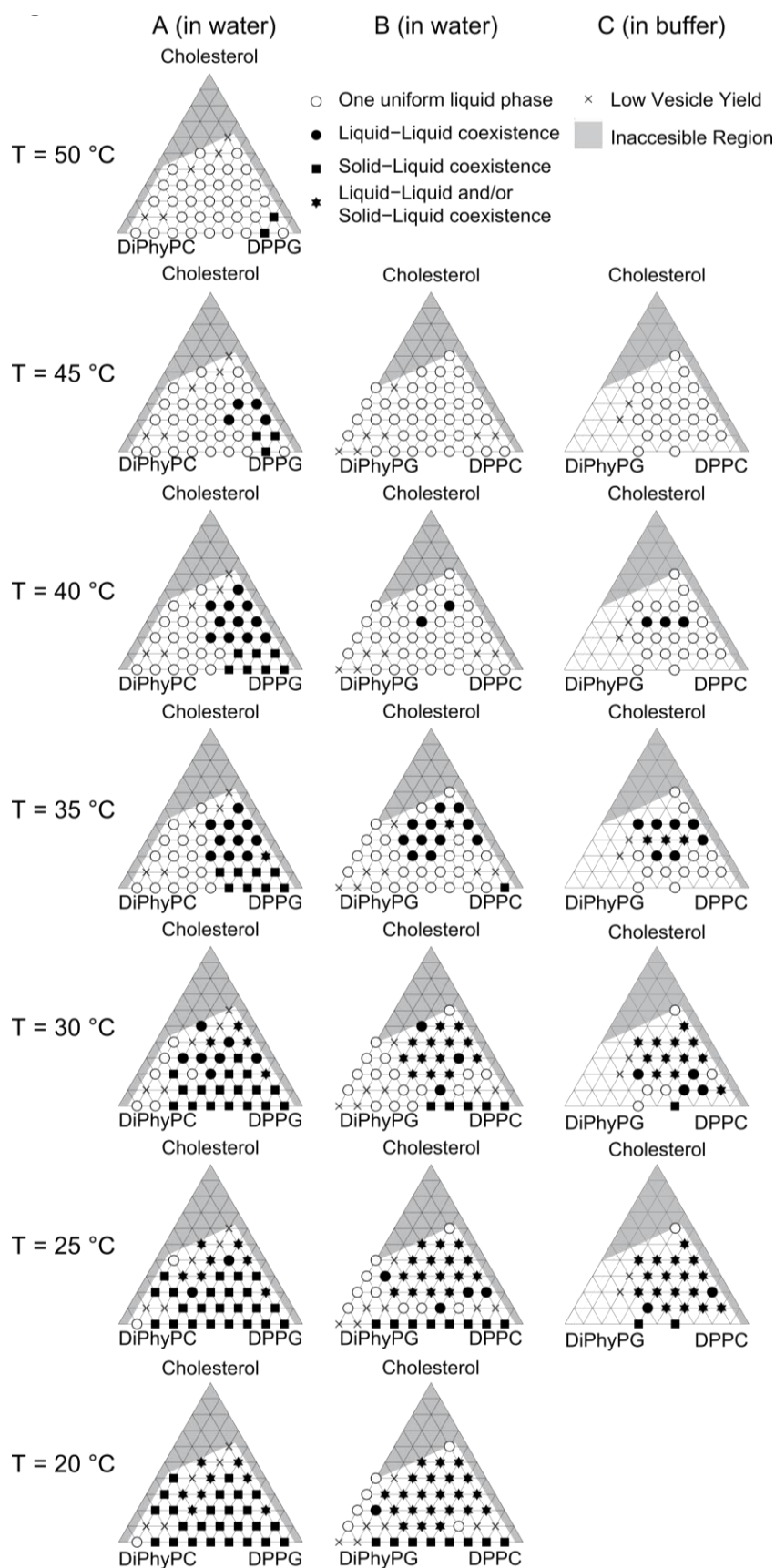


Figure 7 Miscibility phase diagrams at different temperatures for A) DiPhyPC-DPPG-Chol vesicles prepared in water, B) DiPhyPG-DPPC-Chol vesicles prepared in water, and C) DiPhyPG-DPPC-Chol vesicles prepared in 10 mM KCl, 5 mM TRIS, and 0.5 mM EDTA. Regions shaded in gray are inaccessible by our method of gentle hydration and fluorescence microscopy. Star symbols represent phase separation that is coexistence of either L_o/L_d , solid/ L_d , or solid/ L_o/L_d phases. This ambiguity arises because L_o and solid phases can be challenging to distinguish by fluorescence microscopy of vesicles, especially when three

phases (L_d , L_o , and solid) coexist in the same vesicle, and/or when a temperature quench from the $L_d - L_o$ coexistence region nucleates solid domains.

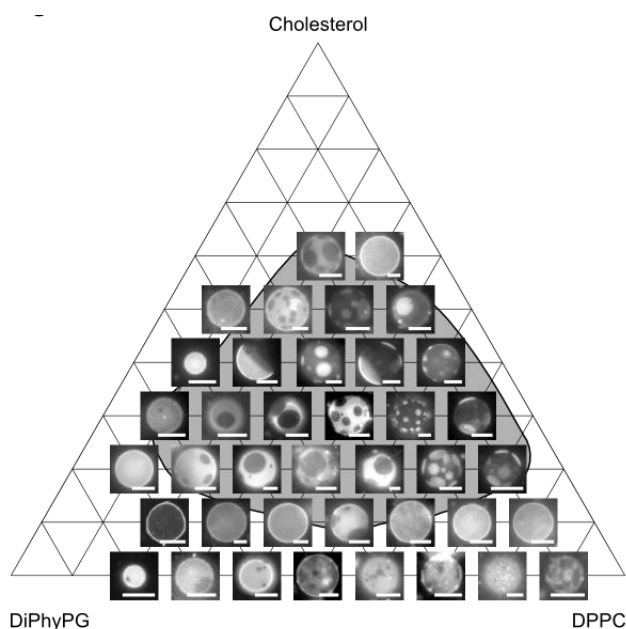


Figure 8 Representative micrographs of DiPhyPG-DPPC-Chol vesicles at 25°C, including cases of low vesicle yield noted in Figure 8. The shaded region encloses all compositions investigated for which vesicle membranes undergo a liquid-liquid transition temperature above 25°C. The fraction of dark, L_o phase increases strongly from left to right in the phase diagram (as DPPC replaces DiPhyPG) and weakly from bottom to top (as cholesterol fraction increases). All scale bars are 15 μm .

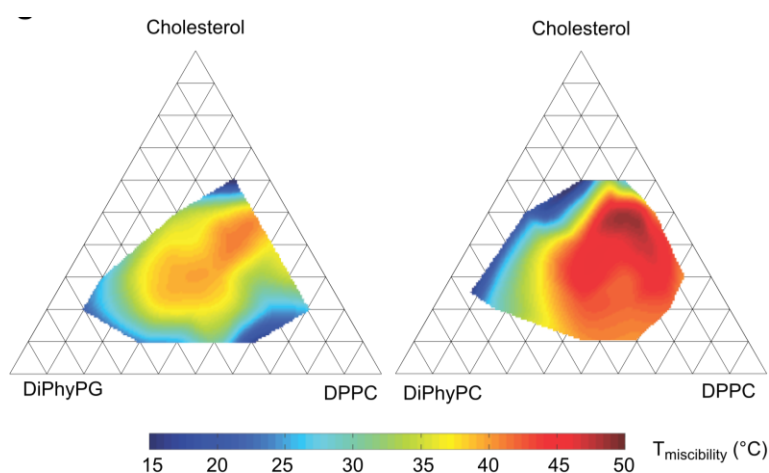


Figure 9 Transition temperature of charged system compared to a neutral system. Data is compiled from Figure 7 to show approximate miscibility transition temperatures of gentle hydration GUVs composed of the charged system DiPhyPG-DPPC-Chol (left) and electroformed GUVs composed of the uncharged system DiPhyPC-DPPC-Chol (right, from Veatch et al.(18)). In both cases, the highest transition temperatures appear near 20 mol% DiPhyPG/PC, 40% DPPC and 40% cholesterol.

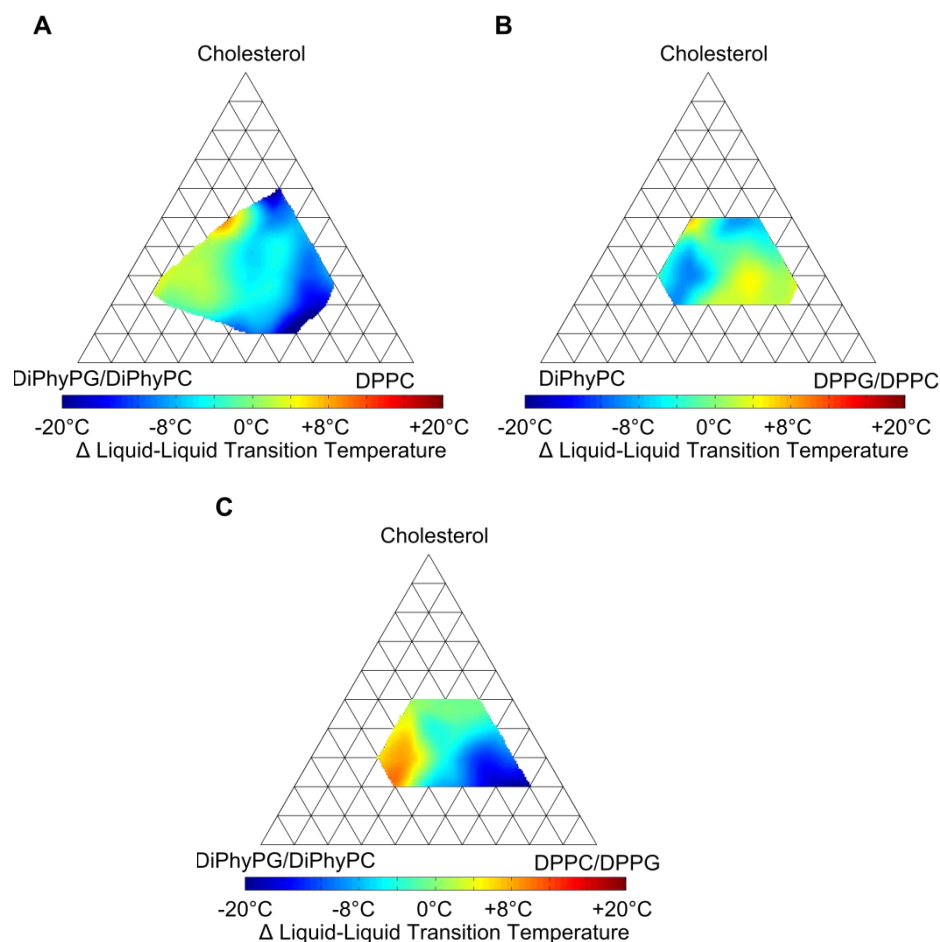


Figure 10 Difference in miscibility transition temperatures (T_{mix}) for different systems of DiPhyX:DPX:Chol, where “X” denotes either a PC-lipid or a PG-lipid. Given that uncertainties in T_{mix} at each composition are $\pm 3^\circ\text{C}$, uncertainties in T_{mix} in the figures above are $\pm 4^\circ\text{C}$ at each point. A) DiPhyPG:DPPC:Chol minus DiPhyPC:DPPC:Chol. B) DiPhyPC:DPPG:Chol minus DiPhyPC:DPPC:Chol. For both A and B, positive values correspond to higher transition temperatures in the charged system. C) DiPhyPG:DPPC:Chol minus DiPhyPC:DPPG:Chol. For A and B, the compositions with the highest values of T_{mix} shift towards the vertex of the charged lipid. For C, the two trends in A and B are additive, and the compositions with the highest values of T_{mix} shift strongly towards the vertex of the low temperature lipid.

Miscibility transition temperatures for both of the charged ternary membrane systems studied here qualitatively mimic those of the corresponding uncharged system DiPhyPC-DPPC-Chol (Figure 9). In particular, all three systems feature high miscibility temperatures and broad composition ranges over which phase separation is observed. This result clearly demonstrates that in our system, monovalent lipids only weakly influence the miscibility of a membrane, even in low conductivity aqueous solutions. Lipid acyl chain identities are far more important. This result is consistent with the observation that binary mixtures of PC and PG lipids have similar melting temperatures as binary mixtures of corresponding PC mixtures with the same acyl chains (74, 76, 77).

Result 2a: Charged membranes demix into two liquid phases at high temperatures

As in the uncharged system DiPhyPC-DPPC-Chol, there are compositions within both of the charged systems studied here (DiPhyPG-DPPC-Chol and DiPhyPC-DPPG-Chol) that phase separate at temperatures above 50°C, even in solutions with low conductivity. This high temperature, which is higher than the melting temperature of either DPPC or DPPG (both 41 °C), implies that favorable interactions between like lipid species are significantly stronger than repulsive interactions between charged head groups.

Result 2b: The charged lipids in our system strongly partition into one of the two liquid phases.

In both the charged and the uncharged vesicle systems studied here, the two liquid phases differ mostly in their phospholipid content, or, visually, the tie lines are more horizontal than vertical. An equivalent statement is that changes in the fraction of membrane area covered by L_d vs. L_o phases are more strongly correlated with changes in phospholipid ratio than with changes in cholesterol content (Figure 8). Specifically, vesicles composed of higher concentrations of the

lipid with a high melting temperature (with dipalmitoyl chains) have higher area fractions of the dark, ordered phase.

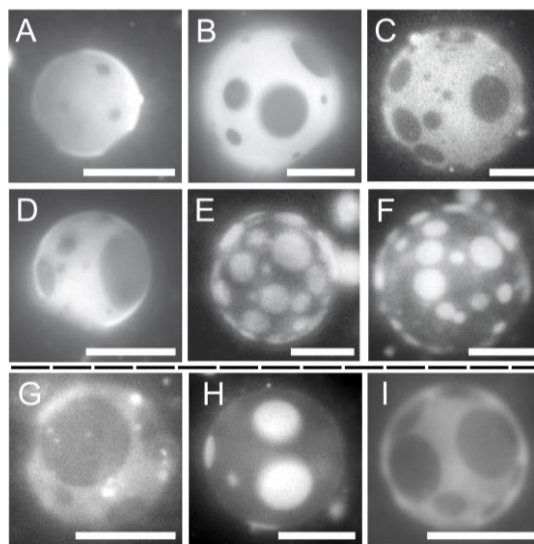


Figure 11 The fraction of membrane area covered by L_o (dark) phase strongly correlates with changes in the ratio of PG to PC lipids. Representative fluorescence micrographs are shown for giant unilamellar vesicles composed of DiPhyPG-DPPC-Chol. Panels A-F are at $T = 20^\circ\text{C}$ with 20 mol% cholesterol, and molar percentages of DiPhyPG and DPPC of A: 60/20, B: 50/30, C: 40/40, D: 30/50, E: 20/60, F: 10/70. The area fraction of L_o phase increases dramatically from panel A to F. Panels G-I are at $T = 25^\circ\text{C}$ with 1:1 DiPhyPC:DPPC and mol% cholesterol of G: 20%, H: 40%, I: 60%. Panels G to I do not show a monotonic change in the L_o area fraction. All scale bars are 20 μm .

This observation is highlighted in Figure 11 in panels A-F. Another way to come to the same conclusion is to note that the lipid compositions that produce vesicles whose surface area is approximately half covered by bright, L_d phase and half by dark, L_o phase are located within an approximately vertical stripe in the middle of the phase diagram, ranging from low to high

cholesterol. In other words, the cholesterol content is only weakly correlated with the area fraction, unlike the phospholipid ratio. This observation is highlighted in Figure 11 in panels G-I.

Since the coexistence regions in the phase diagrams of Figure 7 and Figure 8 are large, the tie line endpoints are far apart, and the two phases have very different compositions. Since the main difference in composition between the two phases is the phospholipid content, they must have a large contrast in phospholipid content. So, charged lipids partition strongly into one phase because of their acyl chains, presumably due to packing interactions. This strong partitioning occurs despite the energetic penalty due to concentrating like charges. Exact directions of tie-lines are difficult to determine without other methods such as NMR (12) or EPR (89). Quantitative tie-lines can be determined by comparing area fractions of the L_d vs. L_o phase only by purposefully neglecting lipid areal densities in the two phases as in recent work (90). Those densities likely differ by less than a factor of two, such that visual inspection of area fractions can be used to estimate tie-lines. These estimates are consistent with quantitative tie-lines determined by NMR, within experimental uncertainty (12).

Result 3: The concentration of salt in solution has only a small effect on membrane miscibility transition temperatures of charged vesicles.

Salt in solution acts to screen electrostatic interactions and shorten the Debye length. This reduces the energetic cost of concentrating charge, and so would be expected to raise transition temperatures. In order to gauge the contribution of electrostatic interactions, we prepared charged DiPhyPG/DPPC/Chol vesicles in a solution of 10 mM KCl, which shortens the Debye length to ~2.8 nm, 5 mM TRIS, and 0.5 mM EDTA. KCl served as a biologically relevant monovalent salt, TRIS stabilized pH to 7.4, and EDTA chelated any divalent cations.

Preparing vesicles in salt solutions vs. water did not have a major effect on miscibility phase behavior; transition temperatures of DiPhyPG-DPPC-Chol vesicles prepared in salt solutions vs. water differed by $\leq 5^\circ\text{C}$ (Figure 12). For the small changes in transition temperatures that were seen, T_{mix} increased for the majority of lipid compositions, in agreement with our expectations. The small decrease in transition temperatures seen in a minority of lipid compositions is inconsistent with a purely electrostatic interaction, so must involve other interactions (e.g. ions sterically disrupting the packing of the ordered phase). For one such composition, the experiment was repeated by measuring T_{mix} after adding salt to vesicles formed in pure water. T_{mix} also decreased in this case, implying that the effect is not an artifact of salt interfering with vesicle preparation.

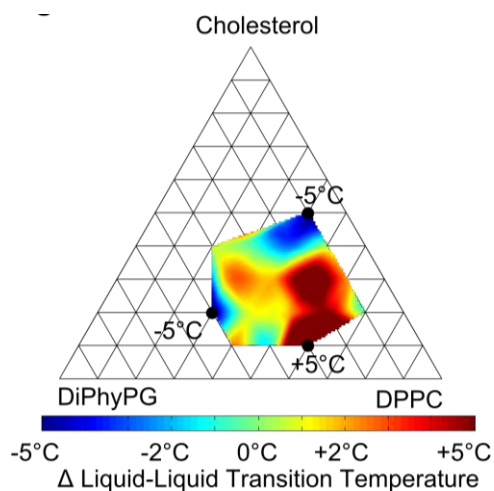


Figure 12 Effect of salt on charged GUVs. The color map represents the change in miscibility transition temperature for charged GUVs of DiPhyPG-DPPC-Chol prepared in a solution of 10 mM KCl, 5 mM TRIS, and 0.5 mM EDTA vs. in water. Positive values indicate a higher transition temperature in the presence of salt.

Figure 12 presents changes in T_{mix} for most but not all possible compositions because vesicles prepared in high salt solutions had significantly lower yields; some compositions had yields so low that no statistically significant transition temperatures could be determined.

Results 4: Results 2 and 3 are valid over a range of experimental conditions.

Table 2 details additional tests in which vesicles were prepared in solutions of various pH, salt concentration (including 100 mM KCl), and EDTA concentration; all support the conclusions above. The only experimental condition that resulted in a significant shift in miscibility temperature (larger than the shift upon changing lipid species in the previous section) was preparation of vesicles in KCl solution without EDTA, presumably due to divalent impurities in the KCl. Divalent cations are known to have a large effect on many physical properties of anionic bilayers, including miscibility transition temperature (91-94).

| Trial | KCl | TRIS (pH) | EDTA | $\Delta T_{\text{mix}} (^{\circ}\text{C})$ |
|--|--------|---------------|--------|--|
| Control $T_{\text{mix}} = 36.5^{\circ}\text{C}$ | — | — | — | 0 |
| 1. | 10 mM | 5 mM; pH 7.4 | 0.5 mM | -5 |
| 2. | 100 mM | 5 mM; pH 7.4 | 0.5 mM | +2 |
| 3. | 10 mM | — | — | +8 |
| 4. | 10 mM | — | 0.5 mM | -1 |
| 5. | — | — | 0.5 mM | -2 |
| 6. | — | 10 mM; pH 8.5 | — | +1 |

Table 2 Effect of buffer on charged vesicles. Shown are the shifts in membrane miscibility temperature (ΔT_{mix}) for charged vesicles of 50:30:20 DiPhyPG:DPPC:Chol prepared in various buffers and/or salt solutions vs. in water (control).

To verify that our main results are general rather than due to specific interactions of PG headgroups, we mapped the boundaries of the liquid-liquid coexistence region for a system incorporating PS, a different monovalent lipid (Figure 13). We found the same results for ternary mixtures containing DiPhyPS as for mixtures containing DiPhyPG. Specifically, we found that immiscible liquid phases persist over a wide range of temperatures and composition in membranes of DiPhyPS-DPPC-Chol, and that the charged lipids strongly partition into one of the two liquid phases.

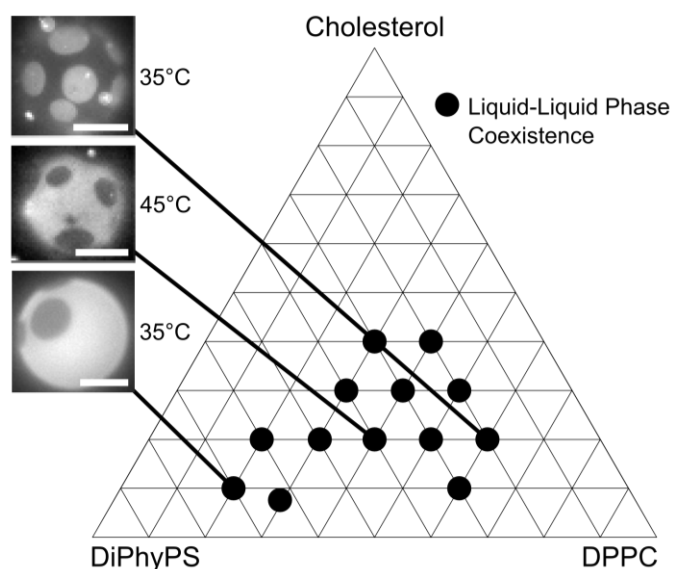


Figure 13 Phase separation of DiPhyPS-DPPC-Chol. Shown are the compositions of DiPhyPS-DPPC-Chol observed to undergo liquid-liquid phase separation within the range of 10-50°C, with representative micrographs for three different compositions. A similar region of observable phase separation exists for membranes containing PG lipids. This region is bounded by both the window where gentle hydration fails to produce sufficient vesicles for characterization and by the compositions that do not separate into liquid phases. As in membranes containing PG lipids,

the amount of L_d (dark) phase is correlated with the ratio of high- T_m to low- T_m lipids. All scale bars are 15 μm .

2.4 Discussion

Our overall result is that replacing PC lipids with PG lipids in ternary lipid membranes results in only small changes in the membranes' miscibility phase behavior, at least in the systems we studied. In other words, coexisting liquid phases are observed over wide ranges of temperatures and compositions in membranes of the uncharged reference system DiPhyPC-DPPC-Chol and in membranes for which PG lipids are substituted for either of the phospholipids. This result is surprising for vesicles grown by gentle hydration in water; the Debye length of the aqueous solution is ~ 15 nm, more than an order of magnitude longer than the lipid-lipid spacing of ~ 5 nm. Neither the long tie lines nor the high miscibility transition temperatures are significantly perturbed by the presence of salt concentrations that are high enough to lower the Debye length to ~ 2.8 nm (at 10 mM KCl). Both point to a relatively minor role for charge in miscibility. Increasing KCl concentrations further to 100 mM does not significantly alter miscibility transition temperatures.

We know of only two other systematic studies of liquid-liquid phase separation involving charged lipids, both of which reported a more pronounced effect of lipid charge. Comparison with these studies, which are by Vequi-Suplicy et al. and Shimokawa et al., is not straightforward. Vequi-Suplicy et al. (95) found that replacing all of the PC lipids by PG lipids in 1:1:1 DOPC-eggSM-Chol depressed the miscibility transition temperature by $> 25^\circ\text{C}$. Here DOPC is dioleoylphosphatidylcholine, which has one double bond in each tail, and eggSM is egg-sphingomyelin.

The system of Vequi-Suplicy et al. differs from ours in both the method of preparation and the types of lipids studied. The more important of the two is the method of preparation. They produced vesicles by electroformation in 0.2 M sugar (sucrose inside and glucose outside).

We find that vesicles formed in this way have significantly lower transition temperatures than vesicles of the same composition formed by gentle hydration (Figure 14). For example, we find that T_{mix} for 50:30:20 DiPhyPG:DPPC:Chol is 36.5 °C for vesicles made by gentle hydration vs. 24 °C for vesicles made by electroformation in 0.2 M glucose. The shift is similar for 30:50:20 DOPG:eggSM:chol. This shift is larger than the shift in T_{mix} upon forming vesicle solutions in either 10 mM monovalent salt or 0.5 mM divalent cations. The shift in measured transition temperatures due to the electroformation of vesicles with charged lipids in sugar accounts for most if not all of the qualitative difference between our results and those of Vequi-Suplicy et al.

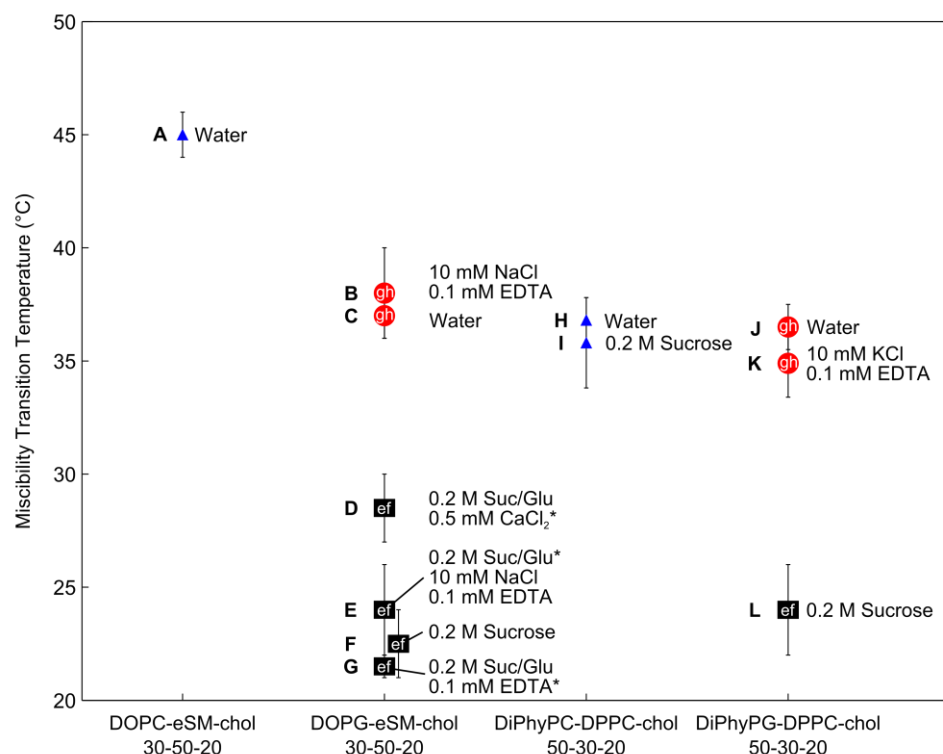




Figure 14 Artifacts of vesicle preparation method. This figure shows transition temperatures of vesicles prepared from four different lipid compositions by different methods and in different solutions. “Suc/Glu” denotes 0.2M sucrose inside of vesicles and 0.2M glucose outside. **ef** denotes vesicles prepared by electroformation that contain PG lipids as the low melting

temperature species and that are in solutions with 0.2M sugar.  denotes vesicles prepared by gentle hydration that contain PG lipids as the low melting temperature species.  denotes vesicles formed by electroformation that contain PC as the low melting temperature lipid (that is, they contain no anionic lipids). The symbol * denotes data from C.C. Vequi-Suplicy et al. (1).

The major finding of this figure is that the difference in miscibility transition temperature between charged vesicles produced by electroformation and those produced by gentle hydration is larger than the effect of adding: monovalent salt, divalent salt, or replacing PG with PC. Specifically, the method of vesicle preparation of charged vesicles (electroformation in sucrose vs. gentle hydration) has a very large effect on miscibility transition temperatures, on the order of 10 °C (compare point C to F, B and E, or point J to L). This effect of preparation method is larger than that of adding monovalent salt (compare point B to point C, E to G, or J to K), and even than that of adding divalent cations (compare point D to point G). Similarly, the effect of preparation method is larger than of replacing PC-lipids with PG-lipids (compare point H to point J, or A to C).

Although determination of the mechanism of the large shift in T_{mix} seen by Vequi-Suplicy et al. is beyond the scope of our work here, we speculate that sugars interact significantly with charged lipids in electroformed membranes. Sugars have previously been found to interact with lipid headgroups (96, 97). Interactions between sugars and uncharged lipids appear to be less important; inclusion of sucrose during electroformation of uncharged vesicles of DiPhyPC-DPPC-chol shifts T_{mix} by only ~1 °C (Figure 14). We were unable to construct experimental conditions that isolated the effect of sugar. Namely, in our hands, vesicle yields were too low to

analyze for charged GUVs produced either by gentle hydration in the presence of sugar or by electroformation in the absence of sugar.

Sugars may affect lipid vesicles in ways besides direct interaction with charged headgroups, but we suspect that the resulting shifts in T_{mix} are small. For example, the use of slightly different concentrations of sucrose and glucose can lead to a difference in osmotic pressure between the inside and outside of the vesicle. A difference in osmotic pressure would alter the membrane tension, which would result in a small change in T_{mix} (98). Also, when sucrose is used to sink vesicles to a glass substrate, interactions may arise between the vesicle and the charged substrate (99) and fluctuations may be suppressed (100). Finally, there remains a possibility that electroformed vesicles of charged lipids are not composed of the same lipid ratios as their stock solutions. The report by Vequi-Suplicy et al. of immiscible phases and of a dependence on mixing composition implies that charged lipids were indeed present at significant concentrations in their vesicles as the authors intended.

The system of Vequi-Suplicy also differed from ours in the lipids studied. Namely, their system was pseudo-ternary (containing a mixture of PC lipids extracted from egg), and we chose to use diphytanoyl lipids instead of mono-unsaturated chains as in their system. In Figure 14 we repeat experiments using the same lipids as Vequi-Suplicy et al. to show that lipid composition does not explain major differences between our results and those of Vequi-Suplicy et al. The minor differences in T_{mix} trends observed in Figure 14 between vesicles of DiPhyPG-DPPC-chol (used here) and DOPG-eggSM-chol (used by Vequi-Suplicy et al.) may be due to the structure of the phytanoyl chains, which have four methyl groups. Lipids with phytanoyl chains are expected to pack poorly; there is no main chain transition temperature above $-120\text{ }^{\circ}\text{C}$ (101). The particular structure of diphytanoyl lipids may well play a role in the membrane's miscibility behavior.

Nevertheless, replacing mono-unsaturated lipid chains in a membrane with phytanoyl chains does not fundamentally alter the membrane's miscibility phase diagram (12). The differences that are observed upon the replacement are as follows: coexisting liquid phases persist in vesicles of DiPhyPC-DPPC-Chol over wider composition ranges and to higher temperatures than in vesicles of analogous mixtures such as DOPC-DPPC-Chol (12). These wide ranges and high temperatures render membranes containing diphytanoyl lipids to be highly amenable for study at laboratory temperatures. A lipid with four unsaturated bonds, as opposed to four methyl groups as in diphytanoyl, would be prohibitively sensitive to photooxidation.

The gentle hydration membranes of Shimokawa et al. (91) also differ from ours in several important aspects. [1] The charged species was phosphatidylserine (PS) instead of PG. We find qualitatively similar results for membranes containing PS lipids (Figure 13) as PG lipids (Figure 7 and Figure 8). Nevertheless, it is worth keeping in mind that PS headgroups have three charges (two negative and one positive), with a $pK_a \sim 1$ pH unit higher than PG. So, under equivalent experimental conditions, a PS headgroup may not be charged when a PG headgroup is (72). In a low salt solution like that used by Shimokawa et al., the pK_a of PS approaches 7 and a significant amount of PS would be uncharged (102). This implies a quaternary system (DPPC, DOPS(-), DOPS+H, and Chol). [2] As noted in the paragraph above, the role of lipid structures (here, of phytanoyl vs. oleoyl chains) may also play a role in membrane miscibility. [3] In some experiments, Shimokawa et al. added $CaCl_2$, a salt containing a divalent cation. Divalent cations have a qualitatively different electrostatic interaction with charged surfaces than monovalent cations (58) and have been shown to interact strongly with anionic lipids, becoming an integral part of the membrane (103). The studies by both Vequi-Suplicy et al. and Shimokawa et al. were

conducted at only one temperature. Here we have provided phase diagrams over a wide range of temperatures to aid future comparison with data from membranes held at any temperature.

A variety of theoretical approaches and conclusions appear in the literature regarding how charge might affect membrane miscibility. Work by Mengistu et al. (57, 104) uses Poisson-Boltzmann theory to estimate the free energetic cost of phase separation in a mixed anionic-zwitterionic system. For our system, given the lowest energy assumptions about tie line endpoints and salt content, their model predicts an energetic cost of $\sim 2 k_B T/\text{lipid}$ ($\sim 1.3 \text{ kcal/mol}$). This is much larger than the interaction energies between lipids that leads to phase separation (105). However, this model makes the mean-field assumption inherent to the Poisson-Boltzmann framework, which ignores ion condensation and fluctuation effects, both of which would decrease the electrostatic penalty.

Work by Lau et al. (106, 107) predicts that in high charge regimes, a significant fraction of counterions are condensed at the membrane surface, effectively renormalizing the charge density. This model has been used to explain experimental observation of attractive forces between like-charged surfaces (108, 109). In our system, the membrane phase containing the most charged lipids has a surface charge density of $\gtrsim 1 \text{ e/nm}^2$, or approximately one charge per square Bjerrum length, which is the cut-off for the highly charged regime at which non-linear effects become important. An extension of the model of Lau et al. that accounts for the zwitterionic headgroup of PC molecules could shed further light on our results.

Lastly, it has been proposed that PG lipids may be capable of hydrogen bonding, unlike PC lipids (62, 74, 110-112). This interaction, or any other short range attraction between PG lipids, could, along with packing considerations, explain why membranes containing charged PG lipids have similar phase behavior as membranes containing only uncharged PC lipids.

2.5 Conclusion

All results that we present are consistent with the conclusion that replacing uncharged lipids with monovalent charged PG lipids within a ternary lipid membrane of DiPhyPC-DPPC-Chol has only a minimal effect on the membrane's miscibility phase behavior. This is supported by observations of the membranes' high temperatures and wide liquid-liquid coexistence regions, whether in the presence or the absence of solutions with significant salt concentrations. These results raise questions about the energetics of liquid-liquid phase separation in lipid bilayers and distribution of counter ions in the vicinity of the membrane. These questions echo concerns raised in measurements of the membrane potential in mixed lipid systems (59, 60) and suggest that new research thrusts that provide more direct measurements of ion distributions associated with a phase separated membrane, either experimentally or in simulation, would be fruitful (113). Biological ramifications of our results follow from suggestions that lipids in the plasma membrane organize in a way similar to phase separation (25). If so, then our results imply that charged lipids are capable of organizing in the same way.

Chapter III: Measuring interleaflet couplet in bilayers under shear

3.1 Introduction

In all cases in which free-standing lipid bilayers demix into coexisting lipid liquid phases (Lo and Ld), the domains in each leaflet are observed by fluorescence microscopy (with roughly 1 μm resolution) to be overlapping, or in registry. This result implies the existence of a transbilayer coupling that drives opposing regions in the two leaflets to have the same phase. This coupling, here referred to as Λ , is the free-energetic cost of misregistration per unit area of misaligned bilayer.

The magnitude of Λ has important implications both for the physical understanding of membrane heterogeneity, and for understanding lipids' role in various biological processes. In theoretical models of phase separation in asymmetric bilayers (those with different global compositions in each leaflet), Λ appears as a parameter that qualitatively changes the membrane phase behavior, for instance, determining if compositional heterogeneity in both leaflets are colocalized (114-117). In biological membranes, Λ sets the energetic scale for lipid mediated transbilayer interactions. Effective transbilayer communication between peripheral proteins mediated by the rearrangement of lipids could then occur in the absence of transmembrane proteins or transmembrane ion fluxes.

There exists little certainty about the scale of Λ . Theoretical predictions vary from 10^{-2} kT/nm² to 0.5 kT/nm² (115, 118, 119), and molecular dynamics simulations have yielded a value of 0.1 kT/nm² (120). To our knowledge, there has been no quantitative measurement of Λ ,

This chapter is adapted from M. C. Blosser, A. R. Honerkamp-Smith, T. Han, M. Haataja, and S. L. Keller. A measurement of interbilayer coupling in phase separated bilayers under high shear. (*in preparation*)

although there are several experiments that have given qualitative measures. Experiments by Subramaniam et al. found that for lipid monolayers supported on alkyl monolayers, the diffusion rate in the lipid monolayer depended on the composition of the alkyl monolayer (121). Experiments by Collins and Keller (122) on asymmetric, unsupported bilayers found that phase separation in one leaflet is capable of inducing phase separation in an apposing leaflet that normally would not phase separate. In fact, it was found that regions in one monolayer leaflet were opposite an ordered domain in the opposing monolayer leaflet always had a different composition from regions that were opposite a disordered domain. Further experiments on asymmetric bilayers by Chiantia et al. (123) found that the order within one leaflet was modified by the composition of the other leaflet, and that this effect was strongest when lipids with one long acyl tail were included, presumably because of interdigitation between leaflets.

Experiments by Stottrup et al. (124) found that when two phase-separated monolayers at an air-water interface were deposited on a glass substrate to form a bilayer, domains in each monolayer leaflet did not move into registration, implying that the registration interaction could be overcome by substrate interactions. Later work with that system by Garg et al. (125) found that varying the distance between the substrate and the bilayers using a polymer spacer allowed domains in each monolayer leaflet to move into registration. Finally, the absence of observable (micron scale) fluctuations away from registration provides an extremely weak bound on Λ of $\Lambda > 10^{-8} \text{ kT/nm}^2$.

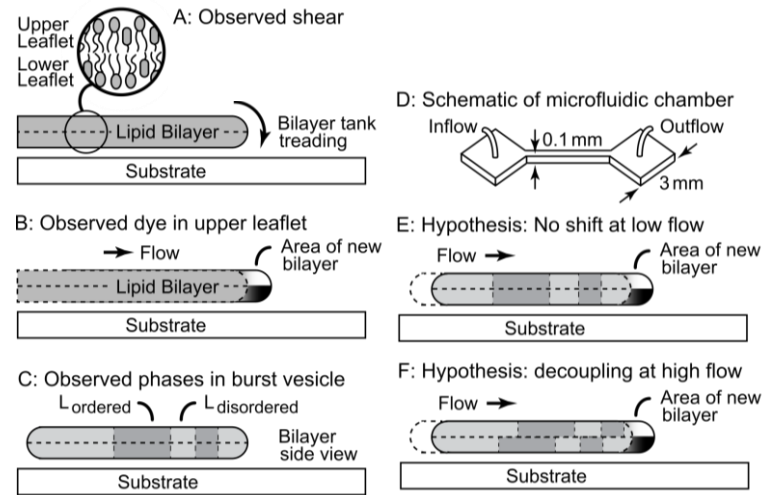


Figure 15. Schematic representation of the experimental system and hypotheses. A) A lipid bilayer on a substrate moves under shear by tank treading. B) Because large fluorophores are excluded from the bottom leaflet during tank treading (126, 127), dye becomes enriched along the leading upper edge of the bilayer. C) Micron scale domains are observed in a supported lipid bilayer formed from a burst giant unilamellar vesicle, GUV (124, 128). D) Hydrodynamic shear is caused by flow of buffer through a microfluidic device. E) A simple hypothesis is that at low flow, corresponding to low shear, domains are stationary even as the bilayer as a whole moves. F) At high flow, corresponding to high shear, a simple hypothesis is that domains move out of registration.

Because equilibrium fluctuations are so difficult to observe, we chose to measure Λ by driving domains out of registration. Here, we present a method for controllably driving deregistration (depicted schematically in Figure 15), develop a model to quantitatively analyze the result, and present a measurement of the interleaflet coupling Λ .

To apply shear to the membrane, we make use of recent work by Jönsson et al. using hydrodynamic flow in a microfluidic device (126). They showed that under shear, bilayers the leading edge of an extensive supported bilayer tank treads across the substrate. The bottom leaflet has velocity ~ 0 , while the top leaflet moves over it, as depicted in Figure 15, A and B. When we produce supported bilayers containing coexisting Lo and Ld phases, as in Figure 15, C, E, and F, we find that for low magnitudes of applied shear, domains of the minority phase stay in place while the bulk phase moves around them. For higher values of the applied shear, the domains become deregistered.

We develop a model that relates the interleaflet coupling to the shear at which a given domain becomes deregistered. Applying this model to our data, we measure a value of $\Lambda = 0.007 \pm 0.004 \text{ kT/nm}^2$, consistent with predictions of a value on the order of 10^{-2} kT/nm^2 (115).

3.2 Materials and Methods

Chemicals

1,2-diphytanoyl-*sn*-glycero-3-phosphocholine (DiPhyPC) and 1,2-dipalmitoyl-*sn*-glycero-3-phosphocholine (DPPC) were obtained from Avanti Polar Lipids (Alabaster, AL). Cholesterol was obtained from Sigma (St. Louis, MO). All lipids were used without further purification and were stored in chloroform at -20°C until use. Texas Red 1,2-dipalmitoyl-*sn*-glycero-3-phosphoethanolamine (TR-DPPE, Invitrogen, Eugene, OR) was included at 0.8 mol% as a dye for contrast between phases in fluorescence experiments. All water was filtered by a Barnstead filtration system to a final conductivity of 18 M Ω -cm. All other chemicals were obtained from Sigma (St. Louis, MO).

Producing Vesicles

We produced GUVs by electroformation as in (56). Briefly, 0.25 mg of lipids, in a mixture of 29.2/32.4/28.4 DiPhyPC/DPPC/chol in chloroform was spread on a clean, ITO-coated glass slide (Delta Technologies, Loveland, CO) at 60°C , which is above the gel-liquid melting transition of all lipids used here. Slides were dried under vacuum for >30 min., then hydrated in 300 μL of aqueous solution. A square wave potential was applied with an amplitude of 1.5 V and a frequency of 10 Hz. GUVs were imaged within 4 hours of production. Vesicles were produced in 200 mM sucrose then diluted into a solution of 200 mM glucose and 5 mM CaCl_2 to induce sedimentation and rupture, respectively.

We produced small unilamellar vesicles (SUVs) by bath sonication as in (129). Briefly, 0.5 mg of lipids in chloroform were dried under nitrogen in a clean glass test tube, and further dried under vacuum for > 30 min. The dried lipid film was hydrated in 1 mL of a buffer of 150 mM NaCl, 10 mM HEPES, 1 mM EDTA at pH 8.0. This solution was briefly vortexed and

placed in a bath sonicator (SharperTek, Detroit, MI) for 2 hours to create SUVs. The vesicle solution was then vortexed for 5 min. to remove any remaining large aggregates. For phase separated systems, SUVs were composed of in a mixture of 68/16.4/15.6/0.8 DiPhyPC/DPPC/cholesterol/Texas Red DPPE. This composition was chosen to be the same as the majority phase of the GUVs (12). For other experiments, lipids were in a mixture of 99.2/0.8 bulk phospholipid/Texas Red DPPE.

Channels

We produced rectangular microfluidic channels arranged in a T-shape of polydimethylsiloxane (PDMS) using replica molding as in (126). Briefly, the master mold was made from SU8 2075 (MicroChem Corp., Newton, MA) and was spun to a thickness of ~ 100 microns and exposed to UV light through a high resolution mask. PDMS replicas were made with a 10:1 mixture of Sylgard 184 to curing agent (Dow Corning, Midland, MI), and were cured at 60-75°C for at least 1 hr. Access holes were made with a .75 mm Uni-Core punch (Ted Pella, Redding, CA).

Immediately before each experiment, glass slides (Menzel-Gläser, Braunschweig, Germany) were cleaned by boiling in 2:1 mixture of water to 7X detergent (ICN Biomedical, Aurora, OH), thoroughly rinsing in water, and drying under nitrogen. The surface of the cured was cleaned with Magic Tape (3M, St. Paul, MN). To create a more hydrophilic surface, the PDMS was plasma cleaned (Harrick Plasma, Ithaca, NY) for 45 seconds. The PDMS was immediately sealed to a clean glass slide. To prevent leakage of fluid from the channel at high flow rates, the channel assembly was gently compressed in a home built clamp consisting of parallel aluminum plates with optical and fluidic access. The interior volume of the channel was connected to Tygon tubing (Saint-Gobain Performance Plastics, Puyallup, WA) via 22 gauge

dispensing needles inserted into access ports with no adhesive. Each channel was used immediately after manufacture.

Supported lipid bilayer formation

Supported lipid bilayers without phase separated domains were formed from SUVs. SUVs were flowed through the channel at a rate of 12 $\mu\text{L}/\text{min}$ for 15 min. The resulting supported lipid bilayer was rinsed with buffer at a rate of 120 $\mu\text{L}/\text{min}$ for 10 min to remove excess SUVs. In order to create a sharp interface at the edge of the supported lipid bilayer, buffer without vesicles was flowed through the opposing arm of the channel, with the both vesicle and buffer solutions exiting from a T-shaped channel.

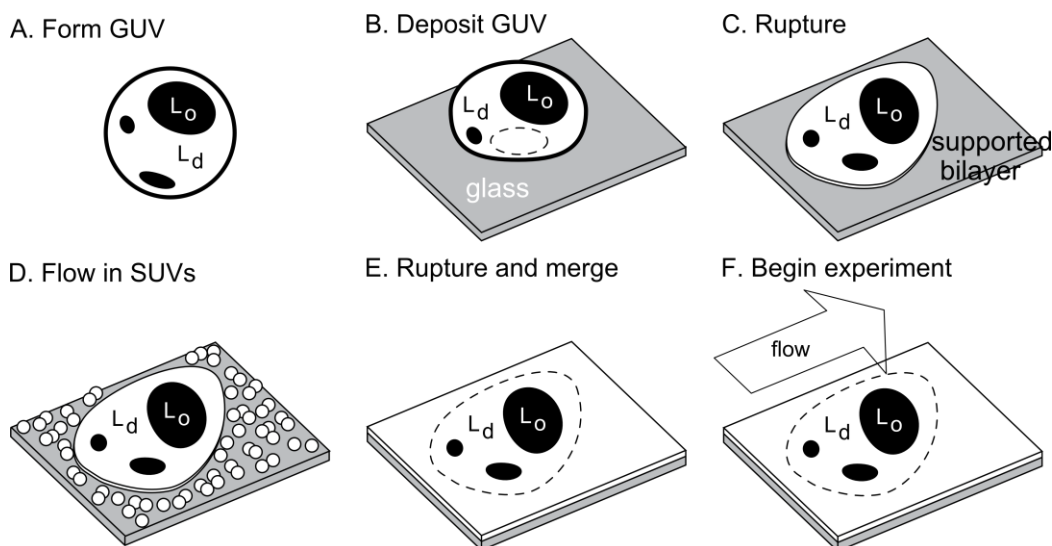


Figure 16 Schematic representation of formation of a supported lipid bilayer from SUVs and phase separated GUVs.

Supported lipid bilayers containing domains were formed from both GUVs and backfilled with SUVs, as schematically represented in Figure 16. Because the diffusion of large scale structures is hydrodynamically hindered in bilayers near a substrate and domain coarsening

is primarily due to the merging of vesicles, domains in a supported lipid bilayer do not grow larger (124, 130). To obtain micron scale domains, we ruptured phase separated GUVs. GUVs were flowed in slowly by hand application of pressure to a syringe filled with GUVs, then allowed to settle and rupture over a period of 5-15 min. with no flow. To avoid artifacts caused by membrane edges as seen in

Figure 17, we then backfilled with SUVs. SUVs were flowed through the channel at a rate of 12 $\mu\text{L}/\text{min}$ for 15 min and then rinsed with buffer at a rate of 0.11 mL/min for 10 min. The bulk flow rate was controlled by a syringe pump (Harvard Apparatus, Holliston, MA).

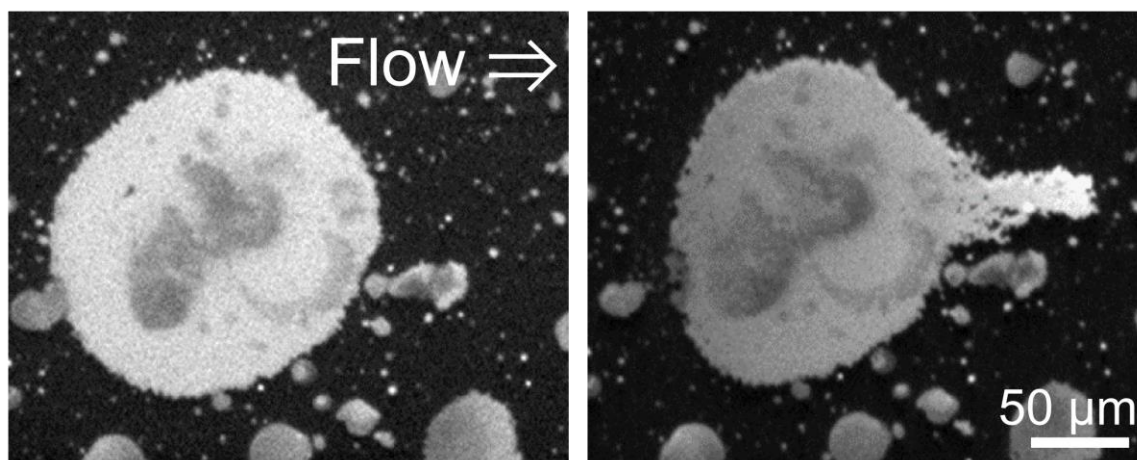


Figure 17 Ruptured GUV under flow. Black areas are bare glass. Dark gray areas within the bright area formed from a ruptured GUV are L_o domains. Under flow of buffer, only a narrow strip of bilayer is displaced, while most of the bilayer edge remains pinned.

Imaging

Epifluorescence microscopy was performed with a 40x objective on a Nikon microscope with a Coolsnap HQ charge-coupled device camera (Photometrics, Tucson, AZ). All image analysis was performed using ImageJ (public domain <http://rsbweb.nih.gov/ij/>).

Interleaflet Friction

To measure the interleaflet friction, we tracked the movement of the edge of a supported lipid bilayer formed from ruptured SUVs tanktreading under shear. The leading edge was determined using ImageJ's edge finding algorithm. The position of the edge at the center of the channel was tracked using code we wrote in Matlab (The MathWorks, Natick, MA). Movement at a given shear was tracked (Figure 18) for at least 5 minutes, and the linear, late time behavior was fit with a line. To control for changes due to time and total distance moved, we tracked bilayer movement at low of a bilayer previously exposed to high shear and found it indistinguishable from a bilayer that had not previously been exposed to high shear. At long times, on the order of hours, the interface became unstable, the movement rate changed and so data after the appearance of defects was discarded. To control for the effect of substrate chemistry and roughness, we measured movement on PDMS and on silicon separately.

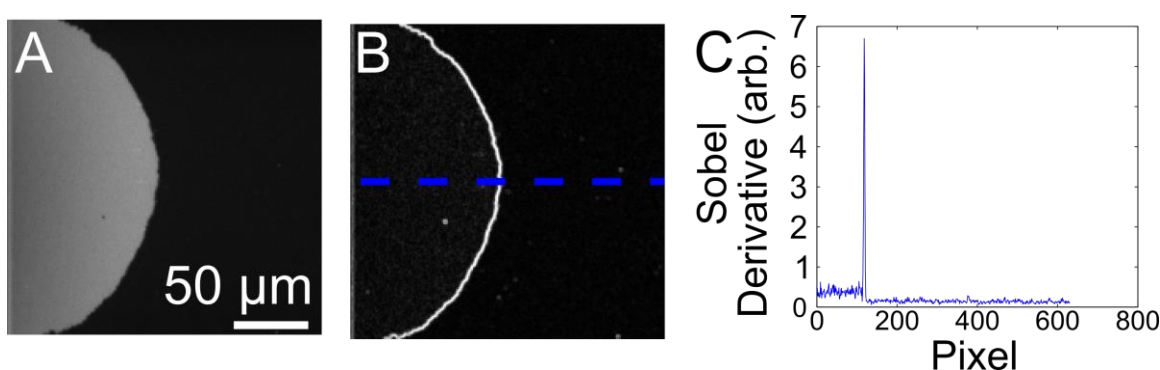


Figure 18 Automated edge tracking process. (A) Micrograph of the bilayer front. (B) A Sobel derivative of (A), where regions of high intensity correspond to regions with the edge of the bilayer in (A). (C) A line scan along the blue dashed line (vertically averaged over the same thickness) in (B). The peak corresponding to the bilayer edge is clearly identifiable.

Deregistration experiment

Supported lipid bilayers were subjected to increasing flows, and each domain was monitored for movement at each flow rate. Only domains with a clear interface completely within the frame of view were measured. Domains that did not move at the highest flow rate were also excluded.

A domain was considered to have moved if the forward edge moved at least 0.85 μm (5 pixels) over the course of 5 min. The area of domains was determined by thresholding the micrograph and summing the pixels in the domain.

Calculating Shear

The behavior of the flow in a channel is described by the Navier-Stokes equation. For a rectangular channel, the shear force on the bottom of the channel at a position z from the center is given by

$$\tau(z) = -\frac{\Delta p}{\Delta x} \frac{h}{2} \left(1 - \frac{8}{\pi^2} \sum_{k \text{ odd}} \frac{1}{k^2} \frac{\cosh(k\pi z/h)}{\cosh(k\pi w/2h)} \right) \quad \text{Eq 2}$$

$$\frac{\Delta p}{\Delta x} = -\frac{12\eta Q}{h^3 w} \left(1 - \frac{192}{\pi^5} \sum_{k \text{ odd}} \frac{h \tanh(k\pi w/2h)}{w k^5} \right)$$

where Q is the bulk flow rate, h is the height of the channel, w is the width of the channel, $\Delta p/\Delta x$ is the change in pressure in the direction of flow, and η is the viscosity of the aqueous phase (131, 132). For domain deregistration experiments, we report the shear experienced by the domain center; for interleaflet friction measurements we report the average shear. Our two channel geometries had widths of 224 μm and 214 μm , both had a height of 105 μm . To calculate the shear we truncated the series after the first 100 terms; including the next 100 terms would change the approximation by less than 1 part in 10^{-10} .

3.3 Model

In order to extract quantitative information from our data, we develop a model of domains deregistering under an applied shear τ . With regard to the domain embedded within the upper, mobile leaflet, the applied shear in the solvent attempts to advect it, while the thermodynamic driving force acts in the opposite direction so as to preserve domain registration. The stationary domain also perturbs the membrane flow field in its vicinity, giving rise to a hydrodynamic drag force on the domain. The forces acting on the mobile domain arise from the induced hydrodynamic flow within the top leaflet (i.e., a drag force F_{drag}), externally applied shear F_{shear} , thermodynamic coupling force F_{reg} , and a static frictional force F_{frict} . We will also consider a static friction force, F_{frict} , that is expected to be important only in gel domains, and we later consider the effect of diffusive transport, which will modify the force balance. As will be shown below, $F_{shear} \propto \tau$ and $F_{drag} \propto \tau$, while F_{reg} and F_{frict} are independent of τ . Hence, for sufficiently large τ , the driving force $F_{shear} + F_{drag}$ overcomes the restoring force $F_{reg} + F_{frict}$, and domain registration can no longer be sustained Figure 15B. In the case of liquid domains, on the other hand, a small displacement of the domains away from registry sets up both diffusive and advective lipid fluxes to counteract the externally imposed membrane flow field. As will be discussed below, this effect is largest when domains are near perfect registry. Once the advective flow exceeds a threshold value, the fluxes are no longer able to sustain domain registration, and the domains are driven apart.

Building on the plan above, we next carry out a detailed analysis of domain deregistration processes in our system of a lipid bilayer spreading over a solid substrate. In particular, we derive analytical formulas to predict the threshold applied shear associated with

such processes as functions of the coupling strength Λ , lipid diffusivity D , interfacial line tension σ , capillary length (or compositional interface width) d_0 , interleaflet friction coefficient of the bulk membrane phase Γ , and static friction coefficient b_s .

We begin our analysis by considering the hydrodynamic behavior of a circular, stationary domain of radius R , which remains in registry as the rest of the membrane moves. Such a domain feels a direct force from the solvent $F_{shear} = \tau \pi R^2$, as well as a hydrodynamic drag force from the surrounding membrane, given by $F_{drag} = \lambda_T v_0$, where λ_T denotes the drag coefficient. We will first derive an analytical expression for λ_T , $\lambda_T = \pi \Gamma R^2$, appropriate for the present problem.

Our starting point are the Navier-Stokes equations for the creeping flow of the incompressible fluid comprising the upper leaflet, $\eta_M \nabla^2 \mathbf{v} - \nabla p + \tau \hat{\mathbf{x}} = \Gamma \mathbf{v}$ and $\nabla \cdot \mathbf{v} = 0$, where $\mathbf{v}(\mathbf{r})$ denotes the membrane velocity relative to the substrate, while η_M denotes the membrane viscosity (133-135). The presence of a shear stress τ in the solvent is accounted for by an effective body force $\tau \hat{\mathbf{x}}$ acting on the membrane. Far away from the stationary gel/liquid domain, $\mathbf{v} \rightarrow v_0 \hat{\mathbf{x}}$, where $v_0 = \tau / \Gamma$, while along the perimeter of the domain and in its interior, $\mathbf{v} = 0$. As shown in (133), it is straightforward to solve the governing equations outside the domain to yield $v_r = \left[v_0 - \frac{C_1}{r^2} - \frac{C_2}{r} K_1\left(\frac{\epsilon r}{R}\right) \right] \cos(\theta)$, $v_\theta = \left[-v_0 - \frac{C_1}{r^2} - \frac{C_2}{r} \left[\left(\frac{\epsilon r}{R}\right) K_0\left(\frac{\epsilon r}{R}\right) + K_1\left(\frac{\epsilon r}{R}\right) \right] \right] \sin(\theta)$, and $p = -\frac{\Gamma C_1}{r} \cos(\theta)$ in polar coordinates, with $C_1 = v_0 R^2 \left[1 + 2 \frac{K_1(\epsilon)}{\epsilon K_0(\epsilon)} \right]$, $C_2 = -2 \frac{v_0 R}{\epsilon K_0(\epsilon)}$, and $\epsilon = R \sqrt{\frac{\Gamma}{\eta_M}}$. Here, K_0 and K_1 denote modified Bessel functions of the second kind of order zero and one, respectively. Finally, from these expressions, the net force acting on the domain in the x-direction (i.e., the drag force) can be extracted to yield $F_{drag} =$

$\pi\eta_M v_0 \left[\epsilon^2 + \frac{4\epsilon K_1(\epsilon)}{K_0(\epsilon)} \right] \simeq \pi\Gamma R^2 v_0$, where the approximation is valid when $R \gg \sqrt{\eta_M/\Gamma} \sim \mathcal{O}(\text{nm})$. Thus, for $\lambda_T = F_{drag}/v_0 \simeq \pi\Gamma R^2$ for $R \gtrsim 0.1 \mu\text{m}$, relevant for optical microscopy experiments. Note that λ_T , which is proportional to the interleaflet friction Γ , is due to increased interleaflet interactions in the bulk membrane phase flowing around a stationary domain, and that the value of Γ does not depend on the material properties of the domain.

In the absence of diffusive fluxes, the threshold applied shear for domain deregistration is obtained from a simple force balance argument. In addition to the shear (F_{shear}) and drag forces (F_{drag}) acting on the mobile domain, the force due to the thermodynamic coupling is given by

$$F_{reg} = -\frac{\partial E}{\partial a} = 2\Lambda \frac{\partial A_{overlap}}{\partial a} = -4\Lambda R \sqrt{1 - \left(\frac{a}{2R}\right)^2} \theta(|a|/d_0), \text{ while the frictional force is}$$

$F_{frict} = -b_s A_{overlap}$, where b_s denotes the static friction coefficient. Here, a denotes the separation between the domain centers, while the domain overlap has been expressed as

$$A_{overlap} = 2R^2 \arccos(a/2R) - aR \sqrt{1 - \left(\frac{a}{2R}\right)^2}, \text{ and } \theta(u) \text{ denotes a smooth step function with}$$

$\theta(0) = 0$ and $\theta(u) \rightarrow 1$ for $u \gtrsim 1$. Thus, the net force acting on the gel domain is given by

$$F_{net} = F_{shear} + F_{drag} + F_{frict} + F_{reg} = 2\pi R^2 \tau - b_s A_{overlap} - 4\Lambda R \sqrt{1 - \left(\frac{a}{2R}\right)^2} \theta(a/d_0),$$

where we have employed the result $\lambda_T = \pi\Gamma R^2$.

In order for the domain to remain stationary in mechanical equilibrium, $F_{net} = 0$. As τ increases, the domain separation a increases as well so as to provide the appropriate restoring force $F_{frict} + F_{reg}$ and maintain equilibrium. The largest possible restoring force occurs for $a \simeq d_0$ with $d_0 \sim \mathcal{O}(\text{nm})$, and it is given by $-b_s \pi R^2 - 4\Lambda R$ for $d_0 \ll R$. Once the driving force $F_{shear} + F_{drag} = 2\pi R^2 \tau$ exceeds this value, equilibrium can no longer be achieved. Domain

de-registration in the case of static friction (as expected in gel domains) thus occurs when $\tau > \tau_{gel}^*$, where $2\pi R^2 \tau_{gel}^* - b_s \pi R^2 - 4\Lambda R = 0$, or

$$\tau_{gel}^* = \frac{b_s}{2} + \frac{2\Lambda}{\pi R} \quad \text{Eq 3}$$

Equation (3) constitutes the first central result of this analysis, and expresses the threshold membrane flow velocity for deregistration of gel domains, τ_{gel}^* , as a function of static friction coefficient b_s , thermodynamic coupling Λ , and domain radius R . The strong $1/R$ behavior of τ_{gel}^* should be noted, which implies that large domains de-register under flow more easily than small ones. This somewhat counter-intuitive result is due to the fact that the driving force scales as $\Gamma R^2 v_0$, while the registration force scales as ΛR . In addition, τ_{gel}^* contains a domain size-independent offset due to static friction.

Before turning to the liquid domain case, we note that the force balance argument leading to Equation (3) can be recast in the form of a velocity condition. To this end, recall that domain registration is sustained when $F_{net} = \lambda_T v_0 + F_{shear} + F_{reg} + F_{frict} = 0$, or $v_0 + \frac{F_{shear} + F_{reg} + F_{frict}}{\lambda_T} = 0$. Upon defining the relative velocity of approach of the two domains as $v_{rel} = v_{rel;adv} \equiv \frac{F_{shear} + F_{reg} + F_{frict}}{\lambda_T}$, the condition for sustained domain registration reads

$$v_0 + v_{rel} = 0 \quad \text{Eq 4}$$

In Equation (4), v_{rel} can be interpreted as the treadmilling speed of the mobile gel domain, and as long as this speed counteracts v_0 , the domain remains in registry.

Now, in the case of liquid domains, their behavior is complicated by the emergence of diffusive lipid fluxes (in addition to advective ones) when the domains are brought out of perfect registry. These fluxes contribute to v_{rel} and help sustain domain registration. To account for

such fluxes, we build on and extend our earlier results for the case of recurrence of domain registration, where the domains of radius R are initially separated by a distance a , and subsequently slide back towards each other to re-establish perfect domain overlap (136). Specifically, the relative velocity of approach of two mobile domains moving in opposite directions due to diffusive transport alone was shown to be $v_{rel;diff} = \frac{4d_0DF_{reg}}{\pi R^2\sigma}$ (136). When only one of the domains is mobile, $v_{rel;diff}$ becomes simply $v_{rel;diff} = \frac{2d_0DF_{reg}}{\pi R^2\sigma}$, while $v_{rel} = v_{rel;adv} + v_{rel;diff} = \frac{F_{shear} + F_{reg} + F_{frict}}{\lambda_T} + \frac{2d_0DF_{reg}}{\pi R^2\sigma}$.

In light of Eq. (4), the condition for sustained domain registration in the case of liquid domains becomes $v_0 + \frac{F_{shear} + F_{reg} + F_{frict}}{\lambda_T} + \frac{2d_0DF_{reg}}{\pi R^2\sigma} = 0$, or $2v_0 + \frac{F_{reg}}{\pi R^2} \left[\frac{1}{\Gamma} + \frac{2d_0D}{\sigma} \right] = 0$, where we have employed the expressions $\lambda_T = \pi\Gamma R^2$ and $F_{shear} = \pi\Gamma R^2 v_0$, and assumed that $F_{frict} = 0$. Given that $|F_{reg}|$ is maximized when $a \simeq d_0$ such that $F_{reg}^{max} = -4\Lambda R$ for $d_0 \ll R$, and that $v_0 = \tau/\Gamma$, the threshold velocity for liquid domains is determined from $2 \frac{\tau_{liquid}^*}{\Gamma} - \frac{4\Lambda}{\pi R} \left[\frac{1}{\Gamma} + \frac{2d_0D}{\sigma} \right] = 0$ or

$$\tau_{liquid}^* = \frac{2\Lambda}{\pi R} \left[1 + \frac{4d_0D\Gamma}{\sigma} \right] \quad \text{Eq 5}$$

Equation (5) constitutes the second central result of this analysis, and expresses the threshold membrane flow velocity for de-registration of liquid domains, τ_{liquid}^* , in terms of interleaflet friction Γ , thermodynamic coupling Λ , capillary length d_0 , lipid diffusivity D , line tension of compositional interface σ , and domain radius R . We note that τ_{liquid}^* displays a strong $1/R$ domain size dependence, similar to the result for τ_{gel}^* in Eq. (3). As expected, the expressions for τ_{gel}^* and τ_{liquid}^* coincide when diffusive contributions are eliminated from τ_{liquid}^*

by setting $D = 0$ in Eq. (5), and when the static friction term is ignored in Eq. (3). The dimensionless term $2d_0D\Gamma/\sigma$ describes the effect of diffusive transport. We take characteristic values of $d_0 = 10^{-9}$ m, $D = 10^{-12}$ m²s⁻¹, $\Gamma = 10^8$ Pa s m⁻¹, and $\sigma = 10^{-12}$ Pa (136), which yields a value of $2d_0D\Gamma/\sigma \sim 0.2$. Because these quantities are not well measured in our particular system, this term introduces some uncertainty that does not decrease with additional data from our experiment. However, when comparing two systems where this parameter is expected to be the same, this uncertainty would not affect the measurement of the difference between coupling constants.

In conclusion, Eqs. (3) and (5) constitute the central results of this work, and provide closed-form analytical expressions for the threshold membrane flow velocity τ^* for induced domain de-registration in lipid bilayer membranes flowing across a solid substrate in case of either gel or liquid domains, respectively.

3.4 Results

GUV and SUV merging

Our goal was to observe micron scale domains far from edge defects. In order to do so, we formed supported lipid bilayers by rupturing GUVs and then covering the remaining bare glass with ruptured SUVs, described as backfilling in the methods. To our knowledge, this method has not been previously employed. This method was inspired by previous methods of backfilling incomplete bilayers formed by microcontact printing (137). We performed controls, summarized in Figure 19, to confirm that a single, continuous bilayer spans the region covered by the ruptured GUVs and the ruptured SUVs.

The first control is in Figure 19A. The left panel shows GUVs ruptured on a glass surface. The bilayer membrane is labeled with Texas Red DPPE, which partitions to the L_d phase. Dark regions within the bilayer are regions of L_o phase. Dark regions surrounding the bilayer are bare glass. The right panel shows the same region after unlabeled SUVs have been ruptured to cover the bare glass. The fluorophores originally in the GUV freely diffuse into the surrounding bilayer formed from SUVs. In the second control, phase separated ruptured GUVs backfilled with L_d SUVs were heated above the transition temperature and then cooled. The resulting (small-scale) domains were distributed over the area originally occupied by GUV and SUV. This shows a large-scale redistribution of all lipids in the sample, not only of a fluorescently labeled lipid.

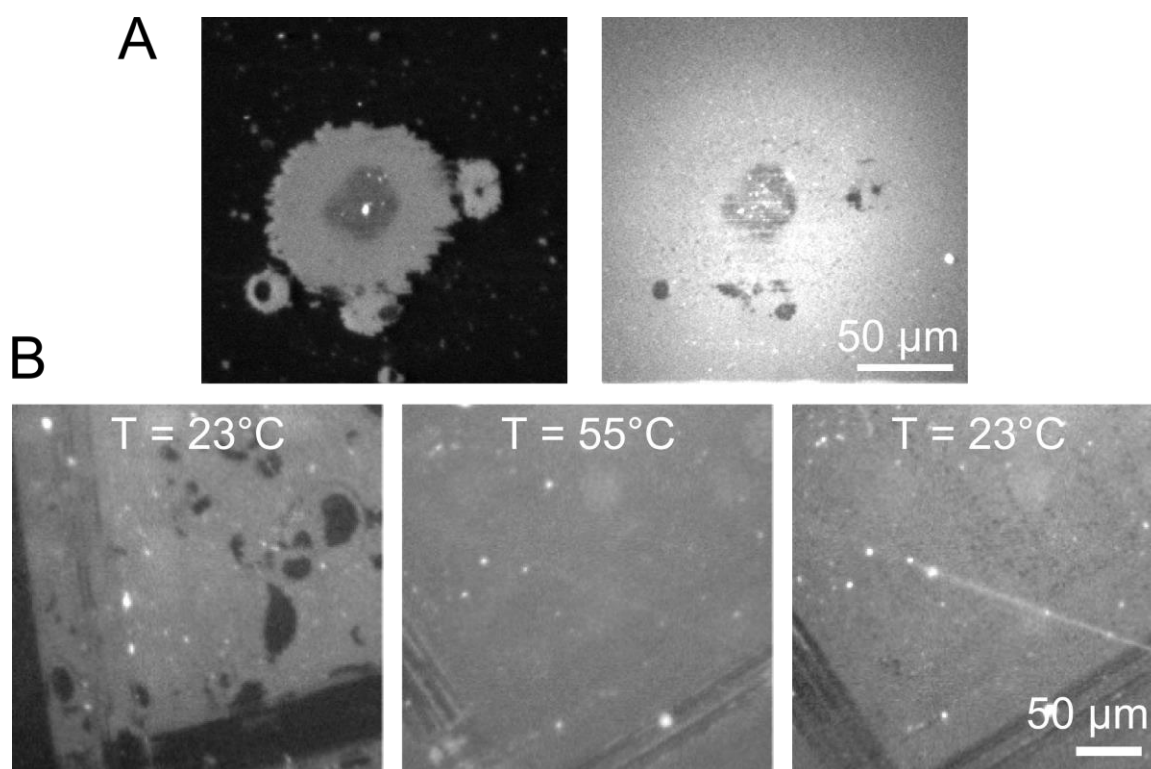


Figure 19 Controls using supported bilayers made from ruptured GUVs backfilled with ruptured SUVs (A) Phase separated GUV backfilled with unlabeled SUVs. After fifteen minutes, the fluorophores (originally associated with the GUV) have diffused throughout the entire field of view of the newly formed bilayer. (B) Phase separated GUVs backfilled with SUVs mixed heated and cooled. When the bilayer is heated, the lipids mix uniformly, and when it is cooled again domains do not reform in their original locations. The uniform distribution of small scale domains across regions originally formed by either SUVs or GUVs implies that lipids mix freely.

Interleaflet Friction

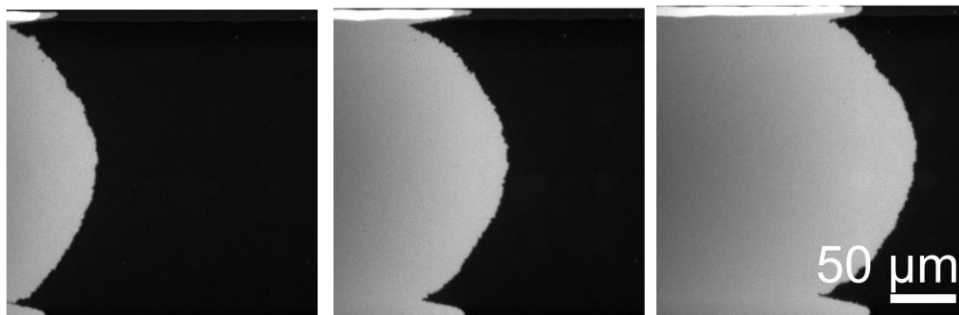


Figure 20 POPC bilayer under a bulk flow. The labeled POPC bilayer was made from ruptured SUVs. It is moving from left to right over a clean glass slide. The bulk flow rate from left to right is 0.22 mL/min, and each micrograph was taken at a 20-minute interval.

A convenient control is to measure the bulk movement of a continuous supported membrane made from only one lipid type Figure 20. The motion of the edge of the supported lipid bilayer edge is linear in time, as seen in Figure 21A. The rate that the bilayer moves is linear in the applied shear, as seen in Figure 21B. Since this motion is dominated by the interleaflet friction, or drag, the slope of Figure 21B is related to the friction coefficient between bilayers by $v = 2 b \sigma$, where v is the velocity of the bilayer front, b is the interleaflet friction coefficient, σ is the applied shear, and the factor of two is from the bilayer front moving at half the velocity of the top leaflet. For supported lipid bilayers made of POPC lipids we obtain a friction coefficient b of $5.8 \pm 0.8 \times 10^7$ Pa s/m, and for DOPC a value of $5.2 \pm 0.4 \times 10^7$ Pa s/m.

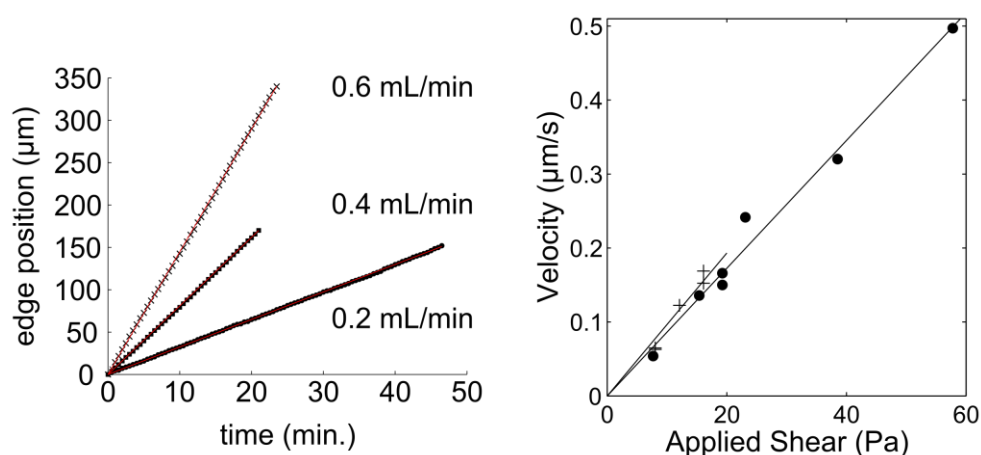


Figure 21 Velocity of the front edge of supported lipid bilayers made from SUVs composed of a single lipid type. (A) Position of a POPC bilayer edge as a function of time for three different bulk flow rates. Points represent the position in an individual frame, and a linear fit is overlaid. (B) Measured velocity as a function of applied shear, determined by taking the slope of tracks as in (A). Circles are POPC, plus signs are DOPC. DOPC bilayers delaminated at lower applied shears, limiting the range of data. Measurement uncertainty is the same as the marker size.

Previous measurements of velocity vs. applied shear for supported bilayers of egg PC lipids obtained a friction coefficient of 2.4×10^7 Pa s/m (132), whereas measurements using other methods and systems have found a range $\sim 10^7$ to 10^8 Pa s/m (138-141). These literature values are consistent with our calculation of the applied shear and with the previously reported result that the primary determinant of the membrane motion is interleaflet interactions (126).

Because the tank treading motion is dominated by interleaflet interactions, the substrate should have no effect. To verify this, we repeated the experiments in Figure 21 using POPC supported lipid bilayers on two additional substrate types: a silicon wafer that replaced the glass in our channel setup, and the PDMS that forms the roof of the channel. The rates on all three

substrates were indistinguishable. Because glass, silicon, and PDMS substrates all have different surface roughnesses, our results imply that the shear experienced by the bilayer does not change with roughness.

Backfilled GUVs under flow

Under sufficiently high flow, domains in supported lipid bilayers moved (Figure 22). The shear required to move a domain was dependent on the size of the domain, and domains in the same bilayer were observed to be either mobile or stationary depending on their size.

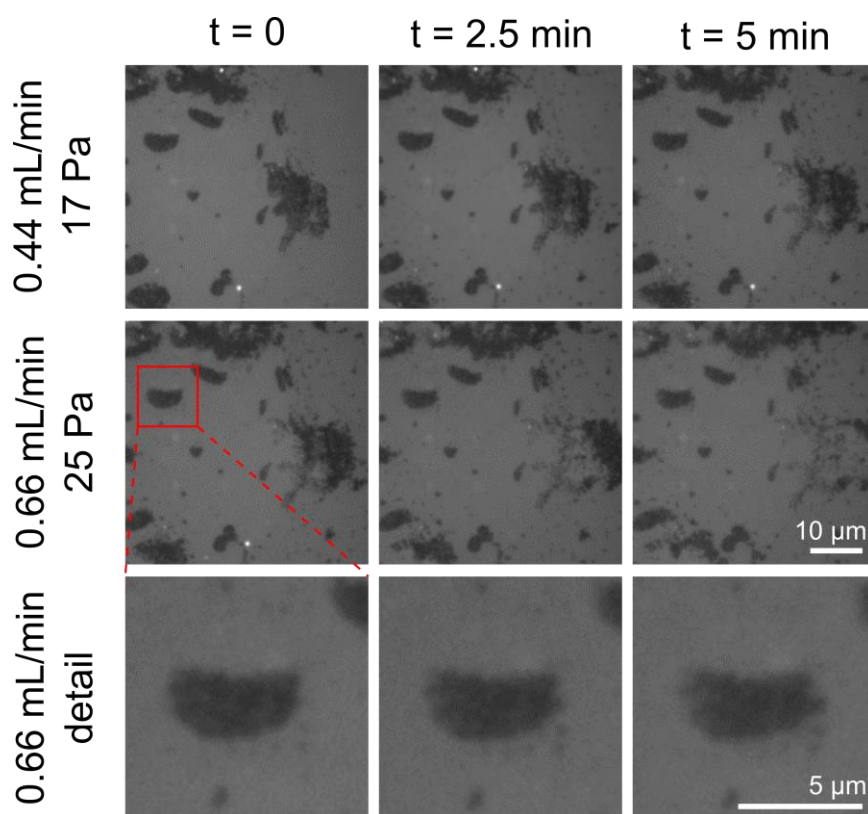


Figure 22 Micrographs of domains under flow. The top row has a bulk flow rate of 0.44 mL/min, which corresponds to a shear of 17 Pa at the center of the image. The second row has a bulk flow rate of 0.66 mL/min, corresponding to 25 Pa. The third row is an inset showing a domain that was stationary at 0.44 mL/min, and moves at 0.66 mL/min. The ten micron scale bar applies to the top two rows, the 5 micron bar to the bottom row.

We chose to focus on the binary outcome of whether or not either moved or did not move. We did not examine trajectories of domains once they started moving for two reasons. First, as domains move their overall shapes change. Second, domain movement was often observed to result in the development of defects in the membrane, which are identified by a bilayer with a speckled appearance rather than a uniform fluorescence level.

As domains move, their overall shape changes. In many cases, defects develop, causing a speckled fluorescence in area newly occupied by a domain. For this reason, we only considered the stability of domains, i.e. whether or not they move, rather than trying to model their behavior while moving.

We expect that the magnitude of shear required to deregister a domain is inversely proportional to its size. A convenient measure of inverse size is the length perpendicular to the direction of flow, r_{perp} , divided by the total area (for a circle this ratio is $2/\pi$ radius⁻¹). In Figure 23, we fit data for shear vs. inverse size to a straight line using a least squares fit weighted by the uncertainty (in this case the range) at each value of inverse size. The best fit slope is 74 ± 42 Pa/ μm , or 0.0089 ± 0.0050 kT/nm². Subtracting our best estimate of the diffusive contribution to domain motion from this value, our best estimate for an interleaflet coupling is 0.007 ± 0.004 kT/nm².

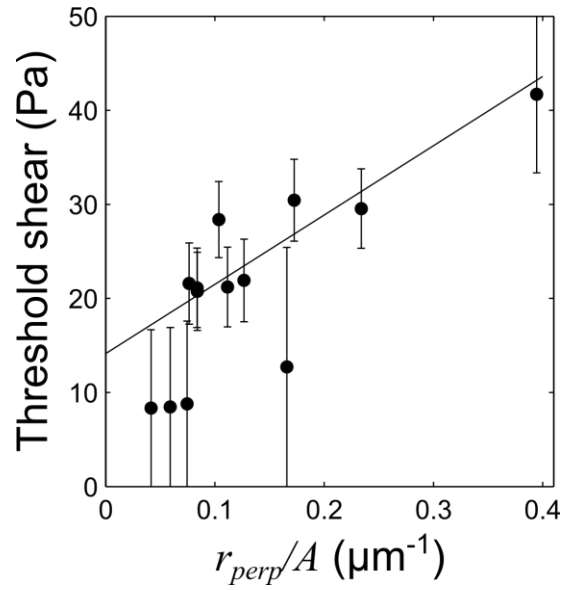


Figure 23 Threshold shear required to move domains, as a function of inverse size r_{perp}/A . Bars show the entire range of all data, from the highest shear at which domains were observed to be stationary to the lowest shear at which they were observed to move. Symbols denote the midpoint of this range, and are present to guide the eye rather than to imply that the central value is most probable. The shear was calculated from the channel geometry, bulk flow rate, and domain center from Eq 2. The line is a least squares fit weighted by the uncertainty at each value of r_{perp}/A .

When the flow was stopped shortly after domains began to move, all movement ceased, and the domain remained stationary for at least 10 minutes. In other words, any domains that were pushed out of registration by the applied shear did not move back into registration when the shear stopped. This is in agreement with previous observations (124, 125) that the substrate proximity is sufficient to prevent micron-scale domains from moving into registration.

In some cases, as in Figure 24, dark regions that appear to be domains disappear instead of translocate. Because the low fluorescence levels of the bare substrate and the Lo-phase membrane are very similar, these dark regions could be holes in the membrane that fill as the membrane is sheared. Another possibility is that the membrane's local lipid composition changes through advection of lipids that the dark region begins as an Lo domain, and that as the membrane in that region moves, the lipid composition of the membrane in that region corresponds to a one-phase region of the phase diagram. A third possibility is that the domains are being moved out of registration, but that the additional cost of misregistration is enough to favor a single phase. In other words, domains out of registration may not be stable, even at a composition where registered domains are stable. In this case we would expect the sub-micron domains to nucleate.

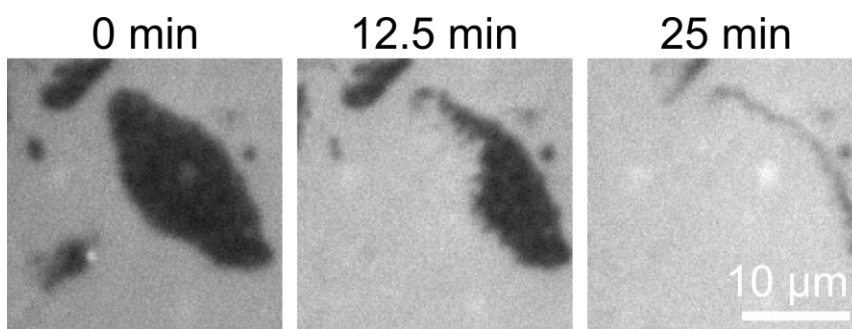


Figure 24 Micrographs of dark regions under flow, increasing from 0.44 mL/min to 0.88 mL/min over 25 minutes. The large domain in the upper right drastically changes in size, whereas the domain in the lower left is undetectable at late times.

3.5 Discussion

Overall, our results show that domains in supported lipid bilayers deregister when subjected to high shear, and that this process is sensitive to interleaflet interactions. From our data we extract the first measured, quantitative value of the interleaflet coupling constant, Λ .

Both qualitative experimental results and quantitative calculations are consistent with our measured value of Λ . Stottrup et al. (124) found that domains within each leaflet of a supported bilayer made by Langmuir-Blodgett deposition do not spontaneously move into registry. Similarly, we find that domains do not spontaneously move into registry, even if the driving force is stopped while a domain is partially deregistered (data not shown). We are justified in ignoring the substrate interaction that prevents registration in our data analysis, as the minimum shear required to deregister a domain (which must be greater than the minimum required to reregister a domain) is small. That is, the y-intercept of Figure 23 is much less than shear at which the majority of domains deregister. Our measured value of Λ is consistent with the theoretical work of Putzel et al. (115), which predicted a value of $\Lambda = 0.01\text{--}0.03\text{ kT/nm}^2$. Our results are inconsistent with previous predictions of $\sim 0.1\text{ kT/nm}^2$, 0.15 kT/nm^2 and 0.5 kT/nm^2 (118, 119).

Determining the mechanism of coupling is beyond the scope of this work. Previous work has found an increase in coupling when bilayers incorporated lipids with one long acyl chain and one short acyl chain, presumably because of increase interdigitation between leaflets (123). Future directions could include using our method to quantify the change in coupling caused by a change in interdigitation.

One unintuitive feature of the micrographs in Figure 22 is that as the domain moves out of registry, there are only two fluorescence levels. This is due to the fact that the overwhelming

majority of fluorophores, which are relatively bulky and charged, partition to the upper leaflet. This effect has been previously reported for charged lipids in bilayers on glass (127), and measured in fluorophores in a supported bilayer in a microfluidic device (126). In effect, the micrographs show only the top leaflet, with the bottom leaflet remaining stationary. Additional evidence for partitioning of fluorophores to the upper leaflet from our results is found in the behavior of bilayers containing a single component in addition to the fluorophore, as in Figure 20. As the bilayer moves from its starting position, the fluorescence level of areas newly covered by bilayers is the same as areas initially covered by ruptured SUVs, except for a bright band at the leading edge. As previously noted (142), this is characteristic of a top leaflet that contains a majority of the fluorophore moving over a stationary bottom leaflet. This motion advects fluorophores to the leading edge, where they are excluded from flipping to the bottom leaflet, and so are concentrated. Far from this bright band, we conclude that fluorescence is due to a labeled top leaflet and unlabeled bottom leaflet.

The scatter in our data in Figure 23 is larger than the measurement uncertainty associated with the plotted quantities, and could be due to several sources. We already mentioned how strong interactions between the bilayer and the substrate is responsible for the positive y -intercept. While most domains were large on the length scale of glass roughness, there could be some variation in the number or strength of pinning sites. If these pinning sites are evenly distributed across the membrane surface, the force from pinning would scale with the area of the domain, just as the applied shear does. Consequently, the change in the measured threshold shear would not depend on the domain size. In other words, the data in Figure 23 would be shifted up by a constant, and so the slope, and our measurement of Λ would not be affected. The relative smoothness of the domain boundary provides evidence that pinning is not concentrated

at domain edges. This is in contrast to the relatively rough edges of bilayer patches made by rupturing GUVs on a substrate, as in

Figure 17, where pinning causes small-scale features. Finally, the existence of pinning interactions concentrated at domain boundaries would artificially increase our measured coupling constant. Because the value we measure is at the low end of theoretical predictions, even if pinning interactions were important, our results would be inconsistent with many of the predictions of Λ .

Another factor possibly introducing scatter in our data is hydrodynamic interactions between domains. We developed a model for single, isolated domain. However, because each GUV in typically had multiple Lo domains, there were generally several domains within the area formed by one GUV. A domain could experience higher or lower effective interleaflet drag λ_T , as the domains around it change the flow field.

Another complicating factor is the non-circularity of domains. Domains in free floating vesicles are kept circular by a line tension that minimizes interfacial length. During the rupturing process, domains are distorted, and these distortions are prevented from relaxing by interactions with the substrate. As a simple correction for the geometry of domains, we considered the length scale $\sim A/l_{perp}$, which accounts for the fact that the applied shear acts on the area of the domain, whereas the deregistration force scales like the interface projected onto the axis perpendicular to flow. If we instead use a length scale of $\sim \sqrt{A}$, we obtain a result of 0.009 ± 0.005 kT/nm², which is within experimental uncertainty of our reported value. Previous work by Han and Haataja has found that the ability of a domain to change shape has a negligible effect on the registration process (135).

Finally, our results hold only for the system considered. Because biological membranes, contain transmembrane proteins, and we expect them to have a substantially higher effective value of Λ . Also, biological membranes contain many more species of lipids. The heterogeneity in chain length might lead to a higher coupling than in our system.

3.6 Conclusion

We presented results showing that domains deregister under sufficient shear, and that this phenomenon gives a measurement of the interleaflet coupling constant, $\Lambda = 0.007 \pm 0.004$ kT/nm². This number rules out several theoretical models of domain registration. It also limits the parameter space for models of asymmetric bilayers to a relatively weak coupling regime.

Future work using this method could identify the mechanism of interleaflet coupling by varying compositional parameters. As has been previously reported (123), varying the length of one of the acyl chains of the saturated lipid presumably increases interdigitation, and consequently increases interleaflet coupling. Another proposed mechanism for interleaflet coupling is the flip-flop of cholesterol, which occurs much faster than most experimental time scales (143). This mechanism could be tested by replacing cholesterol with a sterol less likely to flip-flip, such as cholPC, where the hydroxyl head group of cholesterol has been replaced with the larger, zwitterionic phosphatidylcholine. A third proposed mechanism is coupling between the spontaneous curvatures of each leaflet. This could be varied by the incorporation of phosphatidylethanolamine, which has a negative spontaneous curvature, and lyso-lipids, which have a positive spontaneous curvature (144).

Chapter IV: Fabricating vesicles by cDICE

4.1 Introduction

Quantitative, well-controlled biophysical studies of lipid membranes rely on creating model vesicles *de novo* with known compositions. Giant unilamellar vesicles (GUVs) that have diameters $> 10\ \mu\text{m}$, are especially powerful model systems because they can be readily imaged by optical microscopy. However, current limitations on fabricating GUVs render important regions of parameter space difficult to achieve.

Two of the conditions that are most difficult to achieve with current techniques include the fabrication of GUVs containing high fractions of charged lipids, and fabrication of GUVs in solvents with high ionic strength. The incorporation of charged lipids is of interest because charged lipids are common in biological membranes. Mammalian red blood cells contain ~25% charged lipids (145), almost all of which are located in the cytoplasmic leaflet of the membrane (64). The physical effect of this charge asymmetry is not known. The use of buffers with high ionic strengths is of interest because ionic solutions are widespread in biology. The ionic strength of blood is approximately 0.2 M (146). Moreover, solutions containing ionic cations are essential for several signaling pathways in cells (147). Divalent cations are particularly challenging to work with in a model membrane system.

There are several accepted methods for fabricating GUVs. The most common is electroformation (87). In the limited case of very low concentrations of charged lipids in the membrane and very low concentrations of ions in solution, electroformation has extraordinary

advantages. Electroformation techniques are easy, inexpensive, and produce a high yield of large, defect free vesicles. It is also inexpensive and easy to implement. Unfortunately, incorporation of charged lipids into electroformed vesicles drastically lowers the yield (95) and relies on the presence of sugars, which may induce artifacts (56). Similarly, ionic strengths greater than ~10 mM are difficult to achieve by electroformation.

Because of these difficulties, many studies with charged lipids use a simpler method to produce vesicles, gentle hydration or gentle swelling (83). However, the yield of GUVs containing charged lipids by gentle hydration is low, and multilamellar defects are common. The incorporation of salt further degrades the sample quality. Finally, gentle hydration works only in the presence of charged lipids. Hence, comparison of vesicles with and without charged lipids is difficult, because both the composition and the method of preparation are different. Microfluidic techniques of producing GUVs complement the electroformation and gentle hydration techniques above (148-151). In general, these techniques make using a micron-scale device, and then coat the droplet with lipids to form a vesicle. Microfluidic techniques give the user a high degree of control, but they rely on specialized equipment and are difficult to replicate from one laboratory to another.

As a potential solution to challenges posed by microfluidic techniques, Abkarian et al. developed a novel method for producing vesicles, depicted schematically in Figure 25 (152). While similar to microfluidic techniques, it relies on glass capillaries that are commonly available for patch clamp experiments. The capillary is inserted into a layer of oil in a spinning, sealed petri dish with an opening in the top. Aqueous droplets that emerge from the capillary are driven through an oil layer (where they acquire a monolayer of lipids), through an oil-water interface (where they acquire a second monolayer of lipids), and into a water layer (where the

resulting vesicles are accumulated). This technique was originally developed as a way to incorporate micron-scale objects inside GUVs. Here we evaluate this method's utility for creating vesicles for biophysical studies. We first ensure that it creates vesicles with known, controllable compositions, the primary requirement of membrane biophysics experiments. We then evaluate the efficacy of the technique for creating vesicles containing large fractions of charged lipids and/or vesicles in buffers with high levels of salt.

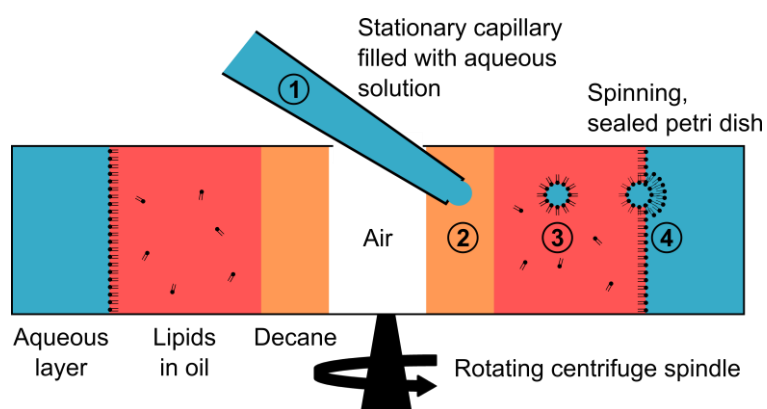


Figure 25 Schematic depiction of the cDICE method for producing vesicles. [1] A glass capillary is inserted into a sealed petri dish that is rotated by a bench top centrifuge. Aqueous solution is pushed through the capillary by a syringe pump or compressed gas. [2] A layer of decane (which is added because of its lower viscosity) flows past the end of the stationary capillary tip. When the aqueous fluid flowed through the capillary forms a droplet of a threshold size (on the order of the capillary inner diameter), the droplet is sheared off. [3] The droplet is forced through the less dense oil by centrifugal force. Lipids dissolved in the oil partition to the interface between the aqueous droplet and the oil. [4] The outer ring of the petri dish contains an aqueous solution, and a monolayer of lipids assembles at the interface between this aqueous solution and the oil. As the droplet reaches the interface, it picks up a second monolayer of lipids.

4.2 Materials and Methods

Materials

1,2-diphytanoyl-*sn*-glycero-3-phosphocholine (DiPhyPC); 1,2-dipalmitoyl-*sn*-glycero-3-phosphocholine (DPPC); 1,2-diphytanoyl-*sn*-glycero-3-phosphoglycerol (DiPhyPG); and 1,2-dipalmitoyl-*sn*-glycero-3-phosphoglycerol (DPPG); were obtained from Avanti Polar Lipids (Alabaster, AL). Cholesterol was obtained from Sigma (St. Louis, MO). All lipids were used without further purification and were stored in chloroform at -20°C until use. Texas Red 1,2-dipalmitoyl-*sn*-glycero-3-phosphoethanolamine (TR-DPPE, Invitrogen, Eugene, OR) was included at 0.8 mol% as a dye for contrast between phases in fluorescence experiments. Phosphate buffered saline (PBS) was obtained from Fisher Scientific (Fair Lawn, NJ). 18 M Ω -cm water was produced by a Barnstead filtration system. All other chemicals were obtained from Sigma (St. Louis, MO).

Preparing a Solution of Lipid in Oil

2 μmole of lipids in chloroform were added to a scintillation vial and dried down under vacuum for at least 30 minutes in a desiccator. The desiccator was opened in a glove box filled with dry nitrogen. 4 mL of heavy mineral oil was added to the scintillation vial, which was then sealed. Lipids were allowed to disperse in the oil for 1 hour and then the solution sonicated for 2 hours.

Preparing vesicles

Vesicles were prepared by the cDICE method, as depicted in Figure 25. A sealed 35 mm petri dish was attached to a centrifuge spindle head rotating at 35 Hz. 1.5 mL of aqueous solution (usually 100 mM glucose), was added to form the outermost layer, then 3.5 mL of 0.5 mM lipids in oil to form an intermediate layer, then 1 mL of decane to form the innermost layer.

These layers remain separate due to their different densities. A silanized capillary with an inner diameter of $\sim 15\ \mu\text{m}$ was connected to a reservoir of aqueous solution (usually 100 mM sucrose). Fluid was driven through the capillary by a syringe pump (Harvard Apparatus, Holliston, MA) at 0.05 mL/min, and the capillary tip was inserted into the decane layer.

Microscopy

Vesicles were examined by fluorescence microscopy as in Veatch et al. (2). Briefly, vesicle solutions were diluted $\sim 5:1$ in an isotonic solution and deposited between two coverslips. The coverslip assembly was sealed with vacuum grease and coupled with thermal paste (Omega Engineering, Stamford, CT) to a stage. Temperature control of the stage was achieved with a Wavelength controller connected to a Peltier device and a thermistor temperature probe with a manufacturer quoted accuracy of 0.02°C (Wavelength Electronics, Bozeman, MT). Epifluorescence microscopy was performed with a 40x objective on a Nikon microscope with either a Coolsnap HQ or QuantEM charge-coupled device camera (Photometrics, Tucson, AZ).

Cholesterol Repletion

Cholesterol repletion by m β CD was performed as in (153). Briefly, 5 mg of cholesterol and 55.6 mg of m β CD were vigorously mixed in a mixture of 1 mL methanol and 0.225 mL chloroform. This mixture was dried under nitrogen and then vacuum for 30 minutes. The resulting crystals were rehydrated at a concentration of 11.2 mg/mL (1 mg/mL of chloroform). The cholesterol repletion solution was titrated into the vesicle solution until liquid-liquid phase separation was observed.

4.3 Results

Phospholipid Composition

Quantitative control of lipid composition within vesicles is essential for their use as model systems. To determine whether the composition of lipids dissolved in oil matched the composition of the vesicles produced by cDICE, we exploited the fact that membrane with binary phospholipid compositions undergo gel-liquid phase transitions at characteristic temperatures. We verified that the transition temperatures of vesicles produced by cDICE are indistinguishable from those produced by electroformation or by gentle hydration. For instance, membranes of 4:1 DiPhyPC:DPPC in both cDICE vesicles and electroformed vesicles exhibited one uniform liquid phase above 20°C and gel-liquid coexistence below 20°C.

This temperature, and the existence of a transition, is sensitive to the presence of oil in the bilayer (150). The agreement in transition temperature between cDICE vesicles and electroformed vesicles suggests that any effect of oil within the bilayer (if any is present) on the membrane physical properties is small.

Cholesterol

Besides phospholipids, sterols are an important component to incorporate in model membranes, both to recapitulate cell membranes (18) and to study their physical effects (9, 10). One unique characteristic of membranes containing phospholipids and cholesterol (or similar sterols) is the ability to phase separate into coexisting liquid phases, as opposed coexisting gel and liquid phases as in mixtures of phospholipids without sterols. To test if the cDICE technique incorporates cholesterol into vesicles, we loaded our cDICE apparatus with an oil layer containing two phospholipids (DOPC and DPPC) and cholesterol. Electroformed vesicles of this

ternary mixture phase separate into gel domains in a liquid background at cholesterol levels less than 10 mol%, and into coexisting liquid phases above 10 mol%. As seen in Figure 26, less than 10 mol% cholesterol incorporates into vesicles produced by cDICE, even when mixed with phospholipids in oil at an initial ratio of 100:1. It is possible that because cholesterol is significantly more hydrophobic than phospholipids, cholesterol does not efficiently partition to the oil-water interface. Another hypothesis is that cholesterol does not dissolve in oil to begin with, possibly because cholesterol crystals are more favorable.

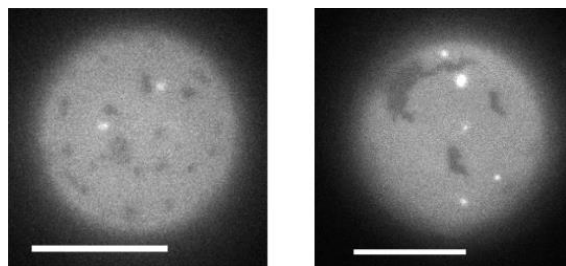


Figure 26 Vesicles made from aqueous droplets traveling through a solution of 1:1:100 DOPC:DPPC:Chol in oil. The presence of solid domains (which have non-circular shapes) implies that cholesterol is present in the membranes at less than 10 mol%. Scale bars correspond to 20 μm .

Previous work (154) has shown that cholesterol partitions to the oil-water interfaces in emulsions. These studies used a silicon oil with a much lower viscosity. When we attempted to form vesicles by cDICE using this oil, no vesicles formed.

One way to overcome this problem is to introduce cholesterol after vesicles have formed using methylated β cyclodextrin (m β CD). We verified that this is compatible with cDICE vesicles by examining their phase behavior. Figure 27 shows a vesicles replenished with cholesterol

using m β CD. The domains merge over time, as is characteristic of liquid-liquid phase coexistence, implying that the cholesterol composition is now at least 10 mol%.

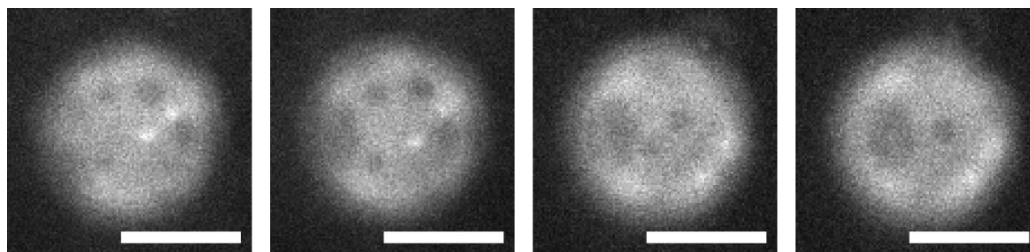


Figure 27 Liquid domains in a cDICE vesicle repleted with cholesterol. Vesicle was initially 1:1 DiPhyPC:DPPC. The collision and merging of domains are indicative of the liquid-liquid phase, as the gel domains are unable to change shape. Micrographs correspond to 5 second intervals. Scale bars correspond to 20 μ m.

Charged lipids

As previously shown, the presence of charged lipids does not inhibit the formation of vesicles (152). Figure 28 shows vesicles containing only charged lipids, 1:1 DiPhyPG:DPPG. This result shows that there is no upper limit on the fraction of charged lipids incorporated into vesicles produced by cDICE.

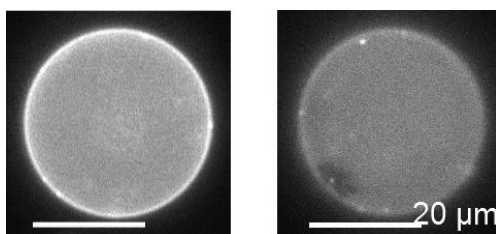


Figure 28 cDICE vesicle composed entirely of charged lipids (50:50 DiPhyPG:DPPG), (left) above the gel-liquid transition temperature and (right) below the transition temperature. Scale bars correspond to 20 μ m.

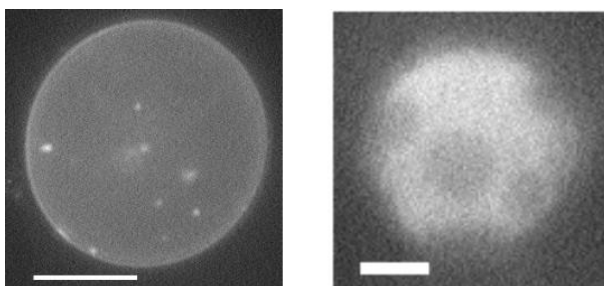


Figure 29 cDICE vesicles of 1:1 DiPhyPG:DPPC in PBS above the transition temperature (left) and below (right). PBS contains 140 mM of monovalent salt, and is often used for biological systems. Vesicles with this density of charged lipid are very challenging to produce in high salt buffers by gentle hydration. Scale bars correspond to 20 μm .

Furthermore, the methods that successfully produce vesicles containing high amounts of charged lipids (gentle hydration, electroformation in the presence of high concentrations of sugar) are not suited to creating vesicles without charged lipids. This introduces systematic error into attempts to determine the effects of charged lipids by comparing neutral systems with charged systems. Using cDICE produces both charged and uncharged vesicles via the same procedure, with qualitatively the same yield.

4.4 Future Challenges

The cDICE method is highly successful for fabricating vesicles containing charged lipids. That success is tempered by the method's inability to incorporate cholesterol into vesicles at significant fractions, which minimizes the technique's applicability to membrane systems that mimic the cell plasma membrane, which contain high fractions of cholesterol. The technique's relatively low overall yield compared to electroformation makes it unlikely to be widely adopted except when charged lipids are required.

One area in which the cDICE technique holds potential for wide use is in the creation of asymmetric vesicles, with different lipid compositions in each leaflet. Current methods for creating asymmetric GUVs involve either microfluidic techniques or exchanging lipids with cyclodextrins, both of which are technically challenging (155). Because cDICE assembles the two leaflets at different places and over different times, it may be possible to exert compositional control over each leaflet independently. One way this could be achieved is depicted in Figure 30. The lipids on the outer leaflet would be dissolved in a different oil than the lipids in the bulk oil, with the two solutions kept separate by a density difference. Because the accumulation of lipids at the oil droplet surface is diffusion limited, it is unlikely that significant lipid exchange would occur with the inner leaflet lipids with the droplet that passes through this thin layer.

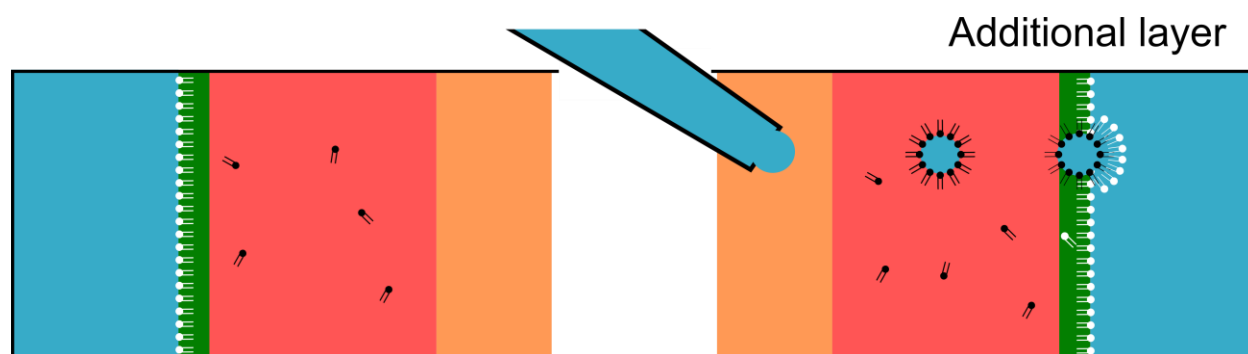


Figure 30 Schematic of proposed production of asymmetric vesicles by cDICE. This figure differs from Figure 25 by the inclusion of an additional oil layer (in green) in which a different composition of lipids is dissolved. The lipids in the first oil layer (shown in black) would form the inner leaflet and the lipids in the second oil layer (shown in white) would form the outer leaflet of vesicles.

Chapter V: Fatty acids and the origin of life

5.1 Introduction

The origin of RNA (157) and how it became associated with amphiphilic membranes in primordial cells is unclear. RNA is a polymer of units containing the sugar ribose covalently bound to one of four nucleobases; amphiphiles are molecules that possess both a hydrophobic and a hydrophilic moiety and can therefore aggregate into membranes in water. We know that two of the four units of RNA can be synthesized under simulated prebiotic conditions (158), that simple amphiphiles such as fatty acids spontaneously aggregate into vesicles in an aqueous environment (159), and that such vesicles can encapsulate nucleic acid and its building blocks (49, 160). Fundamental questions remain, however, regarding how the bases and sugar in RNA were selected from a heterogeneous mixture of prebiotic organic compounds, concentrated sufficiently to react, and co-localized with vesicles. It is also unclear how the first membranes were stabilized in sea water given that fatty acids precipitate at high salt concentrations (46).

Previous lines of research suggest possible answers to these questions. Prebiotic chemical processes could have preferentially generated at least two of the four nucleotides (consisting of a base bound to ribose and phosphate) from simple organic precursors (158). These building blocks, if activated, could then have polymerized on mineral surfaces (161), which also stimulate fatty acid vesicle formation (162). Finally, the incorporation of alcohols and glycerol monoesters in fatty acid membranes could have increased their stability in sea water (49, 163-165).

This chapter is adapted from Black, R. A., M. C. Blosser, B. L. Stottrup, R. Tavakley, D. W. Deamer, and S. L. Keller. 2013. Nucleobases bind to and stabilize aggregates of a prebiotic amphiphile, providing a viable mechanism for the emergence of protocells. *Proc. Natl. Acad. Sci. U. S. A.*, 110:13272-13276. (156)

We hypothesize a simpler, more integrated scenario that complements these mechanisms. In this scenario, aggregates of amphiphiles preceded RNA and facilitated its synthesis by binding and concentrating the bases and sugar of which it is composed. The observation that the assembly of amphiphilic aggregates proceeds spontaneously, whereas the synthesis of RNA requires energy, supports this scenario. Moreover, the planar structure of the bases and the hydrogen-bonding potential of sugars suggest mechanisms by which these compounds could interact with fatty acid aggregates. We further hypothesize a functional consequence of the binding: stabilization of the amphiphilic aggregates in the presence of salt. The mechanisms we hypothesize are mutually reinforcing and under prebiotic conditions could drive the emergence of vesicles enriched in components of RNA.

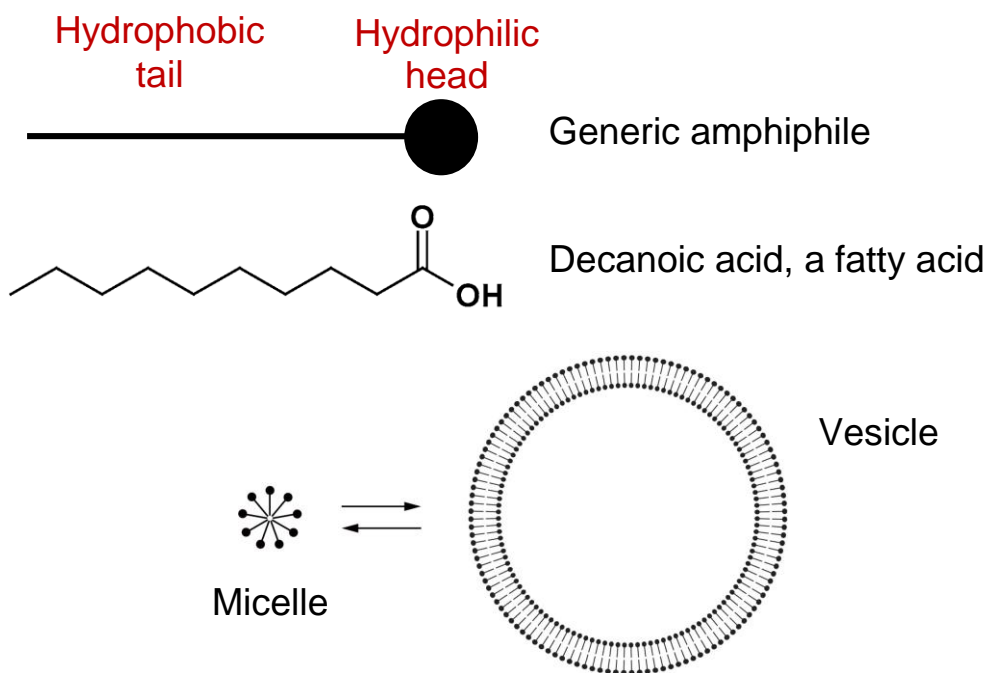


Figure 31 Fatty acids, like other amphiphiles, can form both micelles and vesicles.

The array of bases that we investigated is shown in Figure 37A, including the nucleobases found in RNA: adenine, guanine, cytosine and uracil. We primarily employed decanoic acid (a carboxyl group attached to a chain of nine additional carbons) as our amphiphile because it is synthesized under prebiotic conditions (166) and is long enough to self-assemble into vesicles (167). (We use the term “decanoic acid” to refer to both the protonated and unprotonated forms of the molecule.) Vesicles enclose an aqueous volume, as a cell does, in contrast to smaller aggregates like micelles that have no aqueous core (Figure 31). Above pH 8, decanoic acid forms only micelles. Vesicles typically start to form as the proton concentration becomes sufficient, below pH 8, to bridge carboxyl groups by hydrogen bonding, thereby reducing surface charge (167).

Due to the sensitivity of decanoic acid aggregates to pH, this parameter must be tightly controlled, as we describe below.

5.2 Results:

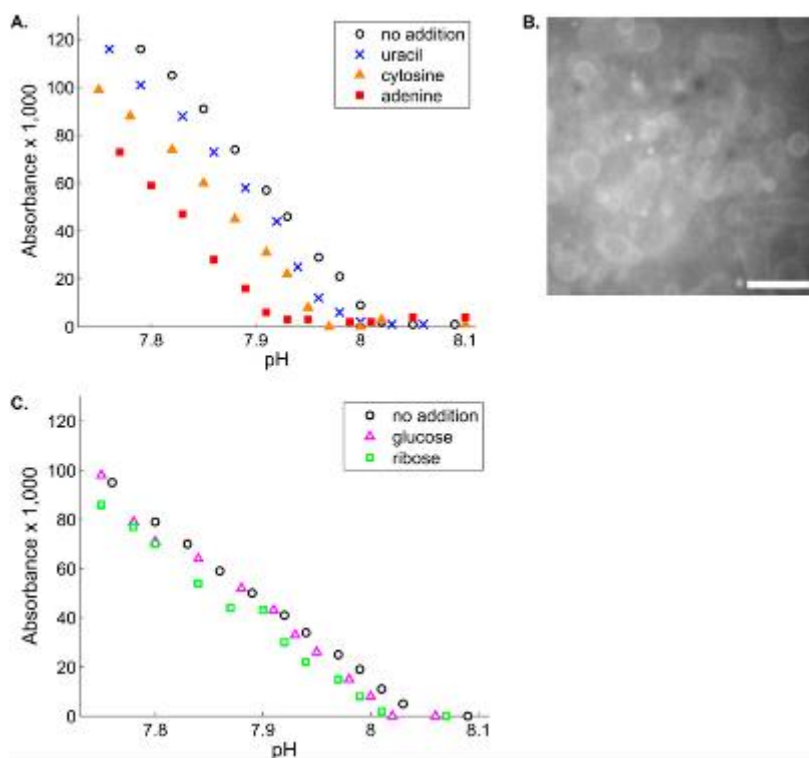


Figure 32 Nucleobases and ribose lower the pH at which vesicles form in decanoic acid solutions when the pH is decreased by titrating with HCl. (A) Nucleobases at 30 mM lower the pH below which 80 mM decanoic acid/100 mM NaCl forms vesicles. The density of vesicles is related to the turbidity of the solution (the absorbance at 490 nm). Results shown are representative of 10 experiments with adenine and 4 with cytosine and uracil. (B) Epifluorescence microscopy shows that the turbidity corresponds with the presence of vesicles. Here, a solution of 80 mM decanoic acid/100 mM NaCl was titrated with HCl to pH 7.8, and 10 μ M rhodamine 6G was added for imaging. Scale bar, 10 μ m. (C) Ribose at 120 mM lowers the pH required for 80 mM decanoic acid/100 mM NaCl to form vesicles, whereas glucose has minimal effect. Results shown are representative of four experiments with ribose and three with glucose.

In a series of preliminary experiments, we found that nucleobases and ribose interact with decanoic acid strongly enough to alter the pH at which vesicles form within a solution of micelles (results summarized in Table 3). Figure 32 shows the effect of adding nucleobases and sugar on the pH at which decanoic acid solutions form vesicles. Figure 33 through Figure 36 show that nucleobases and sugars decrease vesicle formation when pH is lowered by heating decanoic acid solutions containing bicine. To verify and quantify these results, we established an alternate procedure for changing solution pH based on the temperature-dependence of the pK_a of bicine. Heating a solution of 80 mM decanoic acid/100 mM bicine/pH 7.9 from room temperature (24 °C) to 60 °C causes a drop in pH to ~7.6. Among the nucleobases tested, the magnitude of the pH shift was in the order of adenine > cytosine > uracil. (Guanine was not sufficiently soluble to test.) Between the sugars, ribose had a greater effect than glucose. The differences in the magnitudes of these effects suggest that they are due to direct interaction of the compounds with the decanoic acid aggregates, rather than to a change in nonspecific parameters of the solution such as ionic strength or viscosity.

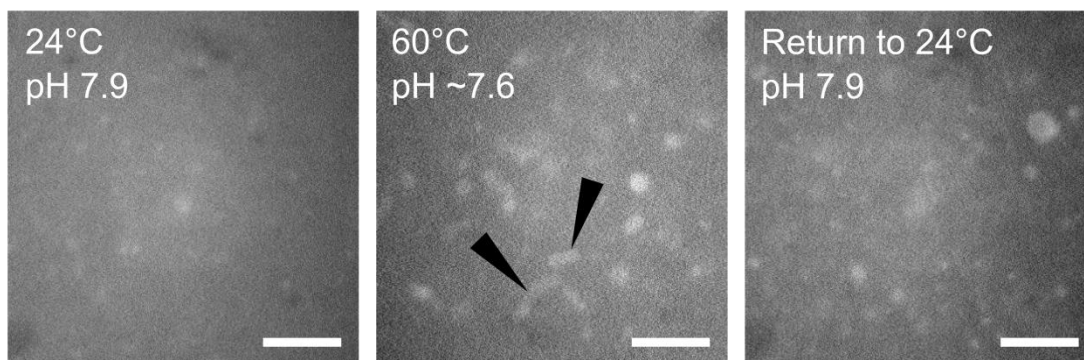


Figure 33 Vesicles form when pH is decreased by heating a decanoic acid solution containing bicine to 60 °C. A solution of 80 mM decanoic acid/100 mM bicine/10 μ M rhodamine 6G was imaged by epifluorescence microscopy as it was cycled from room temperature (24 °C) at pH

7.9, to 60 °C at pH ~7.6, and back again. Arrows indicate the appearance of tubular vesicles, which disappeared rapidly upon the return to 24 °C. Scale bar, 10 μ m.

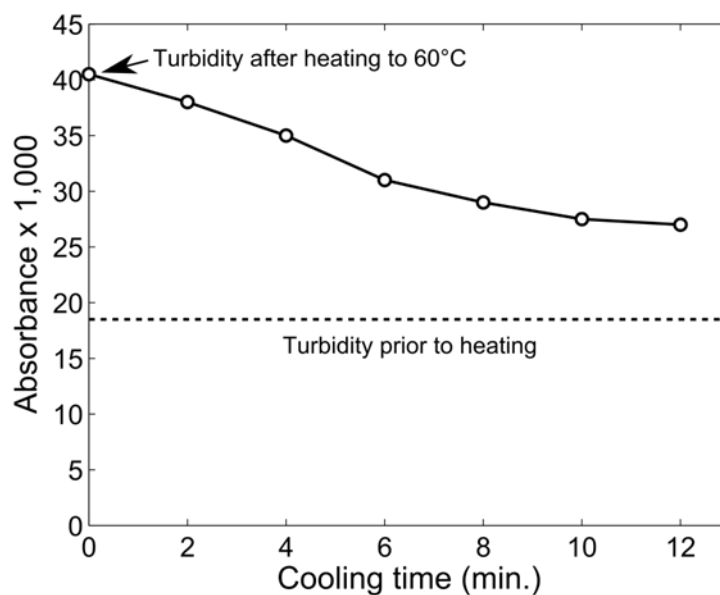


Figure 34 Quantification of the heating-induced increase in vesicle density and subsequent decrease upon cooling. The dotted line shows the absorbance at 490 nm of 80 mM decanoic acid/100 mM bicine/pH 7.9 in a 96-well plate at room temperature (corresponding to first panel in Figure 33). The plate was re-read after heating to 60 °C (0 time, corresponding to the middle panel) and at various times thereafter as the plate cooled (and pH rose). Values are the average of duplicate wells, and average deviations are smaller than the symbols. No increase in absorbance occurs upon heating if bicine is omitted from the solution.

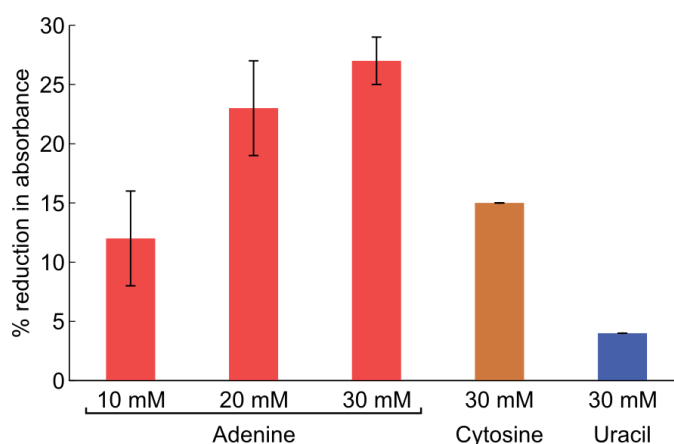


Figure 35 Addition of nucleobases to a solution of 80 mM decanoic acid/100 mM bicine/pH 7.9 decreases the temperature-induced rise in solution absorbance at 490 nm. Values are the average of duplicate wells, and error bars indicate average deviations. % reduction in absorbance is the percentage of the control value (with no base added) by which the base decreased the temperature-induced rise in absorbance.

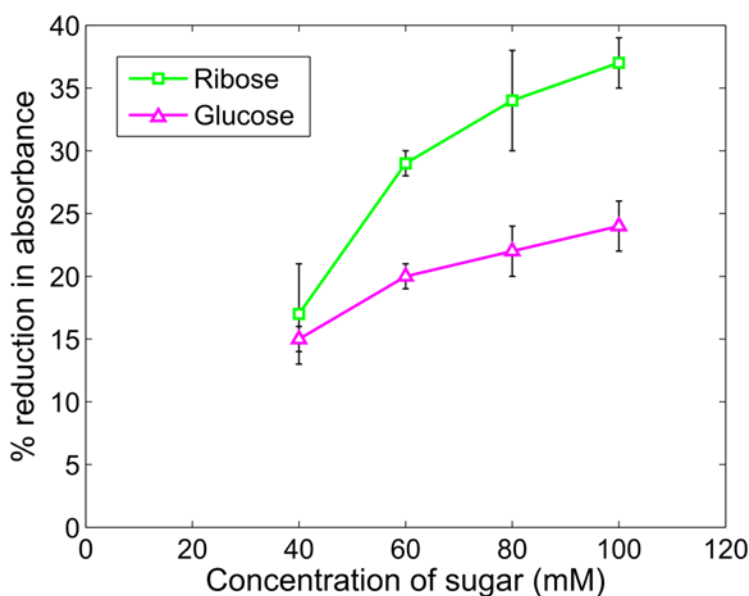


Figure 36 Addition of ribose and glucose to a solution of 80 mM decanoic acid/100 mM bicine/pH 7.9 decreases the temperature-induced rise in solution absorbance at 490 nm. Values are the average of duplicate wells, and error bars indicate average deviations.

Binding of nucleobases to aggregates of fatty acids.

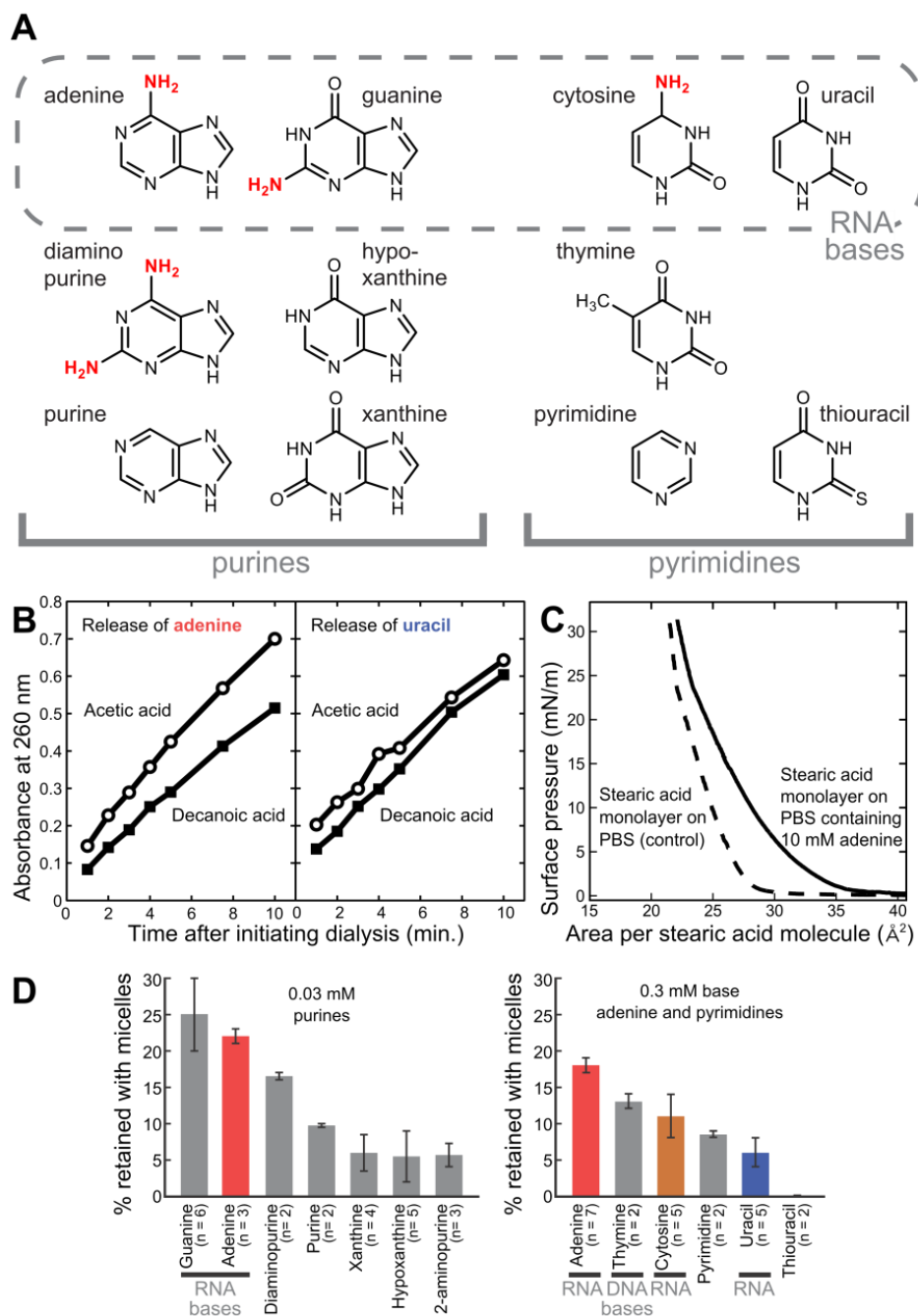


Figure 37 Decanoic acid aggregates selectively bind heterocyclic nitrogenous bases.

(A) Structures of purines and pyrimidines tested for interactions with decanoic acid aggregates.

Diaminopurine contains an amine at the 2-position in addition to the 6-position as in adenine; 2-

aminopurine, not shown, has an amine only at the 2-position. Amine substituents are indicated in red.

(B) Adenine dialyzes more slowly from a decanoic acid solution than from an acetic acid solution. The left panel shows results of a representative experiment in which adenine, at 15 mM, diffused from either 180 mM decanoic acid or from 180 mM acetic acid. Aliquots of dialysis buffer were collected at indicated times and assayed for adenine by measuring absorbance at 260 nm. The rate of release was $24 \pm 5\%$ lower from decanoic acid ($p < 0.05$). The right panel shows results of a corresponding representative control experiment with uracil in place of adenine. The rate of release was $8 \pm 7\%$ greater, not lower, from decanoic acid ($p > 0.05$).

(C) The presence of 10 mM adenine in a subphase of phosphate-buffered saline (PBS) increases the surface pressure of a Langmuir monolayer of stearic acid. Measurement uncertainty is ± 1 mN/m. Stearic acid (18 carbons) was used instead of decanoic acid because the latter does not form a stable Langmuir monolayer.

(D) Nucleobases are retained with decanoic acid micelles during ultrafiltration. A solution of 180 mM decanoic acid and each base at 0.03 mM (for purines) or 0.3 mM (for pyrimidines) was partially centrifuged through a 3 kD-cut-off filter. These concentrations optimize both the percentage of base retained by micelles and the detection of base by absorbance; adenine was evaluated at both 0.3 and 0.03 mM to enable comparison of all the bases. Values are averages, and error bars represent average deviations. (The difference between the means for cytosine and uracil is significant based on Student's t-test: $p=0.028$ by a one-tailed test and 0.056 by a two-tailed test.)

To confirm direct interaction between the bases and the aggregates, as well as to better quantify the strength of interaction, we employed three independent assays for binding. In these experiments, we focused on fatty acid micelles and monolayers rather than vesicles in order to differentiate between adsorption and encapsulation.

| <u>Test for interaction</u> | <u>Bases</u> | <u>Sugars</u> |
|------------------------------------|---------------------------------|---------------------------------|
| Altered pH of vesicle transition | A > C > U (Figure 32-Figure 36) | rib > glu (Figure 32-Figure 36) |
| Retention during dialysis | A > U (Figure 37B) | |
| Retention during ultrafiltration | A ~ G > C > U (Figure 37D) | |
| Reduction in flocculation | A > C > U (Figure 41C) | rib > glu (Figure 41E) |

Table 3 The rank order of effects of nucleobases and sugars is consistent across several tests for interaction with decanoic acid aggregates. The tests are described in the text and figure legends.

First, we determined that adenine dialyzes more slowly from decanoic than from acetic acid ($21 \pm 7\%$ slower averaged over 6 experiments, $p \sim 0.003$; Figure 37B). This result suggests that adenine binds to micelles, because acetic acid has the same hydrophilic moiety as decanoic acid but a hydrophobic tail too short (one carbon) to support micelle formation. To conduct controls, we tested two compounds, uracil and thiouracil, that show weak or no interaction with decanoic acid aggregates by other measures (Figure 32-Figure 36, Figure 37D). We found that the rates of uracil dialysis from decanoic and acetic acids are indistinguishable within experimental uncertainty ($3 \pm 10\%$ faster, not slower, from decanoic acid, $n=2$, $p > 0.05$; Figure 37B), and the difference in rates of thiouracil dialysis is also insignificant ($6 \pm 4\%$ faster, not

slower, from decanoic acid, $n=2$, $p > 0.05$). These results suggest that the slower dialysis of adenine from decanoic versus acetic acid is due to its binding to micelles rather than to a nonspecific property of the solution, such as viscosity.

In a second test for interaction between adenine and long-chain fatty acids, we found that the base interacts with a fatty-acid monolayer in a Langmuir trough. In these experiments, a fatty acid is dispersed over the surface of an aqueous solution, altering the surface tension at the air-solution interface. The change in surface tension is expressed as surface pressure, defined for Langmuir monolayers as the surface tension of pure water minus the surface tension of the system under study. Decreasing the surface area, by moving a barrier, concentrates the fatty acid molecules and increases the surface pressure. We found that the presence of adenine in solution below a stearic acid monolayer increases the surface pressure observed at a given surface area (Figure 37C). This result suggests that adenine adsorbs to or inserts in the monolayer of fatty acid molecules. In the absence of a stearic acid monolayer, surface pressures of an adenine solution and of a buffer-only solution are indistinguishable, indicating that adenine alone does not partition to the air-solution interface enough to measurably affect surface pressure.

We employed ultrafiltration as our third binding assay. Samples were centrifuged through a 3 kD-cut-off filter, which retains decanoic acid micelles and, presumably, any bases associated with them. We found that RNA bases are retained with decanoic acid micelles, and the extent of their retention differs, with adenine \approx guanine $>$ cytosine $>$ uracil (Figure 37D, Table 3). Moreover, adenine and guanine are retained to a greater extent than all five other purines tested, and the three pyrimidines in RNA or DNA are retained to a greater extent than thiouracil (Figure 37D).

We conclude from these three diverse binding assays that (a) nucleobases bind to fatty acid aggregates, (b) the strength of nucleobase binding to fatty acid aggregates correlates well with the magnitude of the pH shifts that they induce in micelle-vesicle transitions (Table 3), and (c) structurally related bases exhibit substantial variation in binding.

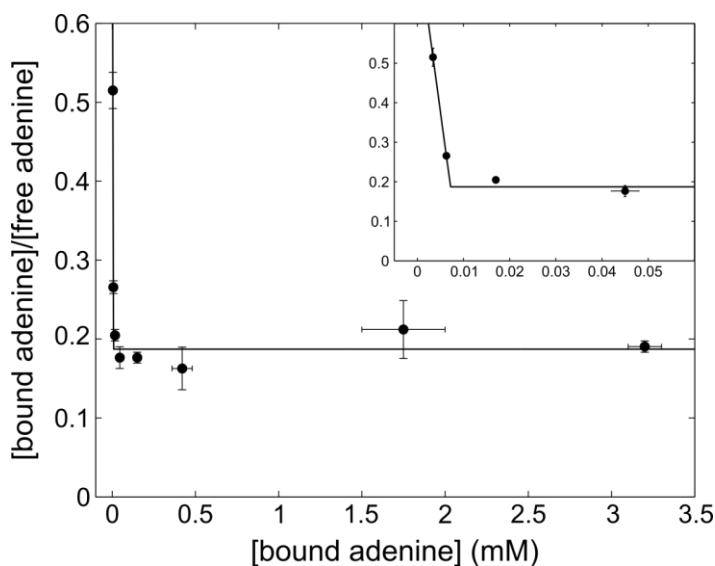


Figure 38 Scatchard analysis of adenine binding to decanoic acid micelles. Binding was measured with the filtration assay described in Methods. We confirmed that the binding is dependent on the presence of micelles across the entire range of adenine concentrations tested: no significant binding was observed when we used decanoic acid at 20 mM, below the critical micelle concentration, instead of 180 mM decanoic acid.

We quantitatively assessed the affinity of adenine binding to decanoic acid micelles by repeating the filtration assay over a range of adenine concentrations, 0.01-3 mM. Scatchard analysis of the results suggests two modes of binding, one with a K_d of about 11 μ M and one, with much lower affinity, that is not saturated at the highest adenine concentration tested (Figure 38). In contrast, 2-aminopurine appears to lack a high affinity binding mode; whereas the

percentage of adenine retained with micelles increases from $18 \pm 1\%$ at 0.3 mM to $22 \pm 1\%$ at 0.03 mM (Figure 37D), retention of 2-aminopurine declines over this concentration range from $9.3 \pm 0.8\%$ (n=3) to $5.7 \pm 1.6\%$ (n=3). The relatively low absorbance of 2-aminopurine and the other purines besides adenine precluded testing them at the low concentrations required to further evaluate for high affinity binding.

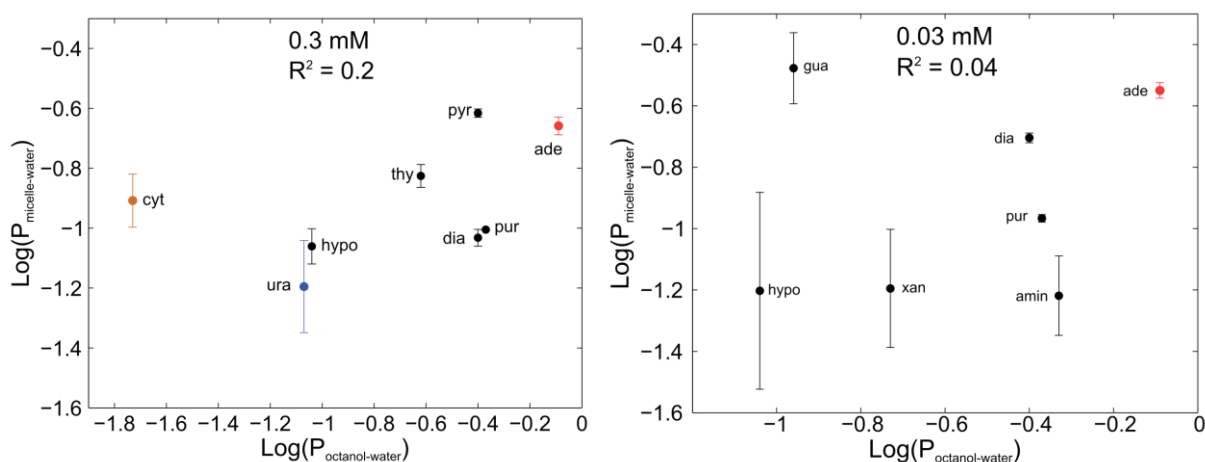


Figure 39 Binding of bases to micelles does not correlate with their hydrophobicity. Binding is expressed as a partitioning between micelles and water; we define $P_{\text{micelle-water}}$ as the ratio of the base associated with micelles to the base that is not. Values are from Fig. 1D. Hydrophobicity is measured by the partitioning between octanol and water; $P_{\text{octanol-water}}$ is defined as $[\text{base in octanol}]/[\text{base in water}]$. Most of the values for octanol-water partitioning are the recommended values from Sangster (<http://logkow.cisti.nrc.ca/logkow/index.jsp>). For diaminopurine and aminopurine, no literature values exist to the best of our knowledge, and we predicted those in the graph, employing Virtual Computational Chemistry Laboratory, <http://www.vcclab.org>, 2005.

We found that the mechanism by which bases bind to decanoic acid micelles is not simply related to hydrophobicity. Including 0.4 M NaCl in the filtration assay with 0.03 mM adenine increased the amount of the base retained with micelles, by $68 \pm 2\%$ (average of duplicates), suggesting that a hydrophobic interaction is involved. However, we found no strong correlation between extent of binding and the hydrophobicity of the bases, as measured by their partitioning into octanol versus water ($R^2 = 0.2$ and 0.04 for binding measured at 0.3 and 0.03 mM respectively) (Figure 39).

Inhibition of decanoic acid flocculation by nucleobases and ribose.

Having established the plausibility of a scenario in which aggregates of amphiphiles could have facilitated RNA synthesis by binding its components, we next tested the functional element of our hypothesis, that these components could have stabilized the aggregates against precipitation by salt. Salt concentrations in ancient oceans were likely at least as high as in modern oceans (168), and decanoic acid flocculates in the presence of even modest concentrations of NaCl (Figure 41A) (a phenomenon previously reported as precipitation (46)). We began our investigation with adenine because it exhibits strong interaction with fatty acid aggregates in all our assays (Table 3).

We found that adenine inhibits salt-induced decanoic acid flocculation, thereby preserving vesicles. Salt-induced flocs in a decanoic acid solution dissolve upon heating, and in the absence of adenine they begin to re-form as the temperature falls to about $32\text{ }^{\circ}\text{C}$ (Figure 41A). With the inclusion of adenine, however, the solution remains relatively clear at this temperature, and epifluorescence microscopy shows that instead of flocs, vesicles as large as $\sim 10\text{ }\mu\text{m}$ form (Figure 41A). Moreover, we found that in addition to inhibiting re-flocculation upon cooling, adenine at $32\text{ }^{\circ}\text{C}$ substantially eliminates pre-existing flocs (Figure 41B). Adenine's

inhibition of flocculation persists to temperatures as low as 30 °C; at room temperature the base has no apparent effect (Figure 41A). Stabilization of vesicles could account for this shift in equilibrium between decanoic acid vesicles and flocs; this explanation is consistent with our finding (in the absence of salt) that vesicles extruded to about 100 nm in diameter grow faster in the presence of adenine than in the presence of the nonbinding base thiouracil (Figure 40).

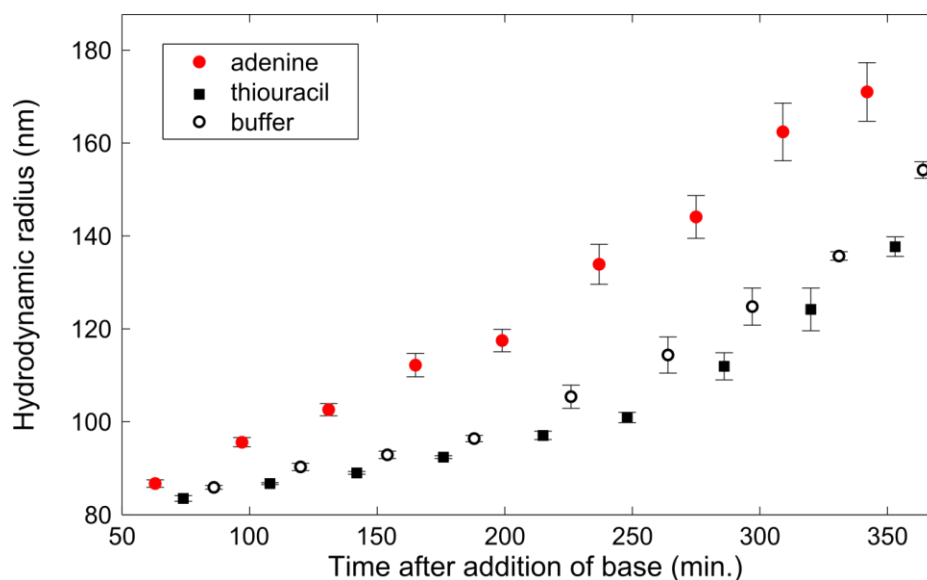


Figure 40 Vesicles grow faster in the presence of adenine. First, vesicles were extruded through 100 nm filters; then buffer, adenine or thiouracil was added (to 10 mM for the bases), and size was measured periodically by dynamic light scattering. Error bars represent the standard error of the 5 runs at each time point. (The plot is representative of three experiments). See Methods for details.

To determine the concentration dependence and specificity of adenine's effect on flocculation temperature, we established the following high-throughput assay using a 96-well plate: Decanoic acid solutions are flocculated by the addition of salt and then heated to 60 °C, which dissolves the flocs and renders the solutions virtually clear. Solution turbidity is then

measured as the solutions cool and flocs re-form. At 32 °C and below, the turbidity of decanoic acid solutions containing 300 mM NaCl is due primarily to flocs (Figure 41A), so turbidity can be used as a measure of flocculation.

We found that as little as 2.5 mM adenine inhibits NaCl-induced flocculation (Figure 41C). The other nucleobases tested also inhibit flocculation, in the order adenine>cytosine>uracil (Figure 41C, inset). This is the same order seen in the extent of their binding to fatty acid aggregates (Figure 37D, Table 3), suggesting that the inhibition of flocculation is related to binding as we hypothesized. Moreover, the correlation between inhibition of flocculation and binding is generalizable to a large group of bases (Figure 41D).

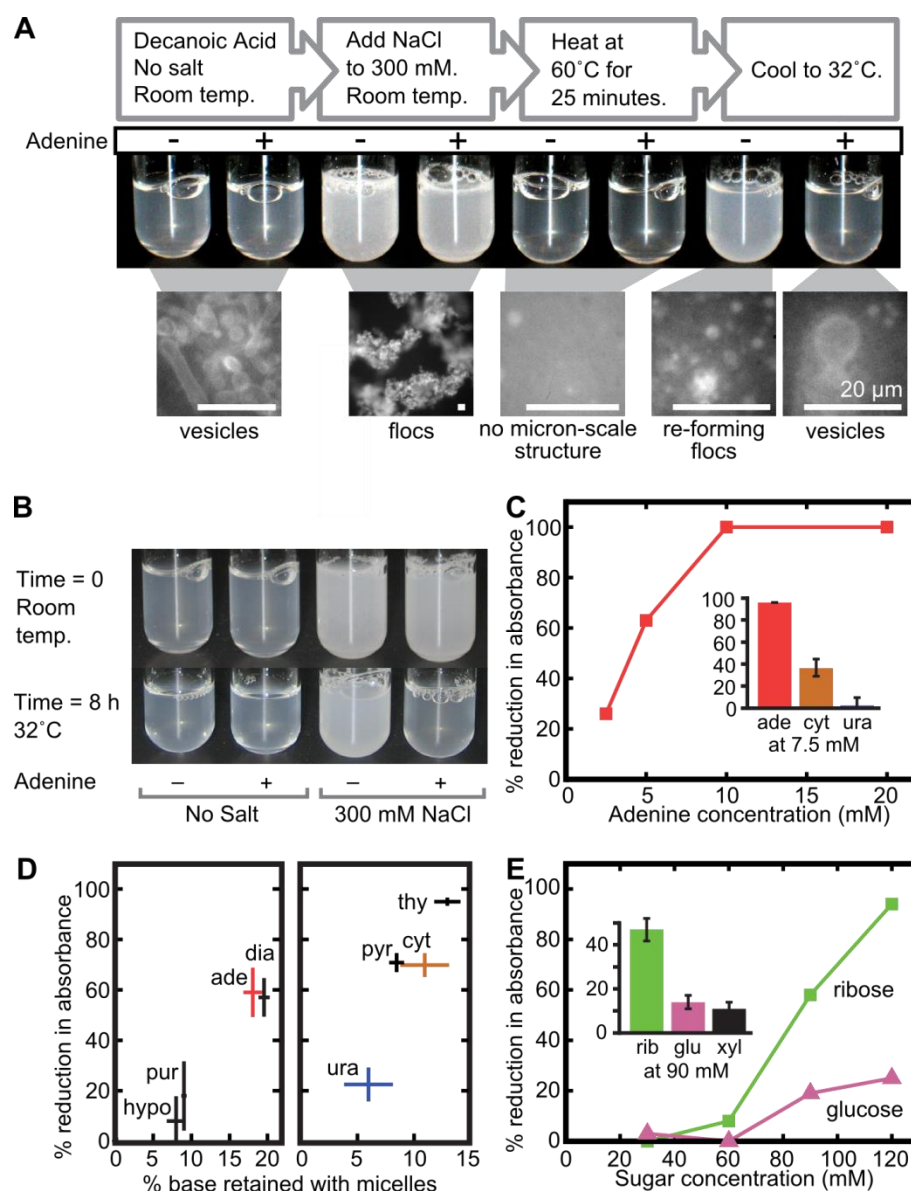


Figure 41 Nucleobases and sugars inhibit flocculation of decanoic acid induced by salt.

(A) Adenine reduces re-flocculation of decanoic acid, and enables vesicle formation, after dissolution of flocs by heat. Test-tube solutions of 80 mM decanoic acid/pH 7.65, without and with 30 mM adenine, were treated as indicated. Corresponding samples for microscopy contained 10 μ M rhodamine 6G as a dye and were heated and cooled to the indicated temperatures on the microscope stage. Scale bars are 20 μ m.

(B) Incubation with adenine at 32 °C reduces pre-existing flocs. 80 mM decanoic acid/pH 7.6, with and without 25 mM adenine and 300 mM NaCl as indicated, is shown before and after incubation at 32 °C for 8 h. (The larger volume used for the pre-incubation set was arbitrarily chosen.) To quantitate the effect, aliquots were incubated in a 96-well plate in parallel, and turbidity was measured after 8 h; the presence of adenine reduced absorbance at 490 nm by $74 \pm 1\%$ (average of duplicates).

(C) Nucleobases inhibit salt-induced flocculation of decanoic acid. The main panel shows the percent reduction in absorbance of a solution of 80 mM decanoic acid/300 mM NaCl (compared to controls with no base added) vs. concentration of adenine, in the plate-based assay for flocculation described in the text; results are representative of three experiments. Inset shows percent reduction in absorbance of a solution of 80 mM decanoic acid/300 mM NaCl containing 7.5 mM adenine, cytosine or uracil (compared to controls with no base added); error bars represent average deviations of duplicate samples.

(D) The inhibition of salt-induced flocculation of decanoic acid by nitrogenous bases correlates with their binding to decanoic acid micelles. The purines (left panel) were tested in the plate-based assay for flocculation at 2.5 mM, and the pyrimidines (right panel) were tested at 10 mM; samples were run in duplicate, and error bars represent average deviations.

Several sugars, too, inhibit flocculation of decanoic acid due to NaCl, and ribose does so more effectively than glucose or xylose (Figure 41E). This order is noteworthy for three reasons. (a) Ribose is the sugar found in RNA and DNA. (b) For sugars, as with bases, the extent of inhibition of flocculation correlates with the shift they cause in pH dependence of vesicle formation (Table 3). (c) Diastereomers are not equally effective, since xylose is less inhibitory than ribose. Ribose is indistinguishable from arabinose in the flocculation assay, and xylose is indistinguishable from lyxose (Table 4). The downward orientation of the C3 hydroxyl group (in standard projections) common to ring structures of ribose and arabinose but not present in xylose or lyxose could cause the difference in efficacy, if hydroxyl groups of sugars are involved in the binding to fatty acid aggregates.

| <u>Sugar</u> | <u>% reduction in absorbance</u> | <u>Number of experiments</u> |
|---------------------|---|-------------------------------------|
| Ribose | 70 \pm 14 | 9 |
| Arabinose | 72 \pm 21 | 9 |
| Xylose | 26 \pm 6 | 5 |
| Lyxose | 32 \pm 5 | 5 |

Table 4 Inhibition of salt-induced flocculation: arabinose is indistinguishable from ribose, and lyxose is indistinguishable from xylose. The flocculation assay was carried out as described in Methods, with all sugars at 90 mM. Ribose and arabinose were assayed side-by-side in the 9 experiments reported, and xylose and lyxose were assayed side-by-side in the 5 experiments reported. The values are means \pm standard deviation.

Finally, we found that the inhibitory effects of adenine and ribose on salt-induced flocculation are approximately additive, at least when adenine alone inhibits by less than 50% and ribose alone inhibits by over 50% (n=5). In one such experiment, for example, 3 mM adenine alone inhibited by $26 \pm 11\%$, 90 mM ribose alone inhibited by $64 \pm 5\%$, and the combination inhibited by $86 \pm 2\%$ (uncertainties expressed as average deviation of duplicate samples). The additivity of the adenine and ribose effects suggests that the two compounds can bind to decanoic acid aggregates simultaneously.

5.3 Discussion

Taken together, our observations support a scenario in which the bases and sugar required for RNA were selected and concentrated by binding to aggregates of prebiotic amphiphiles. Further, the resulting stabilization of the aggregates against salt could have created a positive feedback loop in which vesicles that bound bases and sugar resisted flocculation, thereby preserving more surface area to bind additional bases and sugar, further enhancing stability.

The prebiotic presence of these components at significant concentrations is plausible. Long-chain fatty acids are found in meteorites (169) and can be formed by natural processes on earth (170, 171). Nucleobases have also been found in meteorites (172) and are produced by plausible earth-based prebiotic reactions (173). Recent work describes how ribose could have been generated prebiotically (174, 175). Under prebiotic conditions, organic matter could have been relatively long-lived, and processes such as adsorption could have concentrated these components (176). We suggest that the binding of bases and sugars to amphiphilic aggregates was one of these processes. Since we have shown that multiple compounds bind to these aggregates and that their stabilizing effects are additive, bases and sugars need not have reached concentrations at which they alone would have stabilized vesicles.

Mechanisms by which bases and sugars bind to fatty acid aggregates could involve several variables including planarity, hydrophobicity, and hydrogen bonding. All the bases are planar, and planarity may facilitate insertion in a lipid membrane. The increase in adenine binding in the presence of 0.4 M salt suggests that charge is not a major factor and implicates hydrophobic interactions, despite the lack of a simple correlation between binding and hydrophobicity (Figure 39). Amines on the bases could hydrogen bond with the carboxyl groups of fatty acids, and most of the bases that are retained at higher fractions with micelles have amine

groups. Sugars may interact with a fatty acid aggregate through hydrogen bonding between the carboxyl groups and hydroxyl groups of the sugar, as has been suggested for the hydroxyl groups in glycerol monoesters (165). The unique configuration of hydroxyl groups in ribose has been noted previously to explain its exceptionally rapid permeation of protocells (45, 177).

Following the co-localization of the nucleobases and ribose, the next logical step in the emergence of life is the formation of the glycosidic bond, which may be facilitated by orientation of the base and sugar on amphiphilic aggregates.

5.4 Materials and Methods:

Materials

Flat bottom, nonsterile, clear polystyrene 96-well plates were from Thermo Fisher Scientific (Waltham, MA). Decanoic acid was from Fluka/Sigma (St. Louis, MO), glucose from Thermo Fisher Scientific (Waltham, MA), xylose from Calbiochem/EMD Millipore (Billerica, MA), PBS from Mediatech, Inc. (Manassas, VA), and hypoxanthine from Acros Organics (Geel, Belgium). All other chemicals were from Sigma. All solutions were prepared in 18 M Ω -cm water.

Decanoic acid solutions

Decanoic acid was dissolved, with heating, in 190 mM NaOH, to yield a 180 mM solution. This stock was then diluted to obtain 80 mM decanoic acid with or without 100 mM bicine (diluted from a 1 M stock solution) or 100-300 mM NaCl (diluted from a 4 M stock solution). The pH was adjusted by adding HCl, typically from 0.5 or 1 M solutions.

Imaging vesicles

All samples contained 10 μ M Rhodamine 6G and were placed between two coverslips sealed with vacuum grease. In experiments involving temperature changes, the bottom coverslip was coupled with thermal paste (Omega Engineering, Stamford, CT) to the microscope stage. Temperature control of the stage was achieved with a Wavelength controller connected to a Peltier device and a thermistor temperature probe with a manufacturer-quoted accuracy of 0.02°C (Wavelength Electronics, Bozeman, MT). Epifluorescence microscopy was performed with a 60x or 10x air objective on a Nikon Y-FL microscope (Nikon, Melville, NY) with a Coolsnap HQ charge-coupled device camera (Photometrics, Tucson, AZ).

Dialysis

Adenine, uracil or thiouracil was dissolved to 15 mM in solutions of either 180 mM decanoic acid/190 mM NaOH or 180 mM acetic acid/190 mM NaOH. Solutions were brought to the same temperature and then titrated with HCl to the same pH, typically about 7.8. 0.4 ml of each titrated solution was placed in a Slide-A-Lyzer with a cut-off of 3.5 kD (Pierce/Thermo Fisher Scientific, Rockford, IL). Two solutions were dialyzed side-by-side in beakers containing 200 ml of a 180 mM acetic acid/190 mM NaOH solution adjusted to pH 7.8. Samples of 200 μ l were withdrawn from the dialysis buffer at intervals of 1 or 2.5 minutes, dried down with a centrifugal vacuum evaporator (SPD121P Speedvac, Thermo Fisher Scientific, Pittsburg, PA), and resuspended in 30 μ l water. The absorbance of each sample at 260 nm was measured with a NanoDrop1000 spectrophotometer (Thermo Fisher Scientific, Wilmington, DE).

Absorbance data were fit to a linear function, with best fit slopes and associated fit uncertainties determined using MATLAB software (Mathworks, Natick, MA). Uncertainties stated for individual experiments (*i.e.*, the two discrete experiments shown in Fig. 1B) reflect only the uncertainty in the fit. We set the criterion that differences in slopes are significant only if they are greater than zero with a probability of $p < 0.05$ (equivalent to a difference in slope at least twice as large as the experimental uncertainty). For example, it is significant that the rate of release of adenine was $24 \pm 5\%$ lower from decanoic acid than from acetic acid since $24/5 \sim 5$, *i.e.* a 5-sigma change. Similarly, it is insignificant that the rate of release of uracil was $8 \pm 7\%$ greater from decanoic acid than from acetic acid since $8/7 \sim 1$. Uncertainties quoted in the main text for the mean difference between the rates of release from decanoic versus acetic acids, over several experiments, account for both uncertainty in fit and variation among replicates.

Langmuir trough studies

In Langmuir monolayer studies, the surface pressure is determined by using a balance to measure forces on a plate of filter paper or platinum partially immersed in the subphase. The force on the plate results from three components: buoyant force of water, force of gravity, and surface tension of water. The only one of these terms that changes during our experiments is the surface tension. Our studies were performed as in (178) using a Nima trough (Coventry, England) with a subphase temperature of 22 °C. The subphase contained either 10 mM or no (control) adenine in phosphate-buffered saline, which was prepared from a 10x stock solution; the inclusion of adenine did not detectably change the pH. Stearic acid in chloroform was deposited at the air-water interface using a Hamilton syringe. Ample time (10 minutes) was allowed for chloroform to evaporate before data were taken.

Filtration assay

Bases were dissolved in 180 mM decanoic acid/pH 8.25; at the concentrations employed, ≤ 0.3 mM, the bases did not detectably alter pH. Solutions of guanine and xanthine, which have low solubility, were centrifuged at 3000 x g for 10 minutes in conical-bottomed tubes and the supernates were used for the assay. All base solutions were then treated equally. Typically, 2 ml were placed in an Amicon Ultra-4 3 K filter (Millipore, Billerica, MA) and centrifuged at 3000 x g for 10 minutes in a Sorvall Legend RT swinging-bucket centrifuge (Thermo Fisher Scientific, Waltham, MA). Aliquots of the starting solution (taken prior to centrifugation), the retentate (after gentle agitation to dislodge aggregates on surfaces), and the filtrate were then measured for absorbance at 280 nm for 2,6-diaminopurine, 300 nm for 2-aminopurine, 250 nm for hypoxanthine, 242 nm for pyrimidine, or 260 nm in all other cases. To confirm that decanoic acid micelles are retained in the retentate, we used a pinacyanol chloride assay for aggregated

lipids (13); we found that the retentate contained over 10-fold more aggregated decanoic acid than the filtrate.

The decrease in concentration of base in the filtrate relative to the starting material was used as the measure of base retained with the micelles. This decrease was generally of the same magnitude as the increase in base concentration in the retentate, and was more reproducible. This agreement provides evidence against nonspecific loss of base on the surfaces of the centrifuge tube and filter. Further evidence against nonspecific loss came from control experiments in which bases were dissolved in a 20 mM decanoic acid solution, which is below the critical micelle concentration. The amount of base retained in these experiments was generally only 0-2% of the starting concentration, as expected if retention of base in the experiments with 180 mM decanoic acid is primarily due to binding to micelles.

NaCl-induced flocculation in test tubes

NaCl was added to 80 mM decanoic acid/pH 7.60-7.65 solutions to a final concentration of 300 mM by diluting from a 4 M stock solution, and solutions were briefly vortexed immediately after the addition. Including 30 mM adenine in the solutions only slightly altered pH, lowering it about 0.03 units, and adenine inhibited flocculation equally well when bicine was included to eliminate pH changes. A Canon PowerShot SD600 camera was used to take photos of samples within test tubes in a rack on a black mat. In the case of samples above room temperature, photos were taken promptly upon removal from the indicated temperature.

NaCl-induced flocculation in 96-well plates

Bases and sugars were dissolved in an 80 mM decanoic acid/100 mM bicine/pH 7.9 solution. Inclusion of bicine ensured that effects of bases or sugars on flocculation were not due to changes in pH. Typically, 19 μ l of 4 M NaCl was added to 231 μ l of the test solutions, and

each sample was immediately vortexed. After 5 minutes, samples were vortexed again and 100 μ l aliquots were placed in a 96-well plate. Bubbles introduced due to pipetting were eliminated by lancing with a hypodermic needle. The plate was wrapped in Saranwrap and placed in a 60 °C incubator for 17 min. The plate was then read in a SpectraMax M5 plate-reader (Molecular Devices, Sunnyvale, CA) at 490 nm. On the initial reading, samples showed virtually no absorbance above background (the absorbance of a solution of 80 mM decanoic acid/pH 8.2 with no salt added), because no significant re-flocculation had occurred. The plate was then re-read roughly every minute until control samples with no base or sugar showed substantial absorbance (about 0.5), typically after about 6 min. The reported percent reduction in absorbance (relative to the control value with no base or sugar added) is based on this time point. Values for percent reduction in absorbance vary from experiment to experiment because the cooling time at which the measurement was made varied.

To verify that ribose and glucose, rather than derivatives that formed during heating to 60 °C, inhibit flocculation, we conducted a control experiment in which the sugars were not added until the solutions had cooled to 40 °C; the results were identical within experimental uncertainty to those in Fig. 2E: $81 \pm 6\%$ reduction in absorbance for ribose and $28 \pm 7\%$ for glucose, in duplicate trials, with the sugars at 120 mM. For this control experiment, we made three changes to the general procedure. First, bicine was omitted in order to eliminate any reaction of the sugars with the buffer compound. Second, pH was lowered to 7.5, because the stability of sugars decreases with increasing pH. Third, after heating the 80 mM decanoic acid/300 mM NaCl solution to 60 °C to dissolve the flocs, we cooled it to 40 °C before adding 120 mM sugar; we then transferred the samples to a 96-well plate, and measured absorbance as the solutions cooled further and flocculation occurred.

Titration of decanoic acid solutions

Bases or sugars were dissolved in 80 mM decanoic acid/100 mM NaCl that had been adjusted to pH 8.25 with HCl. Solutions were then titrated in a beaker dropwise with HCl at 0.0625 to 1 M (depending on the volume of the solution and the point in the titration, to yield small, even decreases in pH). After each new pH was established, a 100 μ l aliquot was withdrawn to a 96-well plate for subsequent measuring of the absorbance at 490 nm with a SpectraMax M5 plate-reader (Molecular Devices, Sunnyvale, CA). Ribose and glucose solutions showed some absorbance (< 0.01) even at pH values above the point at which turbidity increased, and baselines were normalized accordingly.

Measuring turbidity induced by heating decanoic acid solutions containing bicine

Bases or sugars were dissolved in 80 mM decanoic acid/100 mM bicine/pH 7.9. 100 μ l of each solution was placed in a well of a 96-well plate, in duplicate, and the absorbance at 490 nm was measured. The plate was then wrapped in Saranwrap, placed in a 60 °C incubator for 10 minutes, and read again. % reduction in absorbance is the percentage of the control value (with no base or sugar added) by which a base or sugar reduced the increase in absorbance of a sample due to the heat-induced drop in pH.

Dynamic light scattering

A solution of 90 mM decanoic acid/100 mM bicine/pH 7.66 was extruded through polycarbonate membranes (Avanti Polar Lipids, Alabaster, AL), first 11 times through an 800 nm pore membrane and then 11 times through a 100 nm pore membrane. 30 mM adenine or thiouracil (or an equivalent volume of buffer) was then diluted into the extruded preparation to yield a final concentration of 10 mM base. Because pH falls when decanoic acid vesicle

preparations are diluted, the additions were in 100 mM bicine at higher pH, such that the pH of the final solution was maintained at 7.66. Dynamic light scattering measurements were carried out on a ZetaPlus analyzer (Brookhaven Instruments, Holtsville, NY) operated at a wavelength of 659 nm and at 25 °C. A 300 μ l sample was used for each measurement. The hydrodynamic radius at each reported time point was determined by averaging 5 two-minute runs. At the end of the experiment, the pH of all solutions was measured to ensure that it had not changed.

References

1. Flory, P. J. 1975. Spatial configuration of macromolecular chains. *Science* 188:1268-1276.
2. Kint, S., J. Scherer, and R. Snyder. 1980. Raman spectra of liquid n - alkanes. III. Energy difference between trans and gauche - butane. *The Journal of Chemical Physics* 73:2599-2602.
3. Nelson, P. 2004. *Biological physics*. WH Freeman New York.
4. Mouritsen, O. G. 2005. *Life-as a matter of fat*. Springer.
5. Weaver, J. C., and Y. A. Chizmadzhev. 1996. Theory of electroporation: a review. *Bioelectrochem. Bioenerg.* 41:135-160.
6. Koynova, R., and M. Caffrey. 1998. Phases and phase transitions of the phosphatidylcholines. *Biochim. Biophys. Acta, Rev. Biomembr.* 1376:91-145.
7. Nagle, J. F., and S. Tristram-Nagle. 2000. Structure of lipid bilayers. *Biochim. Biophys. Acta, Rev. Biomembr.* 1469:159-195.
8. Honerkamp-Smith, A. R., S. L. Veatch, and S. L. Keller. 2009. An introduction to critical points for biophysicists; observations of compositional heterogeneity in lipid membranes. *Biochim. Biophys. Acta, Biomembr.* 1788:53-63.
9. Veatch, S. L., and S. L. Keller. 2003. Separation of liquid phases in giant vesicles of ternary mixtures of phospholipids and cholesterol. *Biophys. J.* 85:3074-3083.
10. Beattie, M. E., S. L. Veatch, B. L. Stottrup, and S. L. Keller. 2005. Sterol structure determines miscibility versus melting transitions in lipid vesicles. *Biophys. J.* 89:1760-1768.
11. Veatch, S., I. Polozov, K. Gawrisch, and S. Keller. 2004. Liquid domains in vesicles investigated by NMR and fluorescence microscopy. *Biophys. J.* 86:2910-2922.
12. Veatch, S. L., K. Gawrisch, and S. L. Keller. 2006. Closed-loop miscibility gap and quantitative tie-lines in ternary membranes containing diphytanoyl PC. *Biophys. J.* 90:4428-4436.
13. Marsh, D. 2009. Cholesterol-induced fluid membrane domains: a compendium of lipid-raft ternary phase diagrams. *Biochim. Biophys. Acta, Biomembr.* 1788:2114-2123.

14. Huang, J., J. T. Buboltz, and G. W. Feigenson. 1999. Maximum solubility of cholesterol in phosphatidylcholine and phosphatidylethanolamine bilayers. *Biochim. Biophys. Acta, Biomembr.* 1417:89-100.
15. Liscovitch, M., and L. C. Cantley. 1994. Lipid second messengers. *Cell* 77:329-334.
16. Ikezawa, H. 2002. Glycosylphosphatidylinositol (GPI)-anchored proteins. *Biol. Pharm. Bull.* 25:409-417.
17. Simons, K., and J. L. Sampaio. 2011. Membrane organization and lipid rafts. *Cold Spring Harbor perspectives in biology* 3:a004697.
18. Van Meer, G., D. R. Voelker, and G. W. Feigenson. 2008. Membrane lipids: where they are and how they behave. *Nat. Rev. Mol. Cell Biol.* 9:112-124.
19. Ekroos, K., C. S. Ejsing, U. Bahr, M. Karas, K. Simons, and A. Shevchenko. 2003. Charting molecular composition of phosphatidylcholines by fatty acid scanning and ion trap MS3 fragmentation. *J. Lipid Res.* 44:2181-2192.
20. Verkleij, A., R. Zwaal, B. Roelofsen, P. Comfurius, D. Kastelijn, and L. Van Deenen. 1973. The asymmetric distribution of phospholipids in the human red cell membrane. A combined study using phospholipases and freeze-etch electron microscopy. *Biochim. Biophys. Acta, Biomembr.* 323:178-193.
21. Dupuy, A. D., and D. M. Engelman. 2008. Protein area occupancy at the center of the red blood cell membrane. *Proc. Natl. Acad. Sci. U. S. A.* 105:2848-2852.
22. Almén, M. S., K. J. Nordström, R. Fredriksson, and H. B. Schiöth. 2009. Mapping the human membrane proteome: a majority of the human membrane proteins can be classified according to function and evolutionary origin. *BMC Biology* 7:50.
23. Filmore, D. 2004. It's a GPCR world. *Modern drug discovery* 7:24-28.
24. Singer, S. J., and G. L. Nicolson. 1972. The fluid mosaic model of the structure of cell membranes. *Science* 175:720-731.
25. Simons, K., and E. Ikonen. 1997. Functional rafts in cell membranes. *Nature* 387:569-572.

26. Karnovsky, M. J., A. M. Kleinfeld, R. L. Hoover, and R. D. Klausner. 1982. The concept of lipid domains in membranes. *J. Cell Biol.* 94:1-6.
27. Pike, L. J. 2006. Rafts defined: a report on the Keystone Symposium on Lipid Rafts and Cell Function. *J. Lipid Res.* 47:1597-1598.
28. Elson, E. L., E. Fried, J. E. Dolbow, and G. M. Genin. 2010. Phase separation in biological membranes: integration of theory and experiment. *Annu. Rev. Biophys.* 39:207-226.
29. Jacobson, K., O. G. Mouritsen, and R. G. Anderson. 2007. Lipid rafts: at a crossroad between cell biology and physics. *Nat. Cell Biol.* 9:7-14.
30. Simons, K., and R. Ehehalt. 2002. Cholesterol, lipid rafts, and disease. *J. Clin. Invest.* 110:597-603.
31. Keller, S. L., S. M. Bezrukov, S. Gruner, M. W. Tate, I. Vodyanoy, and V. A. Parsegian. 1993. Probability of alamethicin conductance states varies with nonlamellar tendency of bilayer phospholipids. *Biophys. J.* 65:23-27.
32. Munro, S. 2003. Lipid rafts: elusive or illusive? *Cell* 115:377-388.
33. Edidin, M. 2003. The state of lipid rafts: from model membranes to cells. *Annu. Rev. Biophys. Biomol. Struct.* 32:257-283.
34. Lingwood, D., and K. Simons. 2007. Detergent resistance as a tool in membrane research. *Nat. Protoc.* 2:2159-2165.
35. Lichtenberg, D., F. M. Goñi, and H. Heerklotz. 2005. Detergent-resistant membranes should not be identified with membrane rafts. *Trends Biochem. Sci.* 30:430-436.
36. Schroeder, R., E. London, and D. Brown. 1994. Interactions between saturated acyl chains confer detergent resistance on lipids and glycosylphosphatidylinositol (GPI)-anchored proteins: GPI-anchored proteins in liposomes and cells show similar behavior. *Proc. Natl. Acad. Sci. U. S. A.* 91:12130-12134.
37. Baumgart, T., A. T. Hammond, P. Sengupta, S. T. Hess, D. A. Holowka, B. A. Baird, and W. W. Webb. 2007. Large-scale fluid/fluid phase separation of proteins and lipids in giant plasma membrane vesicles. *Proc. Natl. Acad. Sci. U. S. A.* 104:3165-3170.

38. Veatch, S. L., P. Cicuta, P. Sengupta, A. Honerkamp-Smith, D. Holowka, and B. Baird. 2008. Critical fluctuations in plasma membrane vesicles. *ACS Chem. Biol.* 3:287-293.
39. Morigaki, K., and P. Walde. 2007. Fatty acid vesicles. *Curr. Opin. Colloid Interface Sci.* 12:75-80.
40. Gebicki, J., and M. Hicks. 1973. Ufasomes are stable particles surrounded by unsaturated fatty acid membranes. *Nature* 243:232-234.
41. Hargreaves, W. R., and D. W. Deamer. 1978. Liposomes from ionic, single-chain amphiphiles. *Biochemistry* 17:3759-3768.
42. Smith, R., and C. Tanford. 1972. The critical micelle concentration of 1- α -dipalmitoylphosphatidylcholine in water and water/methanol solutions. *J. Mol. Biol.* 67:75-83.
43. Walde, P., R. Wick, M. Fresta, A. Mangone, and P. L. Luisi. 1994. Autopoietic self-reproduction of fatty acid vesicles. *J. Am. Chem. Soc.* 116:11649-11654.
44. Chen, I. A., and J. W. Szostak. 2004. Membrane growth can generate a transmembrane pH gradient in fatty acid vesicles. *Proc. Natl. Acad. Sci. U. S. A.* 101:7965-7970.
45. Sacerdote, M., and J. Szostak. 2005. Semipermeable lipid bilayers exhibit diastereoselectivity favoring ribose. *Proc. Natl. Acad. Sci. U. S. A.* 102:6004-6008.
46. Monnard, P.-A., C. L. Apel, A. Kanavarioti, and D. W. Deamer. 2002. Influence of ionic inorganic solutes on self-assembly and polymerization processes related to early forms of life: Implications for a prebiotic aqueous medium. *Astrobiology* 2:139-152.
47. Walde, P. 2006. Surfactant assemblies and their various possible roles for the origin(s) of life. *Origins of Life and Evolution of Biospheres* 36:109-150.
48. Deamer, D. W., and R. Pashley. 1989. Amphiphilic components of the Murchison carbonaceous chondrite: surface properties and membrane formation. *Orig. Life Evol. Biosphere.* 19:21-38.
49. Apel, C. L., D. W. Deamer, and M. N. Mautner. 2002. Self-assembled vesicles of monocarboxylic acids and alcohols: conditions for stability and for the encapsulation of biopolymers. *Biochim. Biophys. Acta, Biomembr.* 1559:1-9.
50. Gilbert, W. 1986. Origin of life: The RNA world. *Nature* 319:618.

51. Johnston, W. K., P. J. Unrau, M. S. Lawrence, M. E. Glasner, and D. P. Bartel. 2001. RNA-catalyzed RNA polymerization: accurate and general RNA-templated primer extension. *Science* 292:1319-1325.
52. Joyce, G. F., and L. E. Orgel. 1993. 1 Prospects for Understanding the Origin of the RNA World. *Cold Spring Harbor Monograph Archive* 24:1-25.
53. Dietrich, C., L. A. Bagatolli, Z. N. Volovyk, N. L. Thompson, M. Levi, K. Jacobson, and E. Gratton. 2001. Lipid rafts reconstituted in model membranes. *Biophys. J.* 80:1417-1428.
54. Polozov, I. V., and K. Gawrisch. 2006. Characterization of the liquid-ordered state by proton MAS NMR. *Biophys. J.* 90:2051-2061.
55. Marsh, D. 2009. Cholesterol-induced fluid membrane domains: A compendium of lipid-raft ternary phase diagrams. *Biochim. Biophys. Acta, Biomembr.* 1788:2114-2123.
56. Blosser, M. C., J. B. Starr, C. W. Turtle, J. Ashcraft, and S. L. Keller. 2013. Minimal effect of lipid charge on membrane miscibility phase behavior in three ternary systems. *Biophys. J.* 104:2629-2638.
57. Mengistu, D. H., and S. May. 2008. Nonlinear Poisson-Boltzmann model of charged lipid membranes: Accounting for the presence of zwitterionic lipids. *J. Chem. Phys.* 129:121105.
58. Lau, A. W. C., D. B. Lukatsky, P. Pincus, and S. A. Safran. 2002. Charge fluctuations and counterion condensation. *Phys. Rev. E* 65:051502.
59. Chakraborty, H., and M. Sarkar. 2007. Interaction of piroxicam and meloxicam with DMPG/DMPC mixed vesicles: Anomalous partitioning behavior. *Biophys. Chem.* 125:306-313.
60. Voinov, Maxim A., I. Rivera-Rivera, and Alex I. Smirnov. 2013. Surface Electrostatics of Lipid Bilayers by EPR of a pH-Sensitive Spin-Labeled Lipid. *Biophys. J.* 104:106-116.
61. Cascales, J. J. L., J. G. de la Torre, S. J. Marrink, and H. J. C. Berendsen. 1996. Molecular dynamics simulation of a charged biological membrane. *J. Chem. Phys.* 104:2713.
62. Zhao, W., T. Róg, A. A. Gurtovenko, I. Vattulainen, and M. Karttunen. 2007. Atomic-Scale Structure and Electrostatics of Anionic Palmitoyloleoylphosphatidylglycerol Lipid Bilayers with Na⁺ Counterions. *Biophys. J.* 92:1114-1124.

63. Mukhopadhyay, P., L. Monticelli, and D. P. Tieleman. 2004. Molecular dynamics simulation of a palmitoyl-oleoyl phosphatidylserine bilayer with Na⁺ counterions and NaCl. *Biophys. J.* 86:1601-1609.
64. Devaux, P. F., and A. Zachowski. 1994. Maintenance and consequences of membrane phospholipid asymmetry. *Chem. Phys. Lipids* 73:107-120.
65. Wang, T.-Y., and J. R. Silvius. 2001. Cholesterol Does Not Induce Segregation of Liquid-Ordered Domains in Bilayers Modeling the Inner Leaflet of the Plasma Membrane. *Biophys. J.* 81:2762-2773.
66. Hinderliter, A., P. F. F. Almeida, C. E. Creutz, and R. L. Biltonen. 2001. Domain Formation in a Fluid Mixed Lipid Bilayer Modulated through Binding of the C2 Protein Motif. *Biochemistry* 40:4181-4191.
67. Mbamala, E. C., A. Ben-Shaul, and S. May. 2005. Domain Formation Induced by the Adsorption of Charged Proteins on Mixed Lipid Membranes. *Biophys. J.* 88:1702-1714.
68. McLaughlin, S., and D. Murray. 2005. Plasma membrane phosphoinositide organization by protein electrostatics. *Nature* 438:605-611.
69. Gambhir, A., G. Hangyás-Mihályiné, I. Zaitseva, D. S. Cafiso, J. Wang, D. Murray, S. N. Pantyala, S. O. Smith, and S. McLaughlin. 2004. Electrostatic sequestration of PIP2 on phospholipid membranes by basic/aromatic regions of proteins. *Biophys. J.* 86:2188-2207.
70. Graber, Z. T., Z. Jiang, A. Gericke, and E. E. Kooijman. 2012. Phosphatidylinositol-4, 5-bisphosphate ionization and domain formation in the presence of lipids with hydrogen bond donor capabilities. *Chem. Phys. Lipids* 165:696-704.
71. Honerkamp-Smith, A. R., P. Cicuta, M. D. Collins, S. L. Veatch, M. den Nijs, M. Schick, and S. L. Keller. 2008. Line tensions, correlation lengths, and critical exponents in lipid membranes near critical points. *Biophys. J.* 95:236-246.
72. van Dijck, P. W. M., B. de Kruijff, A. J. Verkleij, L. L. M. van Deenen, and J. de Gier. 1978. Comparative studies on the effects of pH and Ca²⁺ on bilayers of various negatively charged phospholipids and their mixtures with phosphatidylcholine. *Biochim. Biophys. Acta, Biomembr.* 512:84-96.
73. Watts, A., K. Harlos, W. Maschke, and D. Marsh. 1978. Control of the structure and fluidity of phosphatidylglycerol bilayers by pH titration. *Biochim. Biophys. Acta, Biomembr.* 510:63-74.

74. Garidel, P., C. Johann, L. Mennicke, and A. Blume. 1997. The mixing behavior of pseudobinary phosphatidylcholine phosphatidylglycerol mixtures as a function of pH and chain length. *Eur. Biophys. J.* 26:447-459.
75. Silvius, J. R. 1982. Thermotropic phase transitions of pure lipids in model membranes and their modifications by membrane proteins. In *Lipid-protein interactions*. John Wiley, New York. 239-281.
76. Findlay, E. J., and P. G. Barton. 1978. Phase behavior of synthetic phosphatidylglycerols and binary-mixtures with phosphatidylcholines in presence and absence of calcium-ions. *Biochemistry* 17:2400-2405.
77. Wiedmann, T., A. Salmon, and V. Wong. 1993. Phase-behavior of mixtures of DPPC and POPG. *Biochim. Biophys. Acta* 1167:114-120.
78. Feigenson, G. W. 2009. Phase diagrams and lipid domains in multicomponent lipid bilayer mixtures. *Biochim. Biophys. Acta, Biomembr.* 1788:47-52.
79. Filippov, A., G. Oradd, and G. Lindblom. 2009. Effect of NaCl and CaCl₂ on the lateral diffusion of zwitterionic and anionic lipids in bilayers. *Chem. Phys. Lipids* 159:81-87.
80. Epand, R. M., and S. W. Hui. 1986. Effect of electrostatic repulsion on the morphology and thermotropic transitions of anionic phospholipids. *FEBS Lett.* 209:257-260.
81. Hauser, H. 1991. Effect of inorganic cations on phase transitions. *Chem. Phys. Lipids* 57:309-325.
82. Schneider, M. F., D. Marsh, W. Jahn, B. Kloesgen, and T. Heimburg. 1999. Network formation of lipid membranes: Triggering structural transitions by chain melting. *Proc. Natl. Acad. Sci. U. S. A.* 96.
83. Akashi, K., H. Miyata, H. Itoh, and K. Kinosita. 1996. Preparation of giant liposomes in physiological conditions and their characterization under an optical microscope. *Biophys. J.* 71:3242-3250.
84. Stevens, M. M., A. R. Honerkamp-Smith, and S. L. Keller. 2010. Solubility limits of cholesterol, lanosterol, ergosterol, stigmasterol, and beta-sitosterol in electroformed lipid vesicles. *Soft Matter* 6:5882-5890.

85. Cicuta, P., S. L. Keller, and S. L. Veatch. 2007. Diffusion of liquid domains in lipid bilayer membranes. *J. Phys. Chem. B* 111:3328-3331.
86. Stanich, C. A., A. R. Honerkamp-Smith, G. G. Putzel, C. S. Warth, A. K. Lamprecht, P. Mandal, E. Mann, T.-A. D. Hua, and S. L. Keller. 2013. Coarsening dynamics of domains in lipid membranes. *Biophys. J.* 105:444-454.
87. Angelova, M. I. 1988. Lipid Swelling and Liposome Formation in Electric Fields. In *Institute of Biophysics. Bulgarian Academy of Sciences, Sofia, Bulgaria.*
88. Himeno, H., N. Shimokawa, S. Komura, D. Andelman, T. Hamada, and M. Takagi. 2014. Charge-induced phase separation in lipid membranes. *arXiv preprint arXiv:1405.4650.*
89. Smith, A. K., and J. H. Freed. 2009. Determination of Tie-Line Fields for Coexisting Lipid Phases: An ESR Study. *J. Phys. Chem. B* 113:3957-3971.
90. Husen, P., L. R. Arriaga, F. Monroy, J. H. Ipsen, and L. A. Bagatolli. 2012. Morphometric Image Analysis of Giant Vesicles: A New Tool for Quantitative Thermodynamics Studies of Phase Separation in Lipid Membranes. *Biophys. J.* 103:2304-2310.
91. Shimokawa, N., M. Hishida, H. Seto, and K. Yoshikawa. 2010. Phase separation of a mixture of charged and neutral lipids on a giant vesicle induced by small cations. *Chem. Phys. Lett.* 496:59-63.
92. Boggs, J. M., and G. Rangaraj. 1983. Investigation of the metastable phase-behavior of phosphatidylglycerol with divalent-cations by calorimetry and manganese ion binding measurements. *Biochemistry* 22:5425-5435.
93. Mittler-Neher, S., and W. Knoll. 1993. Ca²⁺-induced lateral phase-separation in black lipid-membranes and its coupling to the ion translocation by gramicidin. *Biochim. Biophys. Acta* 1152:259-269.
94. Riske, K. A., H. G. Dobereiner, and M. T. Lamy-Freund. 2003. Comment on "Gel-Fluid transition in dilute versus concentrated DMPG aqueous dispersions". *J. Phys. Chem. B* 107:5391-5392.
95. Veqi-Suplicy, C. C., K. A. Riske, R. L. Knorr, and R. Dimova. 2010. Vesicles with charged domains. *Biochim. Biophys. Acta, Biomembr.* 1798:1338-1347.

96. Pereira, C. S., and P. H. Hunenberger. 2006. Interaction of the sugars trehalose, maltose and glucose with a phospholipid bilayer: A comparative molecular dynamics study. *J. Phys. Chem. B* 110:15572-15581.
97. Crowe, J. H., F. A. Hoekstra, K. H. N. Nguyen, and L. M. Crowe. 1996. Is vitrification involved in depression of the phase transition temperature in dry phospholipids? *Biochim. Biophys. Acta, Biomembr.* 1280:187-196.
98. Portet, T., S. E. Gordon, and S. L. Keller. 2012. Increasing Membrane Tension Decreases Miscibility Temperatures; an Experimental Demonstration via Micropipette Aspiration. *Biophys. J.* 103:L35-L37.
99. Parthasarathy, R., P. A. Cripe, and J. T. Groves. 2005. Electrostatically driven spatial patterns in lipid membrane composition. *Phys. Rev. Lett.* 95:48101.
100. Gordon, V. D., M. Deserno, C. M. J. Andrew, S. U. Egelhaaf, and W. C. K. Poon. 2008. Adhesion promotes phase separation in mixed-lipid membranes. *Europhys. Lett.* 84:48003.
101. Lindsey, H., N. O. Petersen, and S. I. Chan. 1979. Physicochemical characterization of 1,2-diphytanoyl-sn-glycero-3-phosphocholine in model membrane systems. *Biochim. Biophys. Acta, Biomembr.* 555:147-167.
102. Tokutomi, S., K. Ohki, and S. Ohnishi. 1980. Proton-induced phase separation in phosphatidylserine/phosphatidylcholine membranes. *Biochim. Biophys. Acta, Biomembr.* 596:192-200.
103. Pedersen, U. R., C. Leidy, P. Westh, and G. H. Peters. 2006. The effect of calcium on the properties of charged phospholipid bilayers. *Biochim. Biophys. Acta, Biomembr.* 1758:573-582.
104. Mengistu, D. H., and S. May. 2008. Debye-Huckel theory of mixed charged-zwitterionic lipid layers. *Eur. Phys. J. E* 26:251-260.
105. Almeida, P. F. F. 2009. Thermodynamics of lipid interactions in complex bilayers. *Biochim. Biophys. Acta, Biomembr.* 1788:72-85.
106. Lau, A. W. C., and P. Pincus. 2002. Counterion condensation and fluctuation-induced attraction. *Phys. Rev. E* 66:041501.
107. Lau, A. W. C. 2008. Fluctuation and correlation effects in a charged surface immersed in an electrolyte solution. *Phys. Rev. E* 77:011502.

108. Kjellander, R., S. Marcelja, and J. P. Quirk. 1988. Attractive double-layer interactions between calcium clay particles. *J. Colloid Interface Sci.* 126:194-211.
109. Larsen, A. E., and D. G. Grier. 1997. Like-charge attractions in metastable colloidal crystallites. *Nature* 385:230-233.
110. Pascher, I., S. Sundell, K. Harlos, and H. Eibl. 1987. Conformation and packing properties of membrane lipids: The crystal structure of sodium dimyristoylphosphatidylglycerol. *Biochim. Biophys. Acta, Biomembr.* 896:77-88.
111. Nagle, J. F. 1976. Theory of lipid monolayer and bilayer phase transitions: effect of headgroup interactions. *J. Membr. Biol.* 27:233-250.
112. Garidel, P., and A. Blume. 2000. Miscibility of phosphatidylethanolamine-phosphatidylglycerol mixtures as a function of pH and acyl chain length. *Eur. Biophys. J.* 28:629-638.
113. Laanait, N., M. Mihaylov, B. Hou, H. Yu, P. Vanýsek, M. Meron, B. Lin, I. Benjamin, and M. L. Schlossman. 2012. Tuning ion correlations at an electrified soft interface. *Proc. Natl. Acad. Sci. U. S. A.* 109:20326-20331.
114. Wagner, A. J., S. Loew, and S. May. 2007. Influence of monolayer-monolayer coupling on the phase behavior of a fluid lipid bilayer. *Biophys. J.* 93:4268-4277.
115. Putzel, G. G., M. J. Uline, I. Szleifer, and M. Schick. 2011. Interleaflet Coupling and Domain Registry in Phase-Separated Lipid Bilayers. *Biophys. J.* 100:996-1004.
116. Komura, S., and D. Andelman. 2014. Physical aspects of heterogeneities in multi-component lipid membranes. *Adv. Colloid Interface Sci.* 208:34-46.
117. Shlomovitz, R., and M. Schick. 2013. Model of a raft in both leaves of an asymmetric lipid bilayer. *Biophys. J.* 105:1406-1413.
118. Collins, M. D. 2008. Interleaflet coupling mechanisms in bilayers of lipids and cholesterol. *Biophys. J.* 94:L32-L34.
119. May, S. 2009. Trans-monolayer coupling of fluid domains in lipid bilayers. *Soft Matter* 5:3148-3156.

120. Risselada, H. J., and S. J. Marrink. 2008. The molecular face of lipid rafts in model membranes. *Proc. Natl. Acad. Sci. U. S. A.* 105:17367-17372.
121. Subramaniam, S., M. Seul, and H. McConnell. 1986. Lateral diffusion of specific antibodies bound to lipid monolayers on alkylated substrates. *Proc. Natl. Acad. Sci. U. S. A.* 83:1169-1173.
122. Collins, M. D., and S. L. Keller. 2008. Tuning lipid mixtures to induce or suppress domain formation across leaflets of unsupported asymmetric bilayers. *Proc. Natl. Acad. Sci. U. S. A.* 105.
123. Chiantia, S., and E. London. 2012. Acyl chain length and saturation modulate interleaflet coupling in asymmetric bilayers: effects on dynamics and structural order. *Biophys. J.* 103:2311-2319.
124. Stottrup, B. L., S. L. Veatch, and S. L. Keller. 2004. Nonequilibrium behavior in supported lipid membranes containing cholesterol. *Biophys. J.* 86:2942-2950.
125. Garg, S., J. R  he, K. L  dtke, R. Jordan, and C. A. Naumann. 2007. Domain registration in raft-mimicking lipid mixtures studied using polymer-tethered lipid bilayers. *Biophys. J.* 92:1263-1270.
126. J  nsson, P., J. P. Beech, J. O. Tegenfeldt, and F. H   k. 2009. Shear-driven motion of supported lipid bilayers in microfluidic channels. *J. Am. Chem. Soc.* 131:5294-5297.
127. Shreve, A. P., M. C. Howland, A. R. Sapuri-Butti, T. W. Allen, and A. N. Parikh. 2008. Evidence for leaflet-dependent redistribution of charged molecules in fluid supported phospholipid bilayers. *Langmuir* 24:13250-13253.
128. Bhatia, T., P. Husen, J. H. Ipsen, L. A. Bagatolli, and A. C. Simonsen. 2014. Fluid domain patterns in free-standing membranes captured on a solid support. *Biochim. Biophys. Acta, Biomembr.*
129. Pitcher, W. H., III, and W. H. Huestis. 2002. Preparation and analysis of small unilamellar phospholipid vesicles of a uniform size. *Biochem. Biophys. Res. Commun.* 296:1352-1355.
130. Stone, H. A., and A. Ajdari. 1998. Hydrodynamics of particles embedded in a flat surfactant layer overlying a subphase of finite depth. *J. Fluid Mech.* 369:151-173.
131. Bruus, H. *Theoretical Microfluidics*. 2008. New York: Oxford University Press.

132. Jönsson, P., J. P. Beech, J. O. Tegenfeldt, and F. Höök. 2009. Mechanical behavior of a supported lipid bilayer under external shear forces. *Langmuir* 25:6279-6286.
133. Evans, E., and E. Sackmann. 1988. Translational and rotational drag coefficients for a disk moving in a liquid membrane associated with a rigid substrate. *J. Fluid Mech.* 194:553-561.
134. Ramachandran, S., S. Komura, M. Imai, and K. Seki. 2010. Drag coefficient of a liquid domain in a two-dimensional membrane. *Eur. Phys. J. E* 31:303-310.
135. Han, T., T. P. Bailey, and M. Haataja. 2014. Hydrodynamic interaction between overlapping domains during recurrence of registration within planar lipid bilayer membranes. *Phys. Rev. E* 89:032717.
136. Han, T., and M. Haataja. 2013. Compositional interface dynamics within symmetric and asymmetric planar lipid bilayer membranes. *Soft Matter* 9:2120-2124.
137. Hovis, J. S., and S. G. Boxer. 2001. Patterning and composition arrays of supported lipid bilayers by microcontact printing. *Langmuir* 17:3400-3405.
138. Evans, E., and A. Yeung. 1994. Hidden dynamics in rapid changes of bilayer shape. *Chem. Phys. Lipids* 73:39-56.
139. Merkel, R., E. Sackmann, and E. Evans. 1989. Molecular friction and epitactic coupling between monolayers in supported bilayers. *J. Physique* 50:1535-1555.
140. Den Otter, W., and S. Shkulipa. 2007. Intermonolayer friction and surface shear viscosity of lipid bilayer membranes. *Biophys. J.* 93:423-433.
141. Horner, A., S. A. Akimov, and P. Pohl. 2013. Long and short lipid molecules experience the same interleaflet drag in lipid bilayers. *Phys. Rev. Lett.* 110:268101.
142. Jönsson, P., A. Gunnarsson, and F. Höök. 2010. Accumulation and separation of membrane-bound proteins using hydrodynamic forces. *Anal. Chem.* 83:604-611.
143. Steck, T. L., J. Ye, and Y. Lange. 2002. Probing red cell membrane cholesterol movement with cyclodextrin. *Biophys. J.* 83:2118-2125.
144. Fuller, N., and R. Rand. 2001. The influence of lysolipids on the spontaneous curvature and bending elasticity of phospholipid membranes. *Biophys. J.* 81:243-254.

145. Boesze-Battaglia, K., and R. J. Schimmel. 1997. Cell membrane lipid composition and distribution: Implications for cell function and lessons learned from photoreceptors and platelets. *J. Exp. Biol.* 200:2927-2936.
146. Mouat, M., and K. Manchester. 1998. The intracellular ionic strength of red cells and the influence of complex formation. *Comparative Haematology International* 8:58-60.
147. Berridge, M. J., P. Lipp, and M. D. Bootman. 2000. The versatility and universality of calcium signalling. *Nat. Rev. Mol. Cell Biol.* 1:11-21.
148. Coyne, C. W., K. Patel, J. Heureaux, J. Stachowiak, D. A. Fletcher, and A. P. Liu. 2014. Lipid Bilayer Vesicle Generation Using Microfluidic Jetting. *JoVE (Journal of Visualized Experiments)*:e51510-e51510.
149. Hu, P. C., and N. Malmstadt. 2015. Asymmetric Giant Lipid Vesicle Fabrication. In *Methods in Membrane Lipids*. Springer. 79-90.
150. Arriaga, L. R., S. S. Datta, S. H. Kim, E. Amstad, T. E. Kodger, F. Monroy, and D. A. Weitz. 2014. Ultrathin Shell Double Emulsion Templated Giant Unilamellar Lipid Vesicles with Controlled Microdomain Formation. *Small* 10:950-956.
151. Shum, H. C., J. Thiele, and S.-H. Kim. 2014. Microfluidic Fabrication of Vesicles. In *Advances in Transport Phenomena 2011*. Springer. 1-28.
152. Abkarian, M., E. Loiseau, and G. Massiera. 2011. Continuous droplet interface crossing encapsulation (cDICE) for high throughput monodisperse vesicle design. *Soft Matter* 7:4610-4614.
153. Klein, U., G. Gimpl, and F. Fahrenholz. 1995. Alteration of the Myometrial Plasma Membrane Cholesterol Content with. beta.-Cyclodextrin Modulates the Binding Affinity of the Oxytocin Receptor. *Biochemistry* 34:13784-13793.
154. Haase, M. F., and J. Brujic. 2014. Tailoring of High - Order Multiple Emulsions by the Liquid-Liquid Phase Separation of Ternary Mixtures. *Angewandte Chemie International Edition* 53:11793-11797.
155. Cheng, H.-T., and E. London. 2009. Preparation and properties of asymmetric vesicles that mimic cell membranes effect upon lipid raft formation and transmembrane helix orientation. *J. Biol. Chem.* 284:6079-6092.

156. Black, R. A., M. C. Blosser, B. L. Stottrup, R. Tavakley, D. W. Deamer, and S. L. Keller. 2013. Nucleobases bind to and stabilize aggregates of a prebiotic amphiphile, providing a viable mechanism for the emergence of protocells. *Proc. Natl. Acad. Sci. U. S. A.* 110:13272-13276.
157. Robertson, M. P., and G. F. Joyce. 2012. The origins of the RNA world. *Cold Spring Harbor perspectives in biology* 4:a003608.
158. Powner, M. W., B. Gerland, and J. D. Sutherland. 2009. Synthesis of activated pyrimidine ribonucleotides in prebiotically plausible conditions. *Nature* 459:239-242.
159. Deamer, D., J. P. Dworkin, S. A. Sandford, M. P. Bernstein, and L. J. Allamandola. 2002. The first cell membranes. *Astrobiology* 2:371-381.
160. Mansy, S. S., J. P. Schrum, M. Krishnamurthy, S. Tobé, D. A. Treco, and J. W. Szostak. 2008. Template-directed synthesis of a genetic polymer in a model protocell. *Nature* 454:122-125.
161. Ferris, J. P., A. R. Hill, R. Liu, and L. E. Orgel. 1996. Synthesis of long prebiotic oligomers on mineral surfaces. *Nature* 381:59-61.
162. Hanczyc, M. M., S. M. Fujikawa, and J. W. Szostak. 2003. Experimental models of primitive cellular compartments: encapsulation, growth, and division. *Science* 302:618-622.
163. Chen, I. A., K. Salehi-Ashtiani, and J. W. Szostak. 2005. RNA catalysis in model protocell vesicles. *J. Am. Chem. Soc.* 127:13213-13219.
164. Mansy, S. S., and J. W. Szostak. 2008. Thermostability of model protocell membranes. *Proc. Natl. Acad. Sci. U. S. A.* 105:13351-13355.
165. Maurer, S. E., D. W. Deamer, J. M. Boncella, and P.-A. Monnard. 2009. Chemical evolution of amphiphiles: glycerol monoacyl derivatives stabilize plausible prebiotic membranes. *Astrobiology* 9:979-987.
166. Naraoka, H., A. Shimoyama, and K. Harada. 1999. Molecular distribution of monocarboxylic acids in Asuka carbonaceous chondrites from Antarctica. *Orig. Life Evol. Biosphere.* 29:187-201.
167. Namani, T., and P. Walde. 2005. From decanoate micelles to decanoic acid/dodecylbenzenesulfonate vesicles. *Langmuir* 21:6210-6219.
168. Gornitz, V. 2009. *Encyclopedia of paleoclimatology and ancient environments.* Springer.

169. Lawless, J. G., and G. U. Yuen. 1979. Quantification of monocarboxylic acids in the Murchison carbonaceous meteorite. *Nature* 282:396-398.
170. McCollom, T. M., G. Ritter, and B. R. Simoneit. 1999. Lipid synthesis under hydrothermal conditions by Fischer-Tropsch-type reactions. *Orig. Life Evol. Biosphere*. 29:153-166.
171. Proskurowski, G., M. D. Lilley, J. S. Seewald, G. L. Früh-Green, E. J. Olson, J. E. Lupton, S. P. Sylva, and D. S. Kelley. 2008. Abiogenic hydrocarbon production at Lost City hydrothermal field. *Science* 319:604-607.
172. Callahan, M. P., K. E. Smith, H. J. Cleaves, J. Ruzicka, J. C. Stern, D. P. Glavin, C. H. House, and J. P. Dworkin. 2011. Carbonaceous meteorites contain a wide range of extraterrestrial nucleobases. *Proc. Natl. Acad. Sci. U. S. A.* 108:13995-13998.
173. Luisi, P. L. 2006. *The emergence of life: from chemical origins to synthetic biology*. Cambridge University Press.
174. Ricardo, A., M. Carrigan, A. Olcott, and S. Benner. 2004. Borate minerals stabilize ribose. *Science* 303:196-196.
175. Lambert, J. B., S. A. Gurusamy-Thangavelu, and K. Ma. 2010. The silicate-mediated formose reaction: bottom-up synthesis of sugar silicates. *Science* 327:984-986.
176. Stüeken, E., R. Anderson, J. Bowman, W. Brazelton, J. Colangelo - Lillis, A. Goldman, S. Som, and J. Baross. 2013. Did life originate from a global chemical reactor? *Geobiology* 11:101-126.
177. Wei, C., and A. Pohorille. 2013. Permeation of aldopentoses and nucleosides through fatty acid and phospholipid membranes: Implications to the origins of life. *Astrobiology* 13:177-188.
178. Narayanan, R., B. L. Stottrup, and P. Wang. 2009. Surface packing characterization of Langmuir monolayer-anchored enzyme. *Langmuir* 25:10660-10665.

Appendix I: Code

This appendix contains the text of Matlab code used in data analysis and plotting in this dissertation. The function of each script is given in the initial block of comments. Many scripts contain sections commented out that are useful either for troubleshooting problems or for displaying intermediate outputs.

plot_temp4

```
function plot_temp4(filename, title, lipidA, lipidB)
% Author: Matthew Blosser, matthewblosser@gmail.com
% code stolen liberally from phase_diagram.m by Adrienne Battle
%
% This function reads in a .xls file containing information about phase transition types and temperatures.
% It then outputs a Gibbs triangle plot showing points for all measured compositions, as well as
% a 'rainbow' plot of the transition temperatures for liquid-liquid coexistence.
% Inputs: .xls file (full file name, in same directory), title (as a string), lipidA (string, name of 1st lipid), and lipidB
(string)
% everything but the .xls is optional.
% .xls format: column 1: composition A, 2: composition B, 3: composition of Chol, 4: transition temperature, 5: type
of transition
% type codes:
% 0 = no transition
% 1 = liquid liquid
% 2 = liquid solid
% 3 = solid solid
% 4 = 3 phase
% 5 = no vesicles produced

% defines how many lines of the .xls to skip.
header = 0;

% defaults to plotting a 10 line per size triangle.
L = 10;

% read the .xls
clear data;
data = xlsread(filename);

% identifies the different data from the file.
compA = data(header+1:end, 1);
compB = data(header+1:end, 2);
compC = data(header+1:end, 3);
temp = data(header+1:end, 4);
type = data(header+1:end, 5);

% draws the gibbs triangle, using a .m which would be in the same file as this one.
% gibbs_triangle(L);
figure;
```

```

hold on;
axis([-2 L+2 -2 sqrt(3)*L/2+2]);
axis equal
h=gca;
set(h,'Visible','off');

%read all the liquid liquid transition data to plot transition temperatures
j=1;
for i = 1:size(type, 1)
    x=(L/2)*(1+((100-compC(i))/100).*((compB(i)-compA(i))./(compA(i)+compB(i))));
    y=(L/2)*sqrt(3)*compC(i)/100;

    if type(i) == 1
        xplot(j) = x;
        yplot(j) = y;
        tempplot(j) = temp(i);
        j = j+1;
    end

    %if type(i) == 2
    %   xplot(j) = x;
    %   yplot(j) = y;
    %   tempplot(j) = temp(i);
    %   j = j+1;
    %end
end

%plots transition temperatures. can plot as a 3D surface (surf), which covers up some artifacts, a 2D
%color gradient (pcolor) or a contour plot (contour). Only one of these should be uncommented.
ti=0:0.05:L;
[xI,yI]=meshgrid(ti,ti);
zI=griddata(xplot,yplot,tempplot,xI,yI, 'cubic');
%surf(xI,yI,zI,'EdgeColor','none');
pcolor(xI,yI,zI)
%contour(xI,yI,zI, 15)
shading interp

fontsize = 10;

%plots points for all measured compositions, as well as what kind of transition was observed.
for i = 1:size(type, 1)

    x=(L/2)*(1+((100-compC(i))/100).*((compB(i)-compA(i))./(compA(i)+compB(i))));
    y=(L/2)*sqrt(3)*compC(i)/100;

    marker = 'o';
    markerface = 'k';
    markersize = 10;
    fontsize = 11;

    %no transition
    if type(i)==0;
        marker='o';
        markerface='w';
    end
end

```

```

% liquid-liquid
elseif type(i)==1
    marker='o';
    markerface='k';
%solid-liquid
    elseif type(i)== 2
        marker='s';
        markerface='k';
%solid-solid
elseif type(i)== 3
    marker='^';
    markerface='k';
%3-phase
elseif type(i) == 4
    marker='+';
    markerface='k';
%no vesicles produced
elseif type(i) == 5
    marker='x';
    markerface='k';
end

%plot3(x,y,100, marker,'MarkerFaceColor',markerface,'MarkerEdgeColor','k', 'MarkerSize', markersize)

end

%Initializes title and labels if no inputs are given.
if nargin < 4
    lipidA = 'Low Tmelt Lipid';
    lipidB = 'High Tmelt Lipid';
end

if nargin < 2
    title = '';
end

% Add labels and such
%text(0,sqrt(3)*L/2+1,title,'HorizontalAlignment','right','Interpreter','none', 'FontSize', fontsize);
%text(-2,-2.8,'Temperature (C)','HorizontalAlignment','center', 'FontSize', fontsize);

%symbol half of legend.
%plot(L+0.5,sqrt(3)*L/2+1,'o','MarkerFaceColor','k','MarkerEdgeColor','k', 'MarkerSize', markersize);
%plot(L+0.5,sqrt(3)*L/2,'s','MarkerFaceColor','k','MarkerEdgeColor','k', 'MarkerSize', markersize);
%plot(L+0.5,sqrt(3)*L/2-1,'^','MarkerFaceColor','k','MarkerEdgeColor','k', 'MarkerSize', markersize);
%plot(L+0.5,sqrt(3)*L/2-2,'o','MarkerFaceColor','w','MarkerEdgeColor','k', 'MarkerSize', markersize);
%plot(L+0.5,sqrt(3)*L/2-3,'*','MarkerFaceColor','k','MarkerEdgeColor','k', 'MarkerSize', markersize);
%plot(L+0.5,sqrt(3)*L/2-4,'x','MarkerFaceColor','k','MarkerEdgeColor','k', 'MarkerSize', markersize);
%text half of legend
%text(L+1,sqrt(3)*L/2+1,'L-L coexistence', 'FontSize', fontsize);
%text(L+1,sqrt(3)*L/2,'S-L coexistence', 'FontSize', fontsize);
%text(L+1,sqrt(3)*L/2-1,'S-S coexistence', 'FontSize', fontsize);
%text(L+1,sqrt(3)*L/2-2,'One uniform phase', 'FontSize', fontsize);
%text(L+1,sqrt(3)*L/2-3,'3-phase coexistence', 'FontSize', fontsize);
%text(L+1,sqrt(3)*L/2-4,'No vesicles', 'FontSize', fontsize);

```

```

%composition labels
%text(0,-1, lipidA,'HorizontalAlignment','center', 'FontSize', fontsize);
%text(L,-1,lipidB,'HorizontalAlignment','center', 'FontSize', fontsize);
%text(L/2,sqrt(3)*L/2+1,'Cholesterol','HorizontalAlignment','center', 'FontSize', fontsize);

%color legend
% colormap('hsv')?Col
%set(gca, 'CLim', [15, 50]);
colorbar('Location', 'WestOutside', 'FontSize', fontsize);
axis equal

```

interp_temp

```

function bob = interp_temp(filename)
% Author: Matthew Blosser, matthewblosser@gmail.com
% code stolen liberally from phase_diagram.m by Adrienne Battle
%
% This function reads in a .xls file containing information about phase transition types and temperatures.
% It then asks the user for a composition, and outputs the interpolated
% transition temperature for that composition. Note that it will give a best
% fit value, even if it disagrees with the actual measured temperature at
% that point.
% Inputs: .xls file (full file name, in same directory), title (as a string), lipidA (string, name of 1st lipid), and lipidB
% (string)
% everything but the .xls is optional.
% .xls format: column 1: composition A, 2: composition B, 3: composition of Chol, 4: transition temperature, 5: type
% of transition
% type codes:
% 0 = no transition
% 1 = liquid liquid
% 2 = liquid solid
% 3 = solid solid
% 4 = 3 phase
% 5 = no vesicles produced

% reads the file
data = xlsread(filename);

header = 1;
L = 10;

% identifies the different data from the file.
compA = data(header+1:end, 1);
compB = data(header+1:end, 2);
compC = data(header+1:end, 3);
temp = data(header+1:end, 4);
type = data(header+1:end, 5);

% finds all the liquid liquid transitions. If other transitions are wanted,
% change the line that says 'if type(i) == 1' to the correct type.
j=1;
for i = 1:size(type, 1)

```

```

x=(L/2)*(1+((100-compC(i))/100).*((compB(i)-compA(i))./(compA(i)+compB(i))));
y=(L/2)*sqrt(3)*compC(i)/100;

if type(i) == 1
    xplot(j) = x;
    yplot(j) = y;
    tempplot(j) = temp(i);
    j = j+1;
end
end

%define distance, in mol fraction, between adjacent grid points.
gridsize = .05;

%Does the actual interpolation.
ti=0:gridsize:L;
[xI,yI]=meshgrid(ti,ti);
zI=griddata(xplot,yplot,tempplot,xI,yI, 'cubic');

%asks user for the composition to be looked at.
compA = input('mol fraction of low temperature lipid \n');
compB = input('mol fraction of low temperature lipid \n');

compC = 100 - compA - compB;

%finds the approximate position of the temperature in the gridded data.
xRaw=(L/2)*(1+((100-compC)/100).*((compB-compA)./(compA+compB)))/gridsize;
yRaw=(L/2)*sqrt(3)*compC/100/gridsize;

%fits it to the grid.
x = round(xRaw)+ 1;
y = round(yRaw);

bob = zI(y,x);

```

edgeTrack

```

%written by Matthew Blosser
%For use tracking the edge of bilayers moving under shear
%takes a .tif movie, oriented with flow from left to right. Currently set
%to read tif files already Sobel filtered in ImagedJ, but by uncommenting a
%line this program can do that as well.

function trajectory = edgeTrack(FileTif)

close all

FOLDER = ('C:\Users\matt\Documents\MATLAB\edgeTrack')% Where the movies are
HOME = ('C:\Users\matt\Documents\MATLAB'); % Where work files are
cd(FOLDER)

InfoImage=imfinfo(FileTif);

```



```

mImage=InfoImage(1).Width;
nImage=InfoImage(1).Height;
NumberImages=length(InfoImage);
im=zeros(nImage,mImage,NumberImages,'uint16');
ed = zeros(nImage,mImage,NumberImages);
TifLink = Tiff(FileTif, 'r');

    fitStart = 45;
    % fitEnd = 53;
    fitEnd = NumberImages;
    fitRange = fitStart:fitEnd;

for i=1:NumberImages
    TifLink.setDirectory(i);
    im(:, :, i)=TifLink.read();
    if(i ==1)
        maxInt = max(max(im(:, :, 1)));
        figure(99)
        imshow(im(:, :, 1), [0 maxInt])
        hold on
        center = int16(ginput(1))
        %center(1) = 120

    end
    % uncomment to do edge detecting step, leave commented if using already
    % filtered by ImageJ
    % ed(:, :, i) = edge(im(:, :, i), 'prewitt');
    [holder, throwaway] = imgradient(im(:, :, i));
    ed(:, :, i) = holder;
    % [bob edgeX] = max(sum(ed(center(2)-3:center(2)+3, 20:mImage, i)));
    [bob edgeX] = max(sum(ed(center(2)-3:center(2)+3, 20:mImage, i)));
    track(i,1) = i;
    track(i,2) = edgeX;

end
TifLink.close();

figure(100)

% imshow(im(:, :, 10), [0 maxInt])
% imshow(ed(:, :, 1), [0 maxInt])

hold on
% plot( [center track(10)] )

figure(101)
plot(sum(ed(center(2)-3:center(2)+3, 20:mImage, 1)))
% plot(sum(ed(:, :, 2)))
figure(102)

```

```

slope = fit(track(fitRange,1), track(fitRange,2), 'poly1')
plot(slope, track(fitRange,1), track(fitRange,2))
trajectory = track;

%plot(track(:,1), track(:,2),'o','MarkerFaceColor','k','MarkerEdgeColor','k', 'MarkerSize', 2)

% close all;

```

quantFluor

```

function quantFluor(fileName, diskrad)

% by Matthew Blosser, adapted from Aurelia Honerkamp-Smith
% opens a tiff stack, identifies vesicle meridian using Avesiclemask (or
% Avesiclemask2 or maskFixedRad)and measures the fluorescnse, subtracting
% background, and outputing the number to a txt file.

FOLDER = ('C:\Users\matt\Documents\MATLAB\quantFluor')% Where the movies are
HOME = ('C:\Users\matt\Documents\MATLAB'); % Where work files are
cd(FOLDER)
file = [fileName];

%THIS IS FOR AVIS

% MOV = aviread(file,first:last);%reads the avi movie into the Matlab movie structure MOV.
%MOV has two fields: "cdata" and "colormap"
%aviinfo(file)%prints the info for the avi file onto the command window
%for k=1:useframes,

% in(:,k)=MOV(k).cdata(:,1);%Unsure why, but this replaces the values in in(:,k) with the Matlab MOV
format.

%end

%%% THIS IS FOR TIFFS
%useframes=last-first+1;
%for k=1:useframes,%THIS IS FOR TIFFS
in(:,k,:)=imread(file);
% end

%Have loaded in the movie. Now, take each frame and find the
%center of the vesicle.
%choose a radius, then find the center.
figure(100)
%lastone = in(:, 1);
%firstone = in(:,1);
imshow(in(:, 1))
hold on
%make starting guess
start = ginput(1); %this line lets you click on the first picture to choose the center.
if nargin < 2
edge = ginput(1);

```

```

    diskrad = ((start(1) - edge(1))^2 + (start(2) - edge(2))^2)^(1/2);
end
back = ginput(1);
back(3) = 17;

%if you are automating this, use the next 3 lines, which use
%the center of the picture as the start (this works most of the
%time)
%    xcenter = round(s(1)/2);
%    ycenter = round(s(2)/2);
%    start = [xcenter, ycenter];

%for k = first:useframes,
clear s pic
pic = in(:, :, 1);
s = size(pic);
s1 = double(pic);
figure(11)          %**remove this figure to run faster**
%imagesc(pic), axis square
%hold on

%the last number in this line is your guess for the radius of
%the vesicle in pixels.
%diskrad = ((start(1) - edge(1))^2 + (start(2) - edge(2))^2)^(1/2);
%diskrad = 80;
diskwidth = 4;
vars(1) = start(1);
vars(2) = start(2);
if nargin == 1
    vars(3) = diskrad;
    testFcn = @(vars)Avesiclemask2(vars, s1, diskwidth);
else
    testFcn = @(vars)maskFixedRad(vars, s1, diskrad, diskwidth);
    fit(3) = diskrad;
end

fit = fminsearch(testFcn, vars);

if nargin > 1
    fit(3) = diskrad;
end

%fit = fminsearch(@Avesiclemask, start, s1, 80, []);
if (fit(1) <= 0) | (fit(2) <= 0) | fit(1) >= s(1) | fit(2) >= s(2)
    ERROR = 1
    xxx %crash program if center is outside picture
end
%figure(200)
%fit
%fluorTot = sum(sum(s1));
%fluorTot/(512*512);
%fluor = fluorTot - testFcn(fit);
%fluorScaled = sum(sum(s1)) - fluor

```

```

%fluorDensity = fluor/((fit(3)^2 - (fit(3) - diskwidth)^2)*3.1415927);
fluorDensity = testFcn(fit);
fluorBackDensity = AvesicleMask2([fit(1), fit(2), fit(3)+ 20], s1, diskwidth);
fluorBackDensity2 = AvesicleMask2(back, s1, 15)
fluorDensityDiff = fluorBackDensity - fluorDensity
fluorDensityDiff2 = fluorBackDensity2 - fluorDensity

%pdecirc(fit(2), fit(3), fit(4))
hold on
%figure(11)      %**remove this figure to run faster**
%plot(fit(1), fit(2), 'or', 'LineWidth', 3)
%pause(2)        %**and this pause**

%savefit(k,:) = round(fit);
%picsize(k,:) = s;
%k
start = fit;
%end
%output(1) = fileName;
%output(2) = fluorDensityDiff;
%output(3) = fit(1);
%output(4) = fit(2);
%output(5) = fit(3);
%output

output = strcat(fileName, ',', num2str(-1*fluorDensity), ',', num2str(-1*fluorBackDensity), ',');
output = strcat(output, num2str(fluorDensityDiff), ',', num2str(-1*fluorBackDensity2), ',',
num2str(fluorDensityDiff2), ',');
output = strcat(output, num2str(fit(1)), ',', num2str(fit(2)), ',', num2str(fit(3)), ',', num2str(nargin), '\n')
%save([ file '_center.dat'], 'fileName', 'output', '-ascii', '-tabs', '-double');
fid = fopen('data.txt', 'at');
fprintf(fid, output, 'char');
fclose(fid);
%fwrite(fid, ' ', 'char');
%fwrite(fid, 'fit(1)', 'char');
%fwrite(fid, 'fileName', 'char');
%fwrite(fid, 'fileName', 'char');
%fwrite(fid, 'fileName', 'char');
%fwrite(fid, 'fileName', 'char');

%clear savefit center picsize final
%close all
clear all
close all;

```

quantFluorCrop

% by Matthew Blosser, adapted from Aurelia Honerkamp-Smith
 % opens a tiff stack, identifies vesicle meridian using Avesiclemask (or
 % Avesiclemask2 or maskFixedRad)and measures the fluorescnse, subtracting
 % background, and outputing the number to a txt file.

%Similar to quantFluor, but first asks for user input to crop out a portion

%of the image. Useful if you want to exclude a section of the membrane from
%analysis.

function quantFluorCrop(fileName, diskrad)

% I want to track the location of the vesicle throughout the movie in order
% to compensate for drift. CENTER CROP CALLED AT END!!!!

%clear all

FOLDER = ('C:\Users\matt\Documents\MATLAB\quantFluor')% Where the movies are

HOME = ('C:\Users\matt\Documents\MATLAB'); % Where work files are

cd(FOLDER)

file = [fileName];

%THIS IS FOR AVIS

% MOV = aviread(file,first:last);%reads the avi movie into the Matlab movie structure MOV.

%MOV has two fields: "cdata" and "colormap"

%aviinfo(file)%prints the info for the avi file onto the command window

%for k=1:useframes,

% in(:, :, k)=MOV(k).cdata(:, :, 1);%Unsure why, but this replaces the values in in(:, :, k) with the Matlab MOV
format.

%end

%%%THIS IS FOR TIFFS

%useframes=last-first+1;

%for k=1:useframes,%THIS IS FOR TIFFS

in(:, :, k)=imread(file);

% end

%Have loaded in the movie. Now, take each frame and find the

%center of the vesicle.

%choose a radius, then find the center.

figure(100)

%lastone = in(:, :, 1);

%firstone = in(:, :, 1);

imshow(in(:, :, 1))

hold on

%make starting guess

start = ginput(1); %this line lets you click on the first picture to choose the center.

if nargin < 2

edge = ginput(1);

diskrad = ((start(1) - edge(1))^2 + (start(2) - edge(2))^2)^(1/2);

end

back = ginput(1);

cropUpperLeft = ginput(1)

cropLowerRight = ginput(1)

back(3) = 17;

%if you are automating this, use the next 3 lines, which use

%the center of the picture as the start (this works most of the

%time)

```

%      xcenter = round(s(1)/2);
%      ycenter = round(s(2)/2);
%      start = [xcenter, ycenter];

%for k = first:useframes,
clear s pic
pic = in(:, :, 1);
s = size(pic);
s1 = double(pic);
figure(11)          %**remove this figure to run faster**
%imagesc(pic), axis square
%hold on

%the last number in this line is your guess for the radius of
%the vesicle in pixels.
%diskrad = ((start(1) - edge(1))^2 + (start(2) - edge(2))^2)^(1/2);
%diskrad = 80;
diskwidth = 4;
vars(1) = start(1);
vars(2) = start(2);
if nargin == 1
    vars(3) = diskrad;
    testFcn = @(vars)maskCrop(vars, s1, diskwidth, cropUpperLeft, cropLowerRight);
else
    testFcn = @(vars)maskFixedRad(vars, s1, diskrad, diskwidth);
    fit(3) = diskrad;
end

fit = fminsearch(testFcn, vars);

if nargin > 1
    fit(3) = diskrad;
end

%fit = fminsearch(@Avesiclemask, start, s1, 80, []);
if (fit(1) <= 0) | (fit(2) <= 0) | fit(1) >= s(1) | fit(2) >= s(2)
    ERROR = 1
    xxx %crash program if center is outside picture
end
%figure(200)
%fit
%fluorTot = sum(sum(s1));
%fluorTot/(512*512);
%fluor = fluorTot - testFcn(fit);
%fluorScaled = sum(sum(s1)) - fluor
%fluorDensity = fluor/((fit(3)^2 - (fit(3) - diskwidth)^2)*3.1415927);
fluorDensity = testFcn(fit);
fluorBackDensity = maskCrop([fit(1), fit(2), fit(3)+ 20], s1, diskwidth, cropUpperLeft, cropLowerRight);
fluorBackDensity2 = maskCrop(back, s1, 15, cropUpperLeft, cropLowerRight)
fluorDensityDiff = fluorBackDensity - fluorDensity
fluorDensityDiff2 = fluorBackDensity2 - fluorDensity

%pdecirc(fit(2), fit(3), fit(4))

```

```

hold on
%figure(11)      %**remove this figure to run faster**
%plot(fit(1), fit(2), 'or', 'LineWidth', 3)
%pause(2)        %**and this pause**

%savefit(k,:) = round(fit);
%picsize(k,:) = s;
%k
start = fit;
%end
%output(1) = fileName;
%output(2) = fluorDensityDiff;
%output(3) = fit(1);
%output(4) = fit(2);
%output(5) = fit(3);
%output

output = strcat(fileName, ',', num2str(-1*fluorDensity), ',', num2str(-1*fluorBackDensity), ',');
output = strcat(output, num2str(fluorDensityDiff), ',', num2str(-1*fluorBackDensity2), ',',
num2str(fluorDensityDiff2), ',');
output = strcat(output, num2str(fit(1)), ',', num2str(fit(2)), ',', num2str(fit(3)), ',', num2str(nargin), '\n')
%save([ file '_center.dat'], 'fileName', 'output', '-ascii', '-tabs', '-double');
fid = fopen('data.txt', 'at');
fprintf(fid, output, 'char');
fclose(fid);
%fwrite(fid, ' ', 'char');
%fwrite(fid, 'fit(1)', 'char');
%fwrite(fid, 'fileName', 'char');
%fwrite(fid, 'fileName', 'char');
%fwrite(fid, 'fileName', 'char');
%fwrite(fid, 'fileName', 'char');
clear all
close all;

```

Avesiclemask

% by Matthew Blosser, adapted from Aurelia Honerkamp-Smith
 %creates a mask of a fixed width, for use with quantFluor

```

function g = Avesiclemask(vars, image, diskwidth)

a(1) = vars(1);
a(2) = vars(2);
diskrad = vars(3);

s = size(image);
m = max(max(image));
image = image/m;
new = zeros(s(1), s(2));
inner = diskrad - diskwidth;
%want to make a dark background with a bright ring on it of the specified
%size, and centered at a
for i = 1:s(1),

```

```

for j = 1:s(2),
    rad = sqrt((i-a(2))^2 + (j-a(1))^2);
    if (rad <= diskrad) && (rad>= inner),
        new(i,j) = 1;
    end
end
end
%init = sum(sum(image));
%clear image;
%fin = sum(sum(new));
%clear new
%g = init - fin
diff = abs(image-new);
g = sum(sum(diff));
%fluorReal = sum(sum(image)) - g
figure(13)          %**to run faster, don't show this figure**
imagesc(diff), axis square

```

Avesiclemask2

% by Matthew Blosser, adapted from Aurelia Honerkamp-Smith
 %creates a mask of a fixed width, for use with quantFluor
 %similar to Avesiclemask, but calculates the total fluorescence within the
 %mask, which is more efficient.

```

function g = Avesiclemask2(vars, image, diskwidth)

    a(1) = vars(1);
    a(2) = vars(2);
    diskrad = vars(3);

    s = size(image);
    %m = max(max(image));
    %image = image;

    inner = diskrad - diskwidth;
    fluorInit = sum(sum(image));
    %want to make a dark background with a bright ring on it of the specified
    %size, and centered at a

    area = 0;
    for i = 1:s(1),
        for j = 1:s(2),
            rad = sqrt((i-a(2))^2 + (j-a(1))^2);
            if (rad <= diskrad) && (rad>= inner),
                image(i,j) = 0;
                area = area + 1;
            end
        end
    end
    end

    fluorFinal = sum(sum(image));

```



```

g = (fluorFinal - fluorInit)/area;
%g = (fluorFinal - fluorInit)/((diskrad^2 - (diskrad - diskwidth)^2)*3.1415927);
%g = sum(sum(image));

```

```

figure(13)          %**to run faster, don't show this figure**
imagesc(image), axis square

```

maskCrop

% by Matthew Blosser, adapted from Aurelia Honerkamp-Smith
 %creates a mask of a fixed width, for use with quantFluorCrop
 %similar to Avesiclemask2, but for use with a cropped image.

```

function g = maskCrop(vars, image, diskwidth, cropUpperLeft, cropLowerRight)

    a(1) = vars(1);
    a(2) = vars(2);
    diskrad = vars(3);

    s = size(image);
    %m = max(max(image));
    %image = image;

    inner = diskrad - diskwidth;
    fluorInit = sum(sum(image));
    %want to make a dark background with a bright ring on it of the specified
    %size, and centered at a

    area = 0;
    for i = 1:s(1),
        for j = 1:s(2),
            rad = sqrt((i-a(2))^2 + (j-a(1))^2);
            if (rad <= diskrad) && (rad>= inner),
                if (j < cropUpperLeft(1) || i < cropUpperLeft(2) || j > cropLowerRight(1) || i > cropLowerRight(2)),
                    %if i > cropUpperLeft(1) || j > cropUpperLeft(2) || i < cropLowerRight(1) || j < cropLowerRight(2)
                    image(i,j) = 0;
                    area = area + 1;
                end
            end
        end
    end

    fluorFinal = sum(sum(image));

    g = (fluorFinal - fluorInit)/area;
    %g = (fluorFinal - fluorInit)/((diskrad^2 - (diskrad - diskwidth)^2)*3.1415927);
    %g = sum(sum(image));

    figure(13)          %**to run faster, don't show this figure**
    imagesc(image), axis square

```

quenchFit

```
%By Matthew Blosser
% This is a very standard fitting function, with some of the less used options more obvious. It was originally written
%to fit the results of quenching experiemnts
function param = quenchFit(fluor)
guess = [max(fluor), 1, 1, 1];
param = guess;

f = @(param)residual(fluor, param);
options = optimset('TolFun', 1e-15);

%param = lsqnonlin(f, guess, [],[],options);

param = fminsearch(f, param);

residual(fluor, param)

%plot(fluor);
fit = ones(size(fluor, 1));
fit = param(1)*exp(param(2)*fit) + param(3)*exp(param(4)*fit);
plot(fit);

hold on;

end

function residual = residual(fluor, param)
    temp = 0;
    a = param(1);
    b = param(2);
    c = param(3);
    d = param(4);
    %e = param(5);

    for i = 1:size(fluor, 1)
        temp = temp + (fluor(i) - a*exp(b*i) - c*exp(d*i))^2;
        %temp = temp + (fluor(i) - a*exp(b*i) - c*exp(d*i) - e)^2;
    end

    residual = temp;

end
```

dls

```
function test = dls(fileExt)
%By Matthew Blosser
%This program reads in data files produced by the dynamic light scattering
%machine in Suzie Pun's lab, and the then plots the results

fileList = dir(fullfile(strcat('C:\Users\matt\Documents\MATLAB\DLS\',fileExt)))
test = fileList;
```

```

for i = 1:numel(fileList)

file = fopen(fileList(i).name)
fileList(i).name
crap = textscan(file,'%*[\n]', 5);
crap = textscan(file,'%s', 2);
timeTemp = textscan(file, '%d:%d:%d',1)
hour(i) = timeTemp{1};
minute(i) = timeTemp{2};
second(i) = timeTemp{3};

crap = textscan(file,'%*[\n]', 29);
crap = textscan(file,'%s', 1);
deffTemp = textscan(file, '%f', 1)

deff(i) = deffTemp{1}

crap = textscan(file, '%s', 5);
derrorTemp = textscan(file, '%f', 1);
derror(i) = derrorTemp{1};

fclose(file)

end

time = hour.*60 + minute + second./60 - 9.*60 - 15;

%figure(1)
%plot(time, deff)
errorbar(time, deff, derror, 'ok','MarkerEdgeColor','k','MarkerFaceColor','k','MarkerSize',5)

test = deff;

```